Investigating the heat shock response of bloodstream and procyclic forms of *Trypanosoma spp.*

Abbey Taylor

Lancaster University

Department of Biomedical and Life Sciences

September 2024

This thesis is submitted for the degree of MSc by Research.

Abstract

Trypanosoma congolense, a primary causative agent of Animal African Trypanosomiasis (AAT), inflicts severe economic losses across Sub-Saharan Africa. A key symptom of trypanosome infections is fever, which the parasite counters through its heat shock response, a critical virulence mechanism for survival within the host. Despite the profound impact of AAT, the molecular details of *T. congolense's* heat shock response remain largely unexplored. Given its co-infection with *Trypanosoma brucei*—a parasite with a well-characterised heat shock response—the comparative analysis offers a strategic framework to uncover specific survival strategies in *T. congolense*.

This study aimed to profile the thermal tolerance of *Trypanosoma* spp. and to characterise the molecular responses triggered by heat shock, focusing on key elements such as protein re-localisation, stress granule formation, and mRNA stability. These processes are vital for understanding how these parasites evade host immune defences under stress.

The results reveal that *T. congolense* exhibits a distinct heat shock response compared to *T. brucei*, with significant differences in cellular survival rates, and mRNA dynamics under thermal stress. These findings provide critical insights into the unique biology of *T. congolense*, offering potential avenues for the development of novel therapeutic targets aimed at disrupting the parasite's adaptive mechanisms under heat stress.

Table of Contents

Abstract **1**

List of tables **5**

List of figures **6**

Acknowledgements **8**

Declaration **9**

1. Introduction **10**

1.1. T. brucei and disease *10*

1.2. Host temperature varies in response to parasite burden *13*

1.3. Gene regulation and organisation in trypanosomes is atypical *14*

1.4. Heat shock response in model eukaryotes *15*

1.5. Phosphorylation of eIF2alpha triggers translational arrest *16*

1.6. Formation of Stress granules and P-bodies *16*

1.7. Upregulation of HSP gene *18*

1.8. The HSP70 – HSF1 titration model *18*

1.9. Heat shock response in T. brucei *20*

1.10. PCF T. brucei HS response *20*

1.11. Heat shock-induced stress granule formation *22*

1.12. A summarised timeline of events of the HS response when triggered at 41 ℃ for 2 hours ... *23*

1.13. BSF T. brucei HS response *24*

1.14. The RNA binding protein ZC3H11 is master regulator of HSR in T. brucei *26*

1.15. Changes in early heat shock are dominated by phosphorylation *31*

1.16. Heat shock response in T. congolense *32*

1.17. Project aims *33*

2. Materials and Methods **34**

2.1. Materials *34*

2.1.1. Cell lines 34

2.1.2. Plasmids 34

2.2. Methods *35*

2.2.1. *T. brucei* (BSF) cell culture 35

2.2.2. *T. brucei* (PCF) cell culture 36

2.2.3. *T. congolense* cell culture 36

2.2.4. Generation of cell lines 37

2.2.5. Heat Shock Protocol 38

2.2.6. Flow cytometry 38

2.2.7. Fluorescence microscopy 39

2.2.8. RNA extraction 39

2.2.9. Bioanalyzer 40

2.2.10. Generation of cDNA 40

2.2.11. qPCR 40

2.2.12. gDNA extraction 41
2.2.13. PCR 42
2.2.14. Agarose gel electrophoresis 42
2.2.15. Gel extraction 43
2.2.16. Ligation 43
2.2.17. Transformation 43
2.2.18. DNA mini-preps 44
2.2.19. DNA midi-preps 44
2.2.20. Sequencing 44
2.2.21. Restriction Enzyme Digest 44
2.2.22. Ethanol precipitation 45
2.2.23. Transfection of *T. brucei* 45
2.2.24. Transfection of *T. congolense* 45
2.2.25. SDS-PAGE 46
2.2.26. Western blot 47

3. **Profiling thermal tolerance in *T. brucei* and *T. congolense* 48**

3.1. Introduction 48

3.2. Interrogating T. brucei BSF growth recovery after variable heat shock timeframes 48

3.3. T. brucei BSF Cell cycle analysis across heat shock recovery timeframe 50

3.4. Interrogating T. brucei PCF growth recovery after variable heat shock timeframes 52

3.5. T. brucei PCF Cell cycle analysis across heat shock recovery timeframe 54

3.6. Interrogating BSF T. congolense growth recovery after variable heat shock timeframes 56

3.7. BSF T. congolense Cell cycle analysis across heat shock recovery timeframe 58

3.8. Optimisation of fixation parameters for flow cytometry 60

3.9. Summary 61

4. Genetic modifications to allow molecular characterisation of the HS response 63

4.1. Introduction 63

4.2. In situ tagging of BSF T. brucei proteins 63
4.2.1. PCR Verification of eYFP-TbXRNA cell lines 65
4.2.2. PCR verification of TbPABP1-sfGFP cell lines 66
4.2.3. Western blot verification of eYFP-TbXRNA and TbPABP1-sfGFP cell lines 68
4.2.4. Fluorescence Microscopy Verification of eYFP-TbXRNA 69
4.2.5. Fluorescence Microscopy Verification of TbPABP1-sfGFP 71

4.3. In situ tagging of BSF T. congolense proteins 73
4.3.1. Verification of eYFP-TcoXRNA integration by PCR 74
4.3.2. Verification of TcoHSP100-sfGFP integration by PCR 76
4.3.3. Verification of TcoPABP1- sfGFP integration by PCR 77
4.3.4. Fluorescence Microscopy Verification of *T. congolense* cell lines 78

4.4. Summary 80

5. Characterisation of protein localisation in response to heat shock 82

5.1. Introduction 82

5.2. Characterisation of tagged T. brucei cell lines 82
5.2.1. Characterisation of eYFP-TbXRNA response to heat shock in *T. brucei* 83
5.2.2. eYFP-TbXRNA does not co-localise with the mitochondria 85
5.2.3. Heat shock triggers altered localisation and intensity of PABP1-sfGFP 87
5.2.4. Regions of high sfGFP-PABP1 signal intensity may co-localise with the mitochondria after heat shock 89

5.3. Heat shock triggers altered localisation and intensity of TbDHH1 91

5.4. Summary 93

6. Characterisation of heat-induced transcriptional changes in African trypanosomes 95

6.1. Introduction 95

6.2. T. brucei mRNA levels exhibit both transient and multiphasic temporal changes due to heat shock 95

6.3. T. congolense mRNA levels exhibit both transient and multiphasic temporal changes due to heat shock 99

6.4. Chapter Summary 101

7. Discussion 102

7.1. Growth Recovery 102

7.2. Cell Cycle Disruptions 104

7.3. Stress granule and P-body formation 107

7.4. mRNA changes after HS 109

7.5. Summary 111

8. Appendices 113

References 118

List of tables

Table 1 Plasmid backbones and inserts used for generation of fusion proteins 34
Table 2 *T. congolense* media components 36
Table 3 qPCR Cycle conditions 40
Table 4 PCR Master Mix 42
Table 5 Drug concentration used for transfected cell lines 46
Table 6 Fixation optimisation observations 60
Table 7 Summary of cell lines produced and verified 81

List of figures

Figure 1.1 Digenetic lifecycle of *T. brucei*, illustrating the transmission cycle between the mammalian host and insect vector. 11
Figure 1.2 Variation in host temperature occurs in response to parasite burden. 13
Figure 1.3 Gene expression in kinetoplastids. 15
Figure 1.4 HSP70 – HSF1 titration model. 19
Figure 1.5 The effects of heat shock on BSF cell viability and growth. 25
Figure 1.6 Effects of HS on abundance of ZC3H11 using expression of in-situ tagged V5-ZC3H11. 26
Figure 1.7 ZC3H11 is phosphorylated. 27
Figure 1.8 ZC3H11 depletion is detrimental to BSF but not PCF. 28
Figure 1.9 ZC3H11 is required for survival and recovery of HS in PCF. 28
Figure 1.10 Proposed model of ZC3H11 stabilising mRNA. 30
Figure 2.1 Cloning Strategy. 37
Figure 3.1 Growth Curves of Blood Stream Form *Trypanosoma brucei* Post Heat Shock. 49
Figure 3.2 BSF *T. brucei* under varying heat shock conditions. 50
Figure 3.3 Growth Curves of Procyclic Form *Trypanosoma brucei* Post Heat Shock. 53
Figure 3.4 Cell Cycle disruption of *Trypanosoma brucei* PCF under varying heat shock conditions. 54
Figure 3.5 Growth Curves of Blood Stream Form *Trypanosoma congolense* Post Heat Shock. 57
Figure 3.6 Cell Cycle Distribution of *Trypanosoma congolense* after 0 and 0.5 hours of heat shock. 59
Figure 4.1 Agarose gel electrophoresis of linearised constructs. 64
Figure 4.2 Confirmation of eYFP-TbXRNA transfected cell line by PCR. (a) Schematic of PCR primer design. 65
Figure 4.3 Confirmation of TbPABP1-sfGFP transfected cell line by PCR. (a) Schematic of PCR primer design. 67
Figure 4.4 Western Blot Analysis of *T. brucei* BSF Clones Expressing TbPABP1-sGFP and eYFP-TbXRNA. 68
Figure 4.5 Fluorescence Microscopy Images of *T. brucei* BSF eYFP-TbXRNA cell line. 70
Figure 4.6 Fluorescence Microscopy Images of *T. brucei* BSF TbPABP1-sfGFP cell line. 72
Figure 4.7 Agarose gel electrophoresis of linearised constructs. 73
Figure 4.8 DNA Gel Electrophoresis of PCR Products Confirming Integration of PMA6 (eYFP-TcoXRNA). 75
Figure 4.9 DNA Gel Electrophoresis of PCR Products Confirming Integration of PMA8 (sfGFP-tagged TcoHSP100 Plasmid) into the Genome. 76
Figure 4.10 DNA Gel Electrophoresis of PCR Products Confirm Integration of PMA10 (sfGFP-tagged TcoPABP1 Plasmid) into the Genome. 77
Figure 4.11 Fluorescence Microscopy Images of *T. congolense* BSF eYFP-TcoXRNA, TcoHSP100-sfGFP and TcoPABP1-sfGFP cell lines. 79

Figure 5.1 Time-Course Analysis of TbXRNA Localisation in *T. brucei* BSF eYFP-TbXRNA Cell Line Following Heat Shock. 84
Figure 5.2 Microscopy Analysis of TbXRNA Localisation in *T. brucei* eYFP-TbXRNA Cell Line with Mitochondrial Staining Before and After Heat Shock. 86
Figure 5.3 Time-Course Analysis of PABP1 Localisation in *T. brucei* BSF PABP1-sfGFP Cell Line Following Heat Shock. 88
Figure 5.4 Microscopy Analysis of PABP1 Localisation in *T. brucei* PABP1-sfGFP Cell Line with Mitochondrial Staining Before and After Heat Shock. 90
Figure 5.5 Time-Course Analysis of TbDHH1 Localisation in *T. brucei* mSt-TbDHH1 Cell Line Following Heat Shock. 92
Figure 6.1 Analysis of mRNA Fold Change in Heat Shock Proteins and VSGs in BSF *T. brucei* During Heat Shock and Recovery. 96
Figure 6.2 Analysis of mRNA Fold Change in Heat Shock Proteins and VSG in BSF *T. congolense* During Heat Shock and Recovery. 99
Figure 8.1 Cell cycle analysis of BSF *T. brucei* after heat shock. 117

Acknowledgements

First and foremost, I would like to express my deepest gratitude to my supervisor, Professor Mick Urbaniak, for his unwavering support, guidance, and patience throughout this journey. Your expertise and encouragement have been invaluable, and I feel incredibly fortunate to have had the opportunity to learn and grow under your mentorship. Thank you for taking the gamble on me.

A special thank you to Dr. Caroline Dewar, whose help and wisdom were instrumental to the success of this project. Your constant willingness to provide advice, answer questions, and offer encouragement made all the difference, and I truly could not have achieved this without you.

To Dr. Aro Nugawela, my "lab sister," your friendship and support were the cornerstone of my experience in the lab. I cannot imagine having made it through the challenges of this journey without you by my side, both as a colleague and a dear friend. Thank you for being there through the highs and lows, for all the laughs and tears and for always reminding me that I could do this.

I also want to extend my heartfelt thanks to Professor Jackie Parry, who first ignited my passion for the lab. You were the first person to truly believe in my abilities and encourage me to pursue my path in research. Your belief in me gave me the confidence to embrace my potential, and for that, I am deeply grateful.

I would also like to thank my friends, both in and outside of the lab, for keeping me grounded and reminding me to take breaks when needed. Your kindness and laughter were a constant source of energy that carried me through the tough times.

Finally, I am forever grateful to my family. Your unconditional love and belief in me have been the foundation upon which I have built my academic journey. Thank you for your endless support, for always cheering me on, and for giving me the strength to persevere when things seemed impossible.

This thesis is as much yours as it is mine. Thank you, from the bottom of my heart.

Declaration

I, Abbey Taylor, confirm that the work presented in this thesis is my own and has not been submitted in substantially the same form for the award of a higher degree elsewhere. Where information has been derived from other sources, I confirm this has been indicated in the thesis.

Signed.....

1. Introduction

1.1. *T. brucei* and disease

Trypanosomiasis is a disease which affects both humans and animals across Sub-Saharan Africa. *Trypanosoma brucei gambiense (T. b. gambiense)* and *Trypanosoma brucei rhodesiense (T. b. rhodesiense)* are vector borne parasites and the causative agents of Human African Trypanosomiasis (HAT), otherwise known as sleeping sickness. These two parasites alongside *Trypanosoma brucei brucei (T. brucei), Trypanosoma congolense (T. congolense)* and *Trypanosoma vivax (T. vivax)* are the causative agents of the cattle wasting disease, Animal African Trypanosomiasis (AAT), otherwise known as nagana (CDC, 2019).

The understanding of the diagenetic life cycle of both *T. brucei* and *T. congolense* is furthered by *in vitro* experiments, informing on how we can combat and mitigate the real-world challenges presented by the diverse kinetoplasted lineage. The transmission vector for these parasites is the Tsetse fly, of the genus *Glossina*. In the case of *T. brucei,* once an infected tsetse fly takes a blood meal from a mammal, the mammal is injected with metacyclic trypomastigotes. From here the parasites will enter the lymphatic system subsequently passing into the blood stream. It is here the metacyclic trypomastigotes will transform into bloodstream form (BSF) trypomastigotes and begin to divide. When a tsetse fly takes a bloodmeal from the infected human, the fly will ingest bloodstream from trypomastigotes, pre-adapted for survival in the insect host, as “stumpy-form” parasites. Once the parasites reach the fly midgut, they will differentiate into procyclic form (PCF) trypomastigotes and will begin to divide. Upon leaving the midgut these procyclic trypomastigotes differentiate into epimastigote, once these reach the salivary gland they begin to divide. Finally, these epimastigote transform into metacyclic trypomastigote and the cycle repeats. It is here the life cycles between *T. brucei* and *T. congolense* differ as during a *T. congolense* infection the epimastigote in the tsetse fly transform into metacyclic trypomastigote in the foregut, before moving to the salivary gland (CDC, 2019).

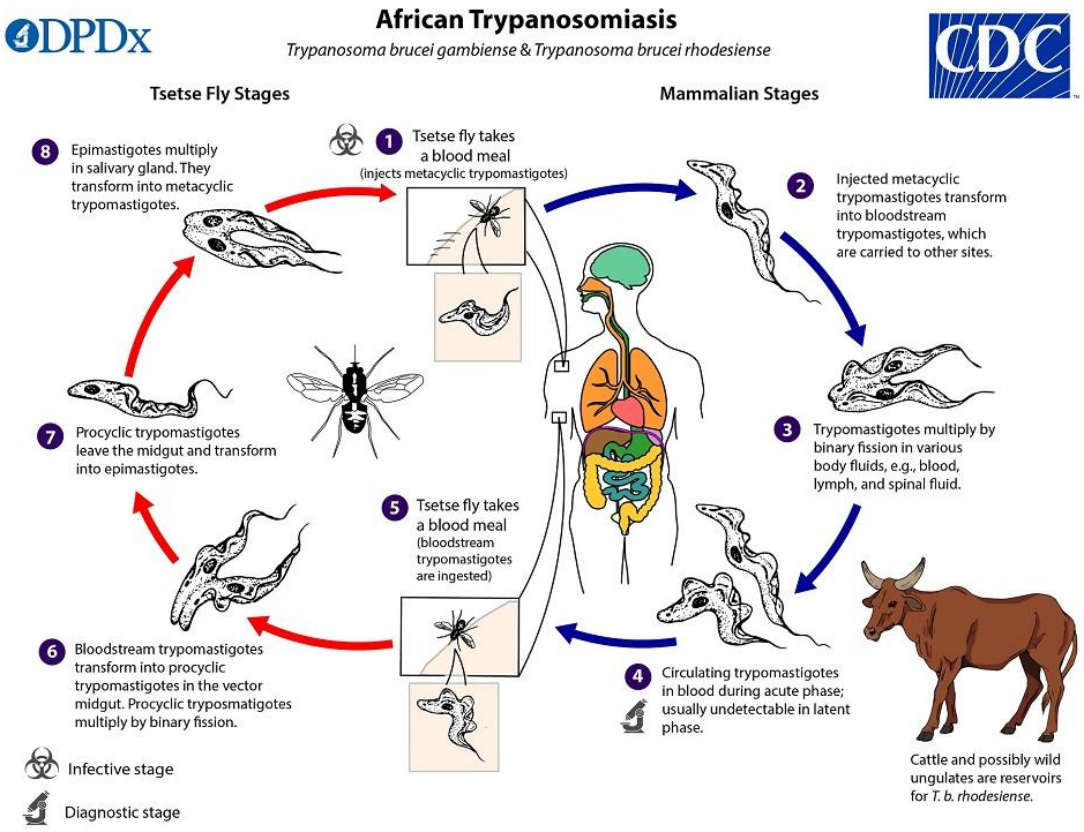

Figure 1.1 Digenetic lifecycle of *T. brucei*, illustrating the transmission cycle between the mammalian host and insect vector. Multiple differentiation events are illustrated here, however, the most promising target to mitigate disease spread is outlined in step 4, where parasites differentiate within the bloodstream to a form adapted to survival within the insect vector (CDC, 2019).

Trypanosomiasis infection progresses through two stages. The first stage occurs when the parasite is present in the blood and is known as the haemolytic stage. During this stage symptoms are rather nonspecific flu-like symptoms such as pyrexia (fever), headaches, joint pain and itching also known as pruritus. As the parasite progresses through the bloodstream and lymphatic system symptoms may include swelling of the lymph nodes. In livestock infection may result in a decline in fertility and weight loss. This first stage can last anywhere from a few weeks to months and if left untreated can develop into the second stage of infection. The second stage of infection occurs when the parasite crosses the blood brain barrier and invades the central nervous system, known as the meningoencephalitic phase. This stage of the disease is fatal if left untreated. It can be characterised by symptoms such as a disruption of the sleep wake

cycle, in which patients may begin to experience extreme tiredness in the daytime and insomnia at night. Further neurological symptoms of this stage include behavioural changes, confusion, and poor coordination. The fatality of these symptoms progress with the infection and can result in paralysis, comas, and irreversible brain damage, and if untreated death (CDC,2019).

The choice of available treatments for HAT depends on the species of parasite and the stage of the infection. For the earliest stages of disease onset (stage 1 infection) pentamidine and suramin were commonly used drugs however NECT (nifurtimox-eflornithine combination therapy) and Fexinidazole have replaced these, with Acoziborole soon to become a first line treatment currently in stage III clinical trials with potential to be a single dose oral cure for both stages (Tarral et al., 2023). These forms of medication aim to eliminate parasites from the bloodstream and prevent progression of the parasite through the blood brain barrier. For a stage two type of infection treatment becomes more difficult, as just as the parasite has done, treatment is required to penetrate the blood brain barrier, this is when the drugs such as melarsoprol would have previously been administered. Melarsoprol is now considered a second line of defence being replaced by the less toxic eflornithine used most commonly in combination with nifurtimox (NECT). These treatments are attached with limitations including the need for intravenous administration, resistance, cost, availability toxicity and potential side effects. Improved diagnostic tools for early detection and further drug development research may address some of the challenges faced (Chappuis et al., 2005).

Treatment of animal African Trypanomiasis is far less studied and developed, treatment strategies consist of chemotherapeutic drugs and vector control. Isometamidium chloride and diminazene aceturate are among the commonly used drugs used for the treatment of AAT. Both drugs are unable to penetrate to blood brain barrier making them ineffective in the management of AAT. The potential emergence of drug resistance, poor quality of drugs and incorrect use of drugs poses significant concern, emphasizing the need for continued research into alternative treatments. Vector control measures are crucial in managing the spread of the disease. Insecticide treated screens and cattle aim

to reduce the tsetse fly populations, in turn limiting the spread of the disease (Venturelli et al., 2022).

1.2. Host temperature varies in response to parasite burden

The fever associated with *T. brucei* is a hallmark of the hosts immune response to parasite burden within the blood. Core body temperature is a highly regulated mechanism, and periods of fever can be used as a defence mechanism to kill not only temperature sensitive bacteria and viruses, but also parasites such as *T. brucei.* The heat shock response is an evolutionarily conserved mechanism, which allows the parasites to survive in these fever conditions. In one of the earliest detailed documentations of Trypanosomiasis, as recorded by Dr Ronald Ross (1910), parasite burden within the bloodstream of a human host was tracked. This study revealed that the number of parasites in the blood, or parasitaemia, exhibited defined peaks and troughs across the time course of infection. Alongside parasite count, host temperature was also measured, revealing that peaks in host temperature occur on the ascending wave of parasitaemia, indicating the immune response against the parasitic infection (Ross & Thomson, 1910).

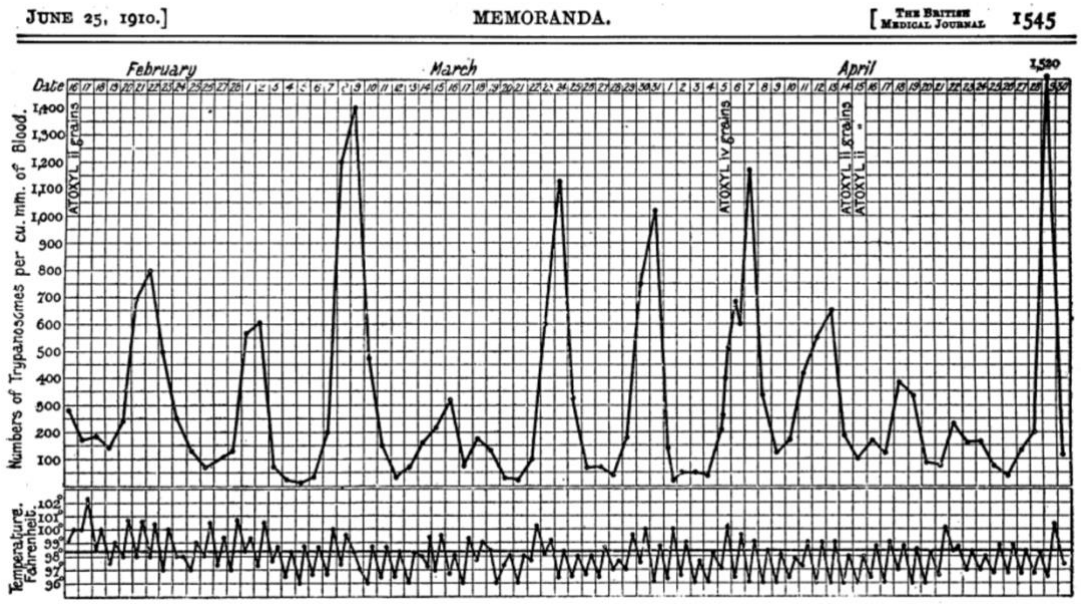

Figure 1.2 Variation in host temperature occurs in response to parasite burden. Peak host temperature corresponds with the ascending wave of parasitaemia, documented by Dr Donald Ross (1910), as one of the earliest indicators that the human body responds

to parasite burden in the same fashion as with bacterial or viral infections (Ross & Thomson, 1910).

1.3. Gene regulation and organisation in trypanosomes is atypical

Trypanosomes exhibit an atypical genome arrangement compared to most eukaryotes. In typical mammalian cells, each gene has its own promoter, allowing for precise transcriptional regulation. In contrast, trypanosomes often use a single promoter to transcribe dozens or even hundreds of genes within a structure known as a *polycistronic transcriptional unit* (PTU). Unlike bacterial operons, the genes within a PTU in trypanosomes are not functionally related and frequently encode proteins with entirely different roles. This lack of functional linkage complicates gene regulation because trypanosomes cannot selectively activate or repress individual genes at the transcriptional level. In mammalian cells, genes are typically composed of exons and introns. After transcription, introns are removed through a process called *cis-splicing*, in which the exons are joined together to form mature mRNA. This process allows for alternative splicing, where multiple protein variants can be produced from a single gene. Mature mRNA contains a 5' methyl cap, untranslated regions (UTRs) flanking the coding sequence, and a 3' poly-A tail, which collectively ensure stability, translation, and export. In trypanosomes, mRNA maturation occurs through a distinct process called *trans-splicing*. Genes are arranged as open reading frames separated by intergenic regions. During transcription by RNA polymerase II, the entire PTU is transcribed into a polycistronic pre-mRNA. This transcript undergoes trans-splicing, where a spliced leader (SL) sequence is added to the 5' end of each individual mRNA. The SL sequence is derived from a capped SL RNA. Concurrently, the 3' end of the pre-mRNA is polyadenylated. This processing produces mature monocistronic mRNAs that resemble those of other eukaryotes but are generated through entirely different mechanisms. Due to the polycistronic nature of transcription, gene expression in trypanosomes cannot be regulated at the level of individual gene transcription. Instead, regulation occurs post-transcriptionally, often through mRNA stability and translation efficiency. mRNA stabilization promotes nuclear export and subsequent

translation, while destabilization leads to degradation. Key mechanisms include the binding of regulatory RNA-binding proteins (RBPs), which either enhance or inhibit translation. Additionally, mRNAs can be sequestered into cytoplasmic granules for storage or degradation, depending on the presence of silencing or aggregating RBPs. This intricate regulatory network allows trypanosomes to adapt to changing environments despite their unconventional transcriptional organisation (Clayton, 2019).

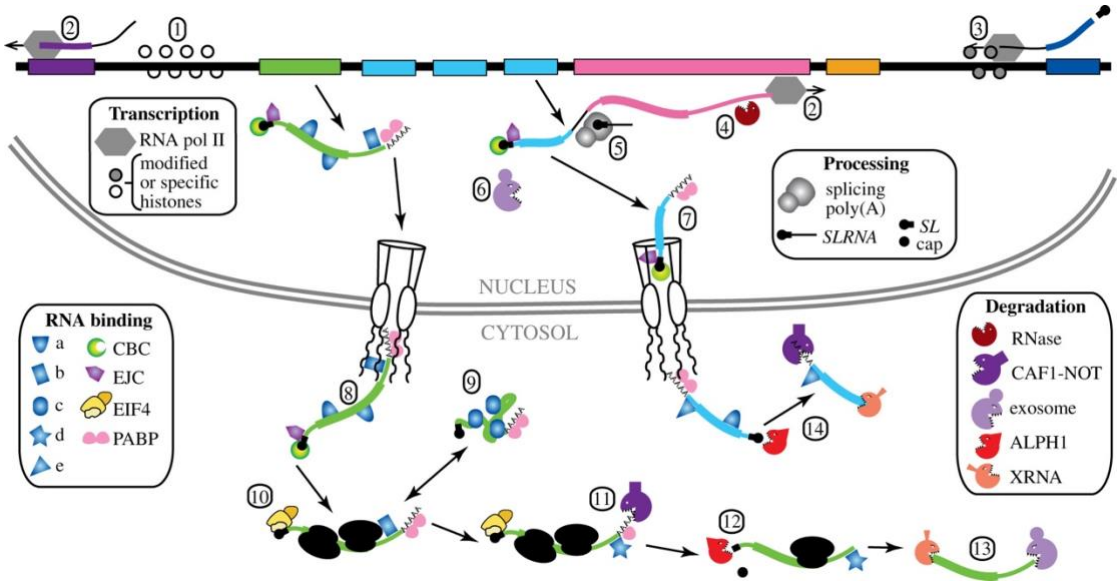

Figure 1.3 Gene expression in kinetoplastids. Schematic representation of transcription and post-transcriptional processing in trypanosomes. RNA polymerase II initiates transcription, producing polycistronic pre-mRNA. The pre-mRNA undergoes trans-splicing, where a spliced leader (SL) RNA adds a 5' cap, and polyadenylation adds a 3' poly-A tail, resulting in mature monocistronic mRNA. The mature mRNA is stabilized by binding proteins and exported from the nucleus to the cytoplasm. In the cytoplasm, RNA-binding proteins regulate translation or sequestration into granules. mRNA degradation occurs when stabilizing proteins are replaced by destabilizing proteins, leading to deadenylation and exonucleolytic decay by the exosome and XRN1 (Clayton, 2019).

1.4. Heat shock response in model eukaryotes

The heat shock stress response is an evolutionarily conserved response employed by many organisms in order to withstand elevations in temperature. Elevations in temperature can be fatal to cells, as they cause protein misfolding and denaturing, disrupting biological pathways. The response is well-studied across yeast and mammals and has revealed a common set of molecular pathways. The response can be characterised by an upregulation in a variety of proteins, termed 'heat shock proteins', and the transcriptional arrest of proteins not vital for survival (commonly, these are proteins required for growth). Put simply the cells enter into a 'survival mode' and prioritise transcription of proteins necessary for survival. A biological state such as this is designed to withstand temperatures exceeding that of a typical human fever. Correspondingly such an extreme modification to cellular processes is not sustainable over long periods of time. While the heat shock response is well characterised in more common and widespread mammalian pathogens, understanding of this survival mechanism is comparatively limited in regard to parasitic protists.

1.5. Phosphorylation of eIF2alpha triggers translational arrest

In the heat shock response, stress is initially sensed through a variety of mechanisms including the accumulation of damaged proteins within the cell. This stress triggers the phosphorylation of eIF2a (eukaryotic initiation factor 2 alpha) at a specific serine residue (serine 51), which initiates a cascade of events within the heat shock response. The phosphorylation of eIF2a results in an inhibition of the eIF2 complex. The eIF2 complex consists of eIF2, GTP and initiator tRNA, it plays a crucial role in initiation for protein synthesis and as a result there is a global reduction in protein synthesis (Kedersha et al., 1999).

1.6. Formation of Stress granules and P-bodies

In eukaryotic cells it is know that heat stress results in the inhibition of translation initiation causing ribosomes to stall on mRNAs. This untranslated mRNA accumulates resulting in the formation of cytoplasmic stress granules. Stress further induces the

relocation of many mRNAs from polysomes to cytoplasmic stress granules. Stress granules provide a vital role in protein regulation within the heat shock response as they allow the cell to prioritize transcription of necessary mRNA for heat shock proteins and a protective role as they have the potential to prevent the degradation of mRNA. Stress granules are able to act as sites of mRNA triage, a process in which the fate of untranslated mRNA is decided. These stress granules contain RNA binding proteins, translation initiation factors, small ribosomal subunits, stress response proteins and enzymes involved in mRNA degradation. The formation of these stress granules is dependent on the phosphorylation of eIF2α at a conserved residue. Stress granules have been shown to interact with processing bodies (P-bodies), which are cytoplasmic granules. Defective mRNAs may be directed by stress granules to P-bodies for degradation, preventing the production of faulty proteins. In a gene regulatory manor stress granules may selectively send mRNAs to P-bodies for degradation this could include mRNAs coding for proteins not immediately needed or mRNAs coding for proteins that could exacerbate stress conditions. Finally, some mRNAs may be stored within stress granules until the stress is resolved at which point, they can be sent to P-bodies to re-initiate translation or be degraded if now longer required, however if the stress persists some mRNAs stored in stress granules may undergo transitions to P-bodies for degradation. P-bodies share some of the components such as exonuclease XRN1, RNA helicase DHH1 and RNA binding proteins SCD6/RAP55/LSM14. Specific to P-bodies is their de-capping enzymes DCP1 and DCP2. RNA binding proteins, translation initiation factors, small ribosomal subunits are specific to stress granules and are not present in P-bodies. Stress granules are involved in translational repression and mRNA stabilisation during stress, containing translation initiation factors and stress response proteins and form specifically in response to cellular stress, whereas P-bodies are primarily involved in mRNA decay and storage, contain protein degradation machinery and are present under normal and stress conditions. As such, P-bodies and Stress granules exhibit not only differential composition, but also manifest with distinct timescales within the lifespan of the cell. Taken together, this suggests involvement in separate pathways and therefore their discrete functionalities within the contexts of housekeeping processes and stress responses (Kramer et al., 2008).

1.7. Upregulation of HSP gene

In mammals, expression of specific genes is either upregulated or downregulated during the heat shock response, and this occurs on the level of transcription. During the response heat shock transcription factors undergo conformational change and translocation to the nucleus, here they bind to heat shock elements (HSEs) which exist in the promoter regions for heat shock genes, resulting in an upregulation of heat shock proteins. Heats shock proteins are chaperone proteins which aid in the refolding of proteins that are misfolded due to heat stress (Alagar Boopathy et al., 2022).

1.8. The HSP70 – HSF1 titration model

HSF1 is one of the key heat shock transcription factors responsible for the upregulation of heat shock proteins such as HSP70. HSF1 is constantly present in the cell allowing for instant response to disruption of proteostasis. HSF1 remains latent in the cells due to its binding with chaperone proteins. HSF1 undergoes a conformational change in response to stress leading to its activation. Once activated HSF1 trimerizes allowing it to become a functional transcription factor and translocate to the nucleus where it binds to HSEs in the promoter regions of heat shock genes. HSF1 recruits RNA Polymerase II, allowing for the formation of a transcription initiation complex, which facilitates the initiation of transcription from these promoter regions. RNA polymerase II is then able to synthesise mRNA transcribed from heat shock genes. Subsequently this transcribed mRNA is translated into heath shock proteins such as HSP70. HSP70 is an essential heat shock protein aiding in refolding misfolded protein, stabilisation and preventing aggregation of denatured proteins. The chaperone titration model suggests that HSF1 is kept inactive in normal conditions due to its binding with HSP70. HSP70 is a limited chaperone protein, once heat stress occurs and the concentration of unfolded protein exceeds the capacity of HSP70, HSP70 is titrated away from HSF1 liberating it and allowing it to become activated and trimerized to induce more HSP70. Once sufficient HSP70 has been produced HSP70 will bind to HSF1 causing it to deactivate, resulting in a negative feedback loop. In summary the activation of HSF1 results in the transcription of more

chaperone proteins including HSP70 allowing for the restoration of proteostasis and subsequently decreasing the activity of HSF1 by allowing it to bind with HSP70 (Masser et al., 2020).

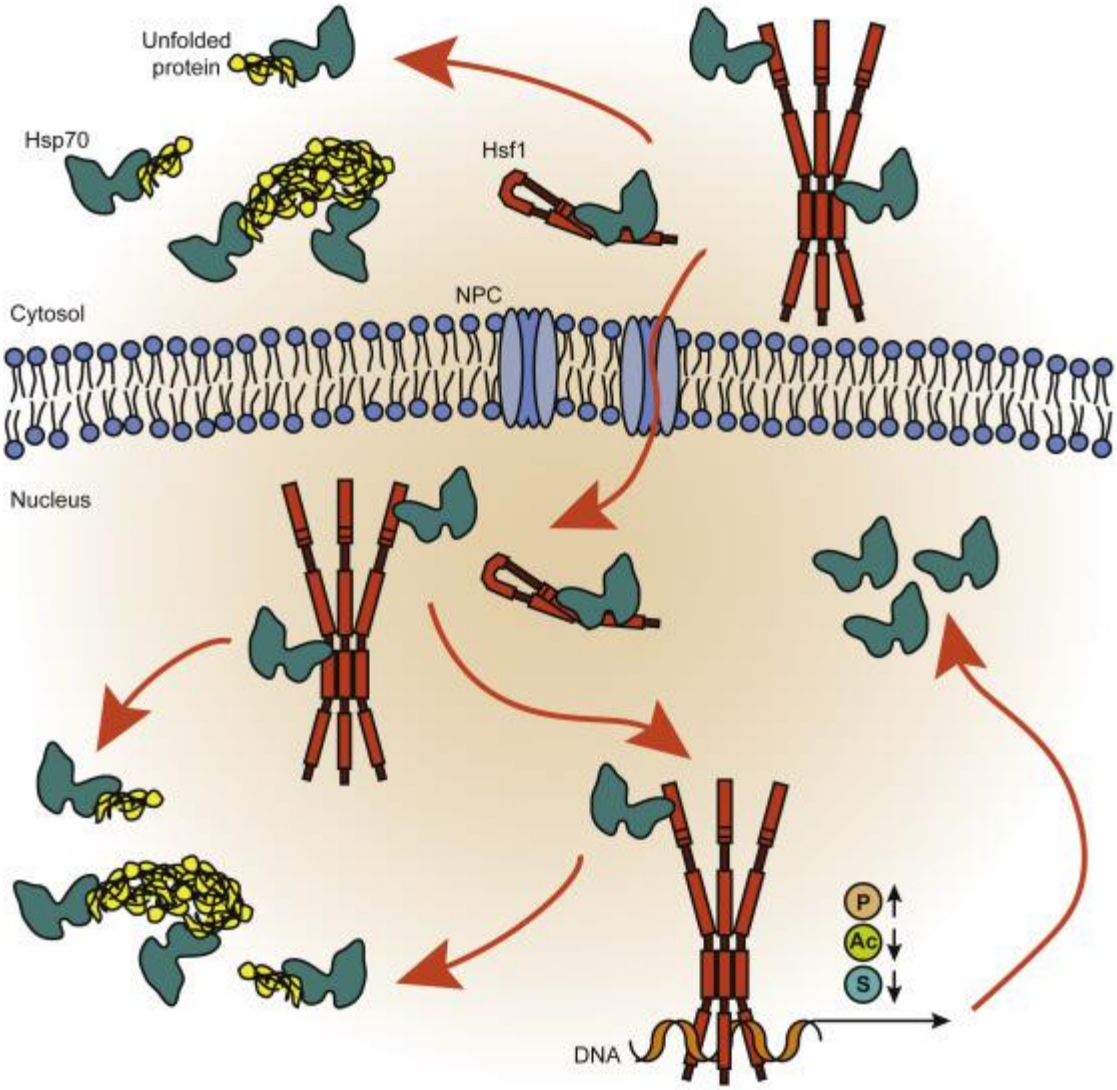

Figure 1.4 HSP70 – HSF1 titration model. Inactive monomers or trimers of HSF1 are bound by HSP70 and reside in the cytosol or the nucleus as a result of active transport through the nuclear-pore complex. Unfolded proteins titrate HSP70 sequestering it away from HSF1 enabling its activation. HSF1 then accumulates in the nucleus resulting in DNA-binding and activation. In order to restore proteostasis post-translational modifications of HSF1 direct the response. Phosphorylation of HSF1 enhances transcription whereas acetylation and SUMOylation represses the transactivation capacity of HSF1 (Masser et al., 2020).

1.9. Heat shock response in *T. brucei*

The heat shock response is employed by *T. brucei* in order to survive the immune response to infection. Once infected with bloodstream form *T. brucei* the mammalian immune response is triggered and elicits a host fever in attempt to kill the parasite. In order to withstand this rise in temperature the trypanosome utilises the heat shock response. The heat shock response has been well studied in procyclic form (PCF), with some studies in bloodstream form *T. brucei* (BSF), but there is little to no research on heat shock response in *T. congolense*.

1.10. PCF *T. brucei* HS response

Characterisation of the heat shock response in PCF *T. brucei* began with the identification and analysis of mRNA transcripts involved. In a response to heat shock (41 °C 1h) there was reduction of up to 50% in the rate of transcription, and a selective block in trans-splicing of tubulin. This suggests that elevations in temperature can disrupt the typical processing of tubulin mRNAs, with tubulin being essential for cytoskeletal structures this has the potential to affect the integrity of the cell. The same study, conducted by Muhic and Boothroyd, found that mRNA transcripts for HSP70 and HSP85 remained steady, if not slightly increased (Muhich & Boothroyd, 1988).

Further studies used ^{35}S methionine labelling to investigate the effects of 60 minutes heat shock at 41 °C and followed the results for up to 5 hours of recovery at 27 °C. Notably the study found a decrease in most newly synthesised polypeptides within the first 30 minutes. It was also discovered that expression of HSP70 and HSP85 remained stable if not increased for up to 5 hours post recovery, suggesting a beneficial role of the proteins during the heat shock response. Most polypeptides recovered to normal levels during the 5 hours they were tracked for, however some remain at a reduced level post the allotted recovery time. The level of polysomes acts as an indicator into a cell's translational activity. In this same study polysome analysis revealed a large decrease in polysomes after 15 and 30 minutes at 41 °C. Taken together, these experiments provide

compelling evidence that in PCF *T. brucei* a temperature of 41 °C triggers a HS response, with characteristics appearing within the first 15 minutes (Kramer et al., 2008).

Due to the polycistronic nature of gene expression in *T. brucei* the effects of heat shock in *T. brucei* must occur post transcription at the level of mRNA or protein. mRNA for unnecessary proteins is made less stable, whereas mRNA for HSPs is made more stable in order to be translated despite a global translational arrest. HSPs are central to the survival of cells and as a result cells undertake adaptions in gene expression to favour the synthesis of HSPs overcoming the general suppression of gene expression. In mammals, fluorescence microscopy has given insight into the spatio-temporal resolution of this gene expression phenomena.

Research has shown that trans-splicing can be disrupted by heat shock and therefore prevent the maturing of mRNA and progression to translation. Disruption of trans-splicing causes an accumulation of polycistronic transcripts. For example, the trans-splicing of tubulin is significantly disrupted by heat shock when heated at 41.5 °C for 2 hours and more significantly at 42.5 °C as reflected by the amount of polycistronic tubulin transcripts. In contrast the trans-splicing of HSP70 and HSP83 appears unaffected and furthermore promoted due to the increase in HSP70 and HSP83 mRNA following a 2-hour treatment at 41.5 °C, with no detectable polycistronic HSP70 or HSP83 transcripts present. At 42.5 °C HSP70 and HSP83 mRNA was elevated however slightly less, furthermore few larger transcripts were detected, suggesting a slight disruption of trans-splicing. The mechanism by which these HSPs avoid trans-splicing disruption is unknown, however it has been theorised to be a result of a region within HSP pre-mRNAs themselves or possibly utilisation of altered splicing machinery. What is known is that the 5'ends of HSP mRNA produced under normal and heat shock conditions are indistinguishable meaning splice-leader addition occurs, and this suggests that the combat mechanism of trans-splicing disruption allows for cap-dependent translation (Muhich & Boothroyd, 1988; Muhich & Boothroyd, 1989).

1.11. Heat shock-induced stress granule formation

It was discovered that heat shock in trypanosomes results in the formation of stress granules. Kramer and colleagues (2008) carried out heat shock on PCF trypanosomes at 41 °C normally grown at 27 °C. Research revealed that the heat shock causes a reduction in polysomes and a decrease in mRNA. They found the decrease in polysomes occurred much faster than the decrease in mRNA, unexplainable by a block in synthesis this suggests an increase in non-polysome associated mRNA. To determine the fate of mRNA released from polysomes researchers used enhanced yellow fluorescent (eYFP) fusion proteins of known homologues of stress granule components. Visualisation prior to heat shock revealed PABP1 and PABP2 appeared predominantly in the cytoplasm, eIF2A, eIF3B, eIF4E3 and eIF4E4 appeared mainly in the cytoplasm with lower concentrations in the nucleus and eIF4E1 and eIF4E2 were equally distributed between both the nucleus and cytoplasm. Following a 1-hour incubation at 41°C all previously mentioned eYFP tagged homologues were found concentrated into distinct cytoplasmic foci of different size and shape. Heat shock granules formed containing PABP1, PABP2, eIF3B, eLF4E1, eLF4E2, eIF4E3 and eIF2A (Kramer et al., 2008). It was discovered in later study that PABP1 and PABP2 do not co-localise. PABP1 co-localised with proteins present in heat shock granules, whereas PABP2 localised with P-body marker XRNA (Kramer et al., 2013). Granule formation occurred after just 30 minutes of heat shock and increased up until 120 minutes of heat shock, while the number of P-bodies containing DHH1, XRNA and SCD6 increased.

Notably, inhibition of mRNA synthesis using actinomycin D did not prevent stress granule formation, indicating newly synthesised mRNA is not required for granule formation. Granule formation was shown to be fully reversible with granules disappearing 5-6 hours upon returning to 27 °C culture. Further tests within the study used Puromycin to dissociate the polysome and this dissociation was insufficient for granule formation. In another condition Cycloheximide was used to stabilise the polysome and they found upon heat shock stress granules could not form. This gives evidence to the requirement of polysome dissociation in the formation of stress granules.

Although heat shock appears to be highly conserved across typical eukaryotes and trypanosomes Kramer et al. showed that the formation of heat shock stress granules is independent of the phosphorylation of eIF2α at the homolog residue in trypanosomes. They showed despite mutation of this homolog to a non-phosphorylation site the heat shock response was unaffected, stress granules formed, polysomes decreased and cells were able to survive increased temperatures. This suggests trypanosomes utilise a novel pathway for triggering the heat shock response (Kramer et al., 2008).

1.12. A summarised timeline of events of the HS response when triggered at 41 °C for 2 hours

0 minutes: HS begins

Trypanosomes are exposed to elevated temperature triggering the heat shock response.

0-5 minutes: Immediate response

Stress responsive signalling pathways are triggered.

5-15 minutes: Transcriptional response

HSPs become upregulated and transcription becomes activated at stress-responsive gene promoters.

15-30 minutes: Post transcriptional regulation and formation of stress granules

Specific mRNAs encoding for stress-responsive proteins are stabilised, mediated by RNA binding proteins. Translation of stress-responsive mRNAs is enhanced, and translation of non-essential mRNAs is inhibited.

Untranslated and nonessential mRNA is aggregated into stress granules containing stress-responsive proteins.

30-60 minutes: Protein folding and stabilisation

Abundant newly synthesised HSPs and activated chaperones aid in protein refolding preventing aggregation.

60-120 minutes: Adaption and maintenance of response

The cell must adjust its metabolic pathways to cope with increased energy demands and sustain expression of stress-responsive genes for survival under prolonged stress.

120-240 minutes: HS subsides

If temperature returns to normal the cell enters a resolution phase gradually returning to homeostasis. Stress-responsive genes are downregulated, stress granules begin to disassemble, and the global translational arrest is lifted.

>240 minutes: Recovery

Cells attempt to repair damage incurred during heat shock including protein misfolding and DNA damage. Depending on the severity of the HS cells will begin to proliferate and return to their typical growth rate.

1.13. BSF *T. brucei* HS response

Most of the early work into the trypanosome heat shock response used the procyclic form of the parasite, which resides in the tsetse fly host. The tsetse fly resides in sub-Saharan Africa and is exposed to a variety of temperatures ranging from 21-34 °C. Their internal temperature is regulated through moving between light and shade throughout the course of the day. This method of temperature regulation as well as the range in internal temperature differs from mammals. Interestingly, research has shown a PCF cell line cultured at 27 °C put into a 37 °C incubator the cells continue to grow for up to 3-4 days, surviving a 10 °C temperature shift. If the temperature of BSF culture was to be increased by 10 °C they would die. It appears the procyclic form of the parasite is much more thermotolerant than the bloodstream form, but only up until the same temperature (Droll et al., 2013). As a result, it can be argued that the mechanisms of heat shock will differ between the procyclic form and bloodstream form of the parasite, or that in the blood stream form the heat shock response is already triggered to some extent.

Ooi et al. have looked at the effects of heat shock on the cell viability of the BSF of the parasite, that are infective in mammals. They used a temperature of 41 °C to induce heat shock. Physiologically this temperature is too hot as it could kill a human within hours, causing irreversible brain damage in 3 hours and death within 8 hours. Whilst some may argue that 41 °C is an unrealistically high temperature, the heat shock treatment used in analysis was up to 2 hours and a human could survive this, research has shown rectal

temperatures of African cows have reached temperatures >41 °C and it is an experimentally tractable temperature to use (Bianca, 1963). Furthermore, 41 °C is the temperature used across previous heat shock investigations adding the element of replicability to the research. Realistically it is more likely that heat shock will occur at a lower temperature but take longer time, so the experiment would have triggered a severe heat shock. The researchers found if the cells were incubated for 30 minutes at 41 °C a slight reduction in motility can be observed. 1 hour of incubation at 41 °C led to a greater reduction in motility with 22% ($p = 0.49$) of cells losing complete motility. The reduction in motility became significant when after 2 hours of incubation at 41 °C 74% ($p = 0.04$) cells had stopped moving. After 4 hours at 41 °C there were no motile cells remaining. The recovery of the surviving heat shocked cells was monitored over 72 hours and plotted on a cumulative growth curve. This revealed cells heat shocked for 0.5 hours at 41 °C grew almost indistinguishably from untreated cells. Cells that were heat shocked for 1 hour at 41 °C experienced an initial stall, followed by a lag in growth lasting up to 24 hours post treatment before recovering to a normal growth rate. Cells that were heat shocked for 2 hours at 41 °C continued to die for up to 24 hours and did not recover to a normal growth rate for up to 72 hours post treatment (Ooi et al., 2020).

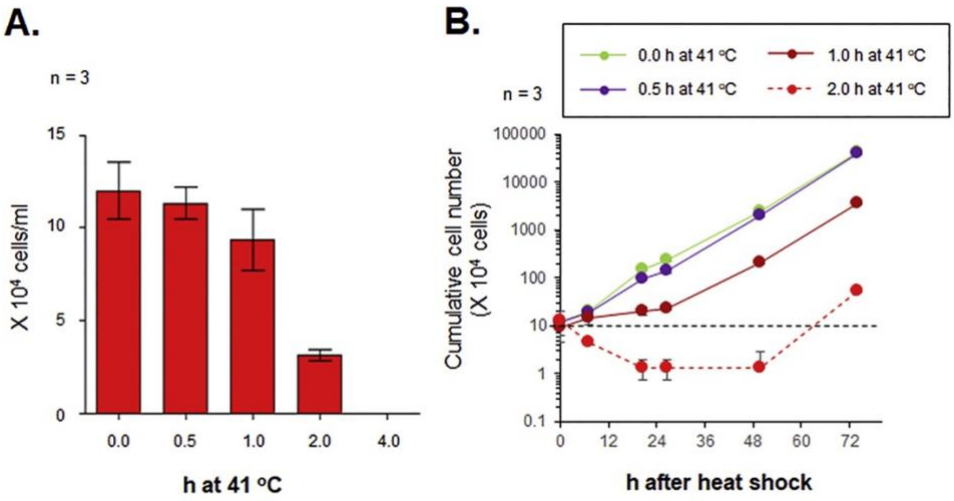

Figure 1.5 The effects of heat shock on BSF cell viability and growth. (A) Count of viable cells after heat shock at 41°C for 0-, 0.5- ,1- ,2-, and 4- hours. (B) Cumulative growth curve of cells monitored for 72 hours after 0-, 0.5-, 1- and 2- hours of heat shock.

They determined that 1 hour of heat shock was a 'sweet spot' as it was interpreted that the data showed almost no cell death had occurred, and yet the cells experienced a lag in growth showing a need for recovery after stress, meaning a response to the heat was triggered just not quite strong enough to kill the cells (Ooi et al., 2020).

1.14. The RNA binding protein ZC3H11 is master regulator of HSR in *T. brucei*

Regulation of the heat shock response occurs primarily post transcriptionally in trypanosomes through mRNA binding proteins. The RNA binding protein ZC3H11 is a master regulator of the HS response that preferentially binds to AU-rich elements in HSP mRNAs stabilising them.

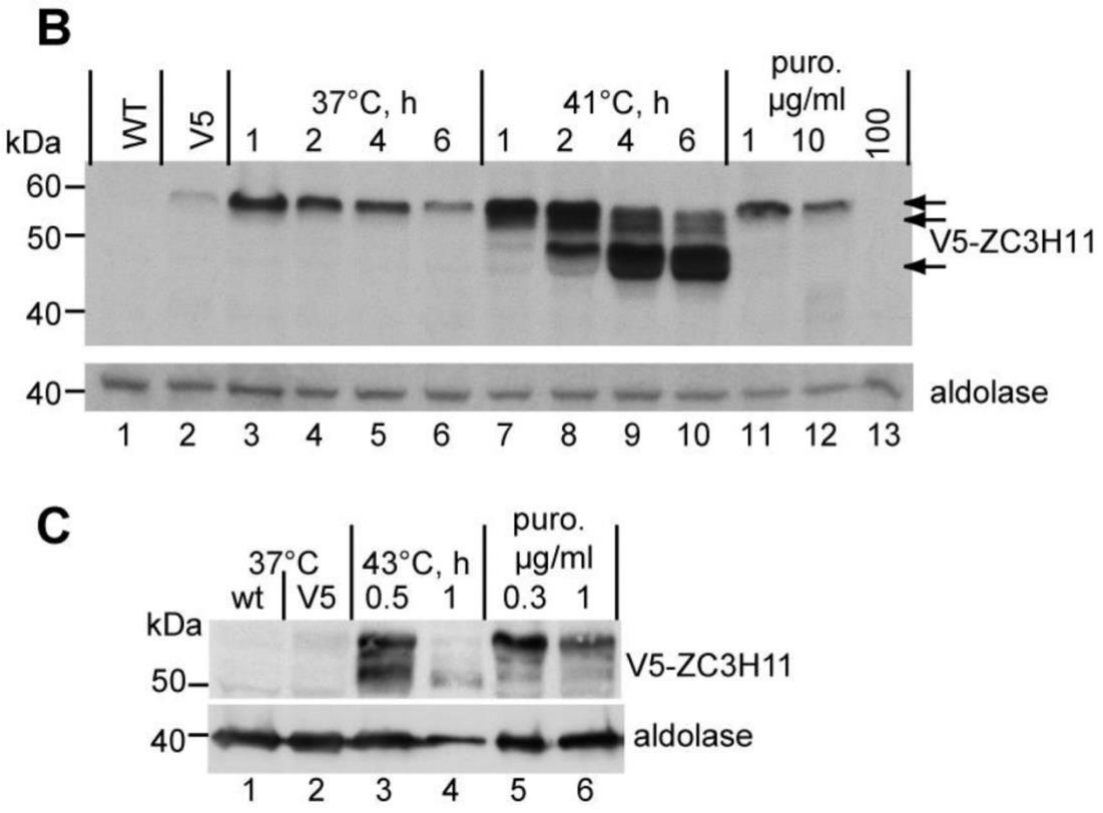

Figure 1.6 Effects of HS on abundance of ZC3H11 using expression of in-situ tagged V5-ZC3H11. Western blot gives insight to (B) PCF *T. brucei* under different conditions. Temperature of incubation is indicated above each lane along with time in hours.

Puromycin treatment was for 1 hour. (C) BSF *T. brucei* following the same details as (C) (Droll et al., 2013).

Through western blotting ZC3H11 was detectable in both the PCF grown at its typical culture temperature of 27 °C (Figure 1.6, B, Lane 1) and BSF when grown at its typical culture temperature of 37 °C (Figure 1.6, C, Lane 1). In PCF the amount of detectable ZC3H11 largely increased after HS at 37 °C however the effects were transient (Figure 1.6, B, Lanes 3-6), at 41 °C the effects were stronger and longer lasting, causing a large increase that was sustained across the 6 hours of incubation (Figure 1.6, B, Lanes, 7-10). It is evident longer incubation periods at this higher temperature resulted in a reduction in cell viability, as the bands begin to migrate suggesting degradation. In BSF it is apparent HS to 43 °C increases the amount of ZCH311 detected after 0.5 hours (Figure 1.6, C, Lane 3), however it is apparent before 1 hour of incubation the cells began to die (Figure 1.6, C, Lane 4). In both forms of the parasite stress induced by puromycin increased levels of ZC3H11 (Figure 1.6, B, Lanes 11-13 and Figure 1.6, C, Lanes 5,6).

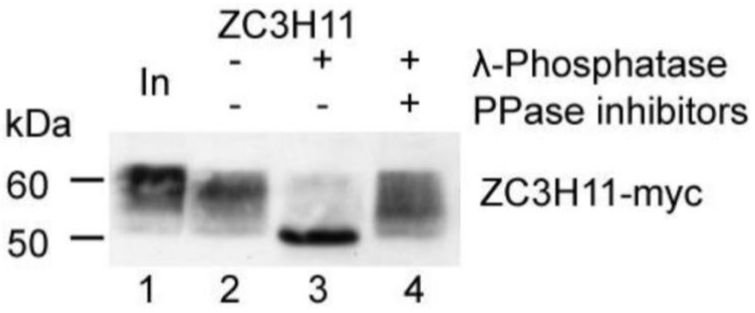

Figure 1.7 ZC3H11 is phosphorylated. Cell extracts incubated with λ-phosphatase (Lanes 2,4) in the presence (Lane 4) or absence (Lane 3) phosphatase inhibitors, effects were detected by Western blot, (Droll et al., 2013).

In attempts to determine the mechanisms by which ZC3H11 expression increases, cell lysates were incubated with λ-phosphatase prior to electrophoresis. It can be seen that the addition of this λ-phosphatase results in a collapse of the band (Figure 1.7, Lane 3) when compared with the control. This original banding pattern was restored by the addition of phosphatase inhibitors (Figure 1.7, Lane 4), suggesting the collapse was due to a lack of phosphorylation. ZC3H11 has shown to be essential in bloodstream forms

and necessary for recovery in procyclic forms of the parasite, very little is currently published on recovery of BSF to heat shock.

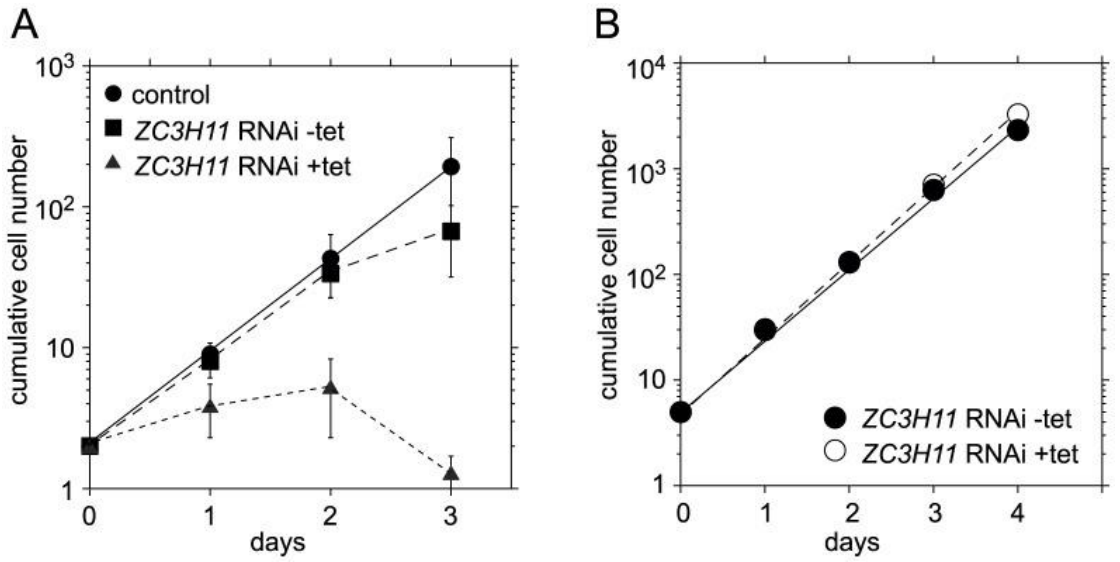

Figure 1.8 ZC3H11 depletion is detrimental to BSF but not PCF. Inducible RNAi of ZC3H11 was used to show effect on growth in BSF (A) and PCF (B) *T. brucei* (Droll et al., 2013).

Tetracycline-inducible RNAi of ZC3H11 in *T. brucei* has shown that depletion of ZC3H11 left PCF unaffected at their normal growth temperature of 28 °C. Contrastingly, induced RNAi of ZC3H11 in BSF cells resulted in death at their typical growth temperature of 37 °C.

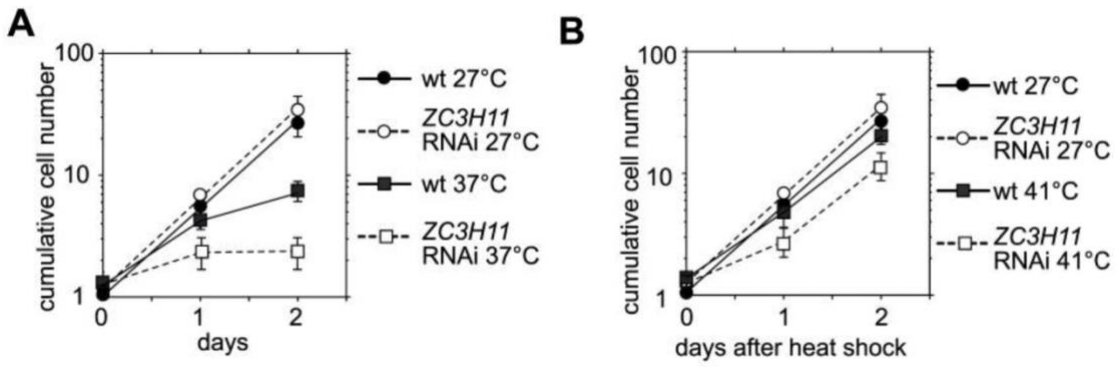

Figure 1.9 ZC3H11 is required for survival and recovery of HS in PCF. Inducible RNAi of ZC3H11 was used to show effect on survival in PCF under normal and elevated culture

temperatures (A) and recovery post 1 hour heat shock at 41°C compared with a control kept at (B) (Droll et al., 2013).

Wildtype PCF cells grown above their typical culture temperature at 37 °C exhibited growth arrest between days 3-4, compared with PCF depleted of ZC3H11, which exhibited a fatal phenotype manifesting at just 2-3 days post RNAi induction (Figure 1.9, A). This suggests ZC3H11 is important in the survival of PCF at high temperatures. Incubation at 41 °C for 1 hour revealed recovery of cells with induced RNAi for ZC3H11 was severely impaired when compared with the recovery of wild type cells (Figure 1.9, B). This highlights the importance of ZC3H11 in the recovery of PCF cells after exposure to elevated temperature. The study concluded ZC3H11 was necessary for retention and stabilisation of HSP chaperone protein mRNAs. The research also concluded the necessity for ZC3H11 in the blood stream form of the parasite even without heat shock. It was found that for ZC3H11 to act as a stabiliser for HSP mRNA it requires additional proteins that form a complex.

Tandem affinity purification-tagging was used in PCF trypanosomes to identify proteins interacting with ZC3H11. Mass spectrometry analysis revealed MKT1, LSM12 and PBP1 as the proteins associated with ZC3H11 to have the highest coverage. Co-immunoprecipitation using tagged proteins was used to confirm these interactions. Results from the study proposed that the binding of ZC3H11 with other proteins was necessary for it to function in stabilising HSP mRNA.

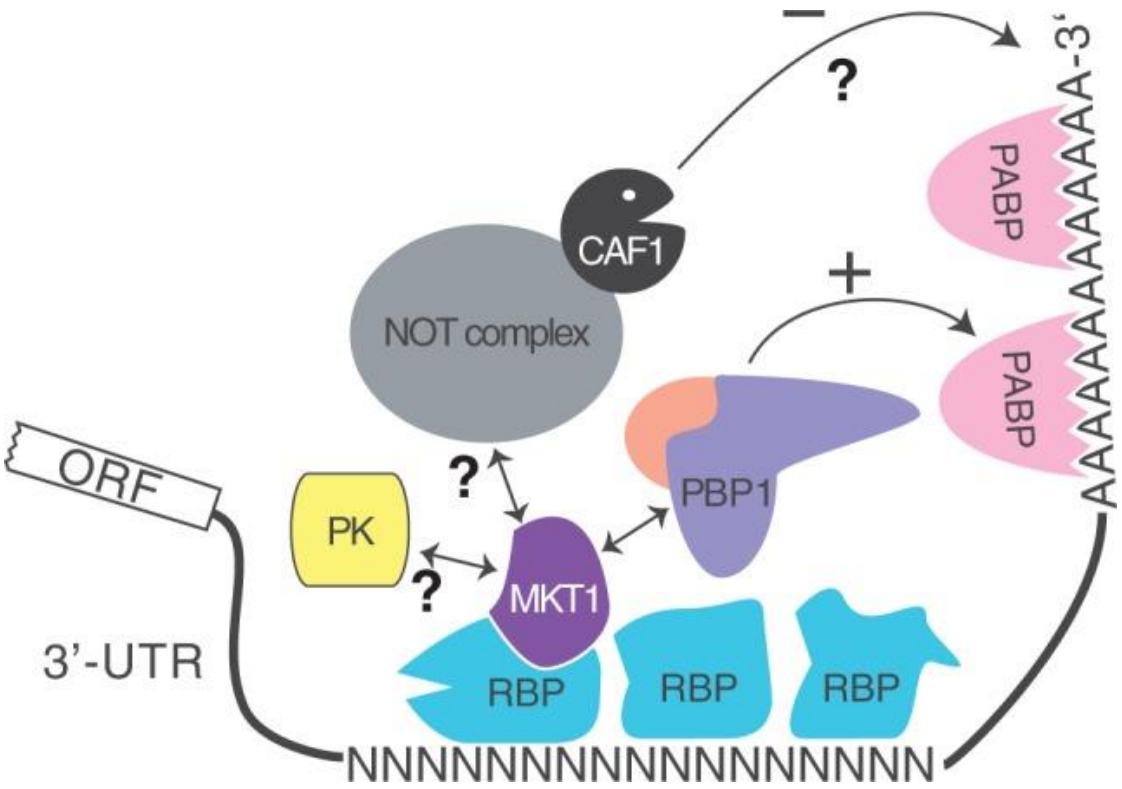

Figure 1.10 Proposed model of ZC3H11 stabilising mRNA. N terminus of ZC3H11 is bound to UAUU elements on mRNA, C terminus interacts with PBP1 and MKT1 recruiting PABP (Singh et al., 2014).

ZC3H11 is a zinc finger RNA binding protein, it was suggested whilst the N-terminus zinc finger is bound to RNA the C-terminus zinc finger interacts with PBP1 and MTK1. This interaction results in the sequestering of further proteins LSM12 and PABP1/2, which in turn interacts with the poly(A) tail and/or eIF4G (Singh et al., 2014).

To further expand upon the knowledge of the mechanisms of heat shock within trypanosomes researchers carried out a SILAC-based quantitation of protein and phosphorylation site abundance changes after one hour of HS at 41 °C. It is evident from this research supported by previous work (Figure 1.7) that phosphorylation events are a determining factor in the regulation of Z3H11 and likely other proteins responsible for thermotolerance. The research found that certain proteins may be responsible for stabilisation of ZC3H11 in order for phosphorylation to occur, namely the protein kinase CK1.2. RNAi of CK1.2 has been shown to reduce phosphorylation of ZC3H11 irrespective of temperature, suggesting a role in its phosphorylation. The Phosphoproteomic study

found CK1.2 to be phosphorylated during HS at residues S19 and S21, also ZC3H11 to be phosphorylated during heat shock at sites S23, S26 and S279. None of these sites found to be phosphorylated in ZC3H11 appear in the recognition motif of CK2.1. This suggests phosphorylation of ZC3H11 by CK2.1 may not be direct (Ooi et al., 2020).

1.15. Changes in early heat shock are dominated by phosphorylation

The overall aims of the SILAC based study were to determine the role of phosphorylation on RNA binding sites in the co-ordination of the heat shock response, the Phosphoproteomic work was carried out on heat shocked BSF trypanosomes. 193 sites of phosphorylation on 148 proteins were found to change in abundance, compared with only 20 heat shock responsive proteins to change in abundance after the 1 hour of heat shock at 41 °C. This suggests that the changes in phosphorylation sites occur much more rapidly after heat shock than the changes in protein abundance, which is to be expected due to the extensive need for post transcriptional modification in the heat shock response. Many of the expected proteins and phosphorylation sites were shown to change in abundance, with the largest increase in phosphorylation site abundance occurring on DHH1. Phosphorylation of Poly(A) binding protein 2 (PABP2) was shown to significantly increase after heat shock unlike phosphorylation of Poly(A) binding protein 1 (PABP1) which was unexpected. However, research has shown the two Poly(A) binding proteins do not co-localise during heat shock. PABP2 co-localised with DHH1 a protein found in P-bodies theorised to be involved in mRNA degradation, whereas PABP1 was found to co-localise with proteins found in heat shock granules theorised to be involved in mRNA storage (Kramer et al., 2013). As a result, it is possible that phosphorylation of PABP2 occurs at a later stage. Furthermore, changes of phosphorylation sites on heat shock proteins 83, 84 and 110 showed no significance and there was no increase in their protein abundance. It is also possible some of these expected changes would occur later in the heat shock response. Effects of heat shock have been shown to occur at later timepoints, this experiment like many others have only looked in detail at events occurring straight after heat shock. Further in-depth research into later timepoints

would provide better insight into a timeline of events and the signalling pathways involved (Ooi et al., 2020).

1.16. Heat shock response in *T. congolense*

Very little experimental work has been carried out on *T. congolense* let alone heat shock specific experiments. IL3000 is the most commonly used and currently sequenced strain of *T. congolense*. This particular strain was originally isolated from bovine in 1966. Until recent advancements, genetic manipulation proved awkward and as a result there is currently a lack of investigation into the infection and survival mechanisms of *T. congolense* (Awuah-Mensah et al., 2021).

Arguably *T. congolense* is a close relative of *T. brucei* they have similar host range and biology, and even co-infect in the same host exposing them to similar evolutionary pressures. This suggests they may have a similar heat shock response mechanism however the evidence is lacking.

Bioinformatic analysis suggests conservation of proteins and phosphorylation across *T. brucei* and *T. congolense*. Six proteins known to have a role in heat shock in PCF *T. brucei* were chosen and homologues in *T. congolense* were analytically compared. The analysis found a 98% conservation across proteins and an 85% conservation across phosphorylation sites. Although these proteins play a role in the PCF *T. brucei* HS response their role in BSF *T. congolense* is not yet known (Aelmans, 2022).

Initial differences in response to temperature are evident in culture temperature. IL3000 *T. congolense* is cultured at 34 °C which is 3 °C lower than 2T1 *T. brucei* strains. Further investigation shows that IL3000 *T. congolense* cannot survive in 37 °C culture, experiencing rapid population decline after just 4 days and being completely eradicated by 7 days. Furthermore, the contents of culture media differ as 2T1 *T. brucei* grows in 10% FBS and IL3000 and TcoSM cells are grown in 15% goat sera (Awuah-Mensah et al., 2021). These differences are unexpected, both BSF parasites co-infect in the same host,

therefore theoretically they should grow at the same temperature and in the same media. It may be argued this is a mutation which has occurred after such long lab culture and may have altered the heat shock response pathway in which case other strains with more recent animal passage should be tested.

1.17. Project aims

The aim of this project is to further characterise the HS response in *T. congolense*, the major cause of AAT, about which very little is currently known. The heat shock response is used as a virulence factor to protect the parasite, enabling survival, and evading the immune response. Research into pathways such as the heat shock response provide a better understanding into the parasites survival mechanisms and has the potential to lead to discovery of novel drug targets.

The first specific aim is to profile thermal tolerance in *T. brucei* & *T. congolense* using and developing on what is currently known. Different severities of HS will be triggered across the 2 different species using different temperatures and durations of HS, generated by a heated water bath. These will be profiled looking at recovery after HS using growth curves and flow cytometry to give insight into the goings on in each cell type. Previous work has demonstrated a G2/M cell cycle arrest occurring in BSF *T. brucei* and BSF *T. congolense* after 1 hour of HS at 41 °C (Aelmans, 2022). Repetition will be used to confirm this as well as testing other durations of HS. This will enable visualisation of the cell cycle distribution across the population at the time of a growth arrest. It has not yet been determined if a G2/M cell cycle arrest occurs in PCF *T. brucei* so this will also be determined. This will give insight into the cause of the cell cycle arrest depending on whether it is seen in both life stages of the parasite.

The next aim is to further characterise the HS response at the molecular level. Previous work identified homologs of 5 conserved HS proteins across *T. brucei* and *T. congolense*. Genetic manipulation was used to begin to fluorescently tag these proteins the same procedure will be carried out to tag the remaining proteins (Aelmans, 2022). The increase in abundance of P-bodies and HS granules after heat shock will be followed by immunofluorescence microscopy. Furthermore, the this will provide insight of specific

protein proximity before and after heat shock. Finally, the translational arrest and alteration mRNA abundance in *T. congolense* upon HS will be confirmed, and HSPs that are up regulated will be identified using qPCR.

2. Materials and Methods

2.1. Materials

2.1.1. Cell lines

T. brucei 2T1 BSF, *T. brucei* 427 PCF (Alsford et al., 2005) and *T. congolense* IL3000 TcoSM (Awuah- Mensah et al., 2021) were the cell lines used for all experiments.

2.1.2. Plasmids

Plasmids pEnNmSt0-N, pEnNY0 and pSIS-HHsfG (Wickstead et al., 2010) were used for N-terminal and C-terminal tagging of proteins in both *T. brucei* and *T. congolense.* Vector maps of pEnNY0 and pSIS-HHsfG are shown in Appendix 3 and 4 respectively.

Table 1 Plasmid backbones and inserts used for generation of fusion proteins

Backbone	Tagged Protein	Species	Inserts	Generated Plasmid
pEnNmSt0-N	mst-DHH1	BSF *T. brucei* (2T1)	MA12 (ORF), MA34 (5'UTR)	pMA1
pEnNmSt0-N	mst-DHH1	BSF *T. congolense* (IL3000)	MA56 (ORF), MA78 (5'UTR)	pMA2
pEnNYo	eYFP-ZC3H11	BSF *T. brucei* (2T1)	MA910 (ORF), MA1112 (5'UTR)	pMA3

pEnNYo	eYFP-ZC3H11	BSF *T. congolense* (IL3000)	MA1314 (ORF), MA1516 (5'UTR)	pMA4
pEnNYo	eYFP-XRNA	BSF *T. brucei* (2T1)	MA1718 (ORF), MA1920 (5'UTR)	pMA5
pEnNYo	eYFP-XRNA	BSF *T. congolense* (IL3000)	MA2122 (ORF), MA2324 (5'UTR)	pMA6
pSIS-HHsfG	HSP100-sfGFP	BSF *T. brucei* (2T1)	MA2526 (ORF), MA2728 (3'UTR)	pMA7
pSIS-HHsfG	HSP100-sfGFP	BSF *T. congolense* (IL3000)	MA2930 (ORF), MA3132 (3'UTR)	pMA8
pSIS-HHsfG	PABP1-sfGFP	BSF *T. brucei* (2T1)	MA3334 (ORF), MA3536 (3'UTR)	pMA9
pSIS-HHsfG	PABP1-sfGFP	BSF *T. congolense* (IL3000)	MA3738 (ORF), MA3940 (3'UTR)	pMA10

2.2. Methods

2.2.1. *T. brucei* (BSF) cell culture

T. brucei (BSF) 2T1 cells were cultured at 37 °C with 5% CO_2, 100% humidity. Cells were cultured in 5 ml of HMI-11 media (Hirumi & Hirumi, 1989), and maintained in a logarithmic growth phase. Five L of HMI11-T media consists of 1 pack of HMI-9 powder (Invitrogen) to which 10 g of sodium bicarbonate (Sigma) is added, followed by 500 ml of Fetal Bovine Serum (Biosera) and 4.4 L of double-distilled water. The pH is adjusted to 7.3 with NaOH, before the addition of 50 ml of L-glutamine (Labtech) and 50 ml of Penicillin-Streptomycin (100×, Labtech). This is then filtered through a 0.2 μm filter under sterile conditions and stored in 500 ml sterile bottles in the dark at 4 °C.

2.2.2. *T. brucei* (PCF) cell culture

T. brucei (PCF) 427 cells were cultured at 27 °C. Cells were cultured in 5 ml of SDM79 media and maintained in a logarithmic growth phase. 1 L of SDM79 media contains 25.48 g of SDM79 powder (Invitrogen) to which 2 g of sodium bicarbonate (Sigma) was added, followed by 0.75 ml of hemin (Sigma) and 150 ml of Fetal Bovine Serum (Biosera). The pH is adjusted to 7.3 with NaOH, before the addition of 10 ml of L-glutamine (Labtech) and 10ml of Penicillin-Streptomycin (100×, Labtech). This is then filtered through a 0.2 μm filter under sterile conditions and stored in 500 ml sterile bottles in the dark at 4 °C.

2.2.3. *T. congolense* cell culture

T. congolense cells were cultured at 34 °C with 5% CO_2, 100% humidity and maintained in a logarithmic growth phase. Cells were grown in TcBSF-1 (Coustou et al., 2010). To make 850 ml of the media the components in Table 2 were combined, filtered through a 0.2 μm filter and stored as 2 × 425 ml in sterile 500ml glass bottles. Prior to use 42.5 ml of media was combined with 7.5 ml of Goat serum (Gibco), the pH was adjusted to 7.3 and finally the 50 ml of complete media was filtered through a 0.2 μm filter into a sterile 50 ml falcon, in a sterile environment.

Table 2 *T. congolense* media components

Component	**Amount in 850 ml media**
MEM powder (Sigma)	9.6 g
Sodium Bicarbonate (Sigma)	2.2 g
HEPES (Melford)	5.96 g
Glucose (Duschefa)	1.10 g
Sodium Pyruvate (Sigma)	110 mg
Adenosine (Sigma)	5.3 mg
Hypoxanthine (100 mM)*	1 ml

Thymidine (Sigma)	4.84 mg
Barthocuproinedisuplonic acid (Sigma)	11.3 mg
2-mercaptoethanol (Sigma) (14.3 M)	14 µl
L- glutamine (Labtech) (100×)	10 ml
Penicillin Streptomycin (Labetch) (100×)	5 ml

* Hypoxanthine stock -1.36g in 100mL of 0.1M NaOH (0.4g/ 100 mL), warm to dissolve. Aliquot and store at -20 °C.

2.2.4. Generation of cell lines

Utilising constructs designed by Aelmans (2022), presented in Table 1, *T. brucei* and *T. congolense* BSF parasites were engineered to express fusion proteins for eYFP-XRNA, HSP100-sfGFP and PABP1-sfGFP, cloning process shown in Figure 2.1.

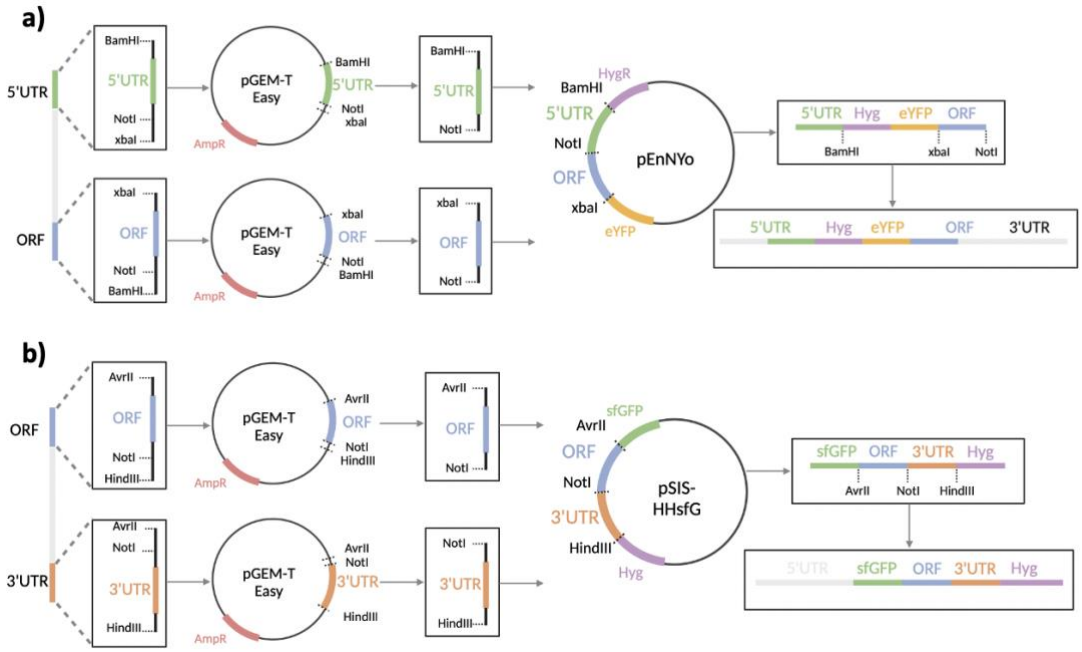

Figure 2.1 Cloning Strategy. Sections of the ORF and either the 5'UTR (a) or 3'UTR (b) of the selected gene are amplified with PCR and inserted into the initial vector (pGEM-T Easy). Restriction enzymes cut sites are incorporated into the PCR primers flanking the inserts. Once replicated, these inserts are digested out of these initial vectors and are ligated one by one into the final vector. pEnNYo was used for N-terminal tagging **(a)** and pSIS-HHsfG for C-terminal tagging **(b)**. The final construct is then linearised and

incorporated into the trypanosome genome through homologous recombination, ensuring the integration of the drug resistance cassette and fluorescent protein sequence.

Figure 2.1 shows a simplified diagram of the cloning strategy. Expanding on this explanation of cloning the pGEM-T Easy vector serves as a back bone for ligation with the amplified inserts containing a Ampicillin resistance cassette (AmpR) in high-efficiency *Escherichia coli*. These bacterial cultures are mini prepped, and the sequential DNA is sequenced to ensure no mutations have occurred. These inserts were then digested out of pGEM-T Easy and ligated into one of the final vectors, which contains the drug resistance cassette and fluorescent protein sequence. The final plasmid was transformed in to bacteria for replication, mini prepped (for *T. brucei*) or midi prepped (for *T. congolense*) in line with manufacturer guidelines, and sequenced. Subsequently the plasmid was linearised using *Not*I restriction enzyme, ethanol precipitated, and transfected into the parental cell line. Homologous recombination facilitated the integration of the plasmid DNA into the correct site of the trypanosome genome, with selection achieved via drugging to identify successful transformants.

2.2.5. Heat Shock Protocol

In order to keep cells at an ideal mid-log density 5-10 ml cells at a density of 5×10^5 cells/ml for BSF cells or 4×10^6 cells/ml for PCF cells were used. Cells were placed in 50 ml falcon tubes with loose lids for BSF cells and tight lids for PCF cells and placed into a pre-equilibrated recirculating water bath (Clifton NE4) at the specified temperature (41-42 °C) for the specified amount of time (0-2 hours). Cell density was determined either using a haemocytometer or an automated cell counter (CellDrop FL Flourescence Cell Counter, DeNovix). The temperature of the bath and a blank tube of equal volume to the sample was checked and recorded with an digital thermometer (RS).

2.2.6. Flow cytometry

For flow cytometry, samples were prepared using 1×10^6 cells fixed in 70% methanol. For *T. congolense* cells were initially fixed in 50% methanol and then adjusted to 70% after 1 hour to prevent cell rupture. The samples were fixed overnight at 4 °C. Following fixation, cells were washed, resuspended in PBS, and stained with 10μg/ml propidium iodide (Invitrogen) and 10 μg/ml RNase (Sigma). The samples were then analysed using a Beckman Coulter Cytoflex flow cytometer using Cytoflex software. For analysis cells were gated firstly using forward scatter against side scatter to allow for size discrimination. This population of cells (P1) were then gated using Phycoerythrin (PE) signal width against PE signal height allowing for doublet discrimination. The resulting population of cells (P2) were gated using PE signal area against PE signal height allowing further gating for DNA content generating the final population of cells for analysis (P3). P3 cells were plotted on a histogram and sequential peaks are gated based on to separate cell cycle phases G1, S and G2M. Gates were also added for abnormal cells that did not conform to these peaks and are labelled <G1 and >G2M here referring specifically to DNA content not to a cell cycle phase.

2.2.7. Fluorescence microscopy

To make slides, 5×10^5 2T1 *T. brucei* or *T. congolense* cells were centrifuged for 3 minutes at 1800 g, then washed in PBS. Cells were centrifuged again and resuspended in 25 µl PBS and 50 µl of 4% PFA and left to incubate for 10 minuets at room temperature. Cells were then placed on a superfrost plus adhesion slide (Epredia) and left to air dry in the dark. Once dry slides were placed into a humidity chamber, rehydrated with PBS, and treated with 0.01% Triton for 5 minutes, before 5 washes with PBS. Flouroshield mounting medium (Sigma) was then used to stain genetic material with 4',6-diamidino-2-phenylindole (DAPI) before adding a coverslip and sealing with nail polish. Slides were stored at 4 °C in the dark, then visualised using a DeltaVision Elite deconvolution microscope.

2.2.8. RNA extraction

1×10^7 cells were prepared, and RNA was extracted using the RNeasy Plus Mini Kit according to the manufacturer's instructions. Subsequent experiments indicated that RNA extraction for *T. congolense* required the Direct-zol RNA MiniPrep Kit, which was then used according to the manufacturers protocol for RNA purification.

2.2.9. Bioanalyzer

Integrity of RNA was confirmed using the Agilent RNA 6000 Nano Kit per manufactures instructions and samples were analysed using an Agilent 2100 bioanalyzer, with the Eukaryotic total RNA Nana series II assay.

2.2.10. Generation of cDNA

Extracted RNA was DNase treated using Amplification grade DNase I (Sigma) per manufactures instruction to digest DNA isolating and purifying extracted RNA. This purified RNA was then used for the synthesis of cDNA using the Omniscript reverse transcriptase kit (Qiagen) per manufacturers instruction.

2.2.11. qPCR

White 96-well qPCR plates (BIORAD) were loaded with generated cDNA and primers designed for Actin (control) and different heat shock proteins. Fast SYBR Green Master Mix (Thermo fisher) was used to allow for quantification of PCR product. qPCR was carried out on a BIO-RAD C1000 Thermal Cycler. Pre-established cycle conditions for detection of Actin using SYBR-green were used. Express loading conditions were set for 'Quick Plate 96 wells SYBR Only white' and scan mode was set for SYBR FAM only. Quantification Cq results were used for analysis.

Table 3 qPCR Cycle conditions

1	95 °C	20 seconds

2	95 °C	3 seconds
3	60 °C	30 seconds
+ Plate read		
4	Go to 2 39 more times	
5	Melt curve 65 °C to 95 °C Increment 0.5 °C	5 Seconds
+ Plate read		
End		

2.2.12. qPCR statistical analysis

To evaluate the significance of mRNA fold changes in HSPs in response to heat stress, Student's t-tests were performed using technical replicates derived from the qPCR Ct readings. Ideally this analysis would have been conducted using biological replicates, however, due to time constraints, this was not feasible. The analysis focused on mRNA fold changes of HSPs before, during and after heat shock, normalised to actin which was assumed to remain unaffected. For each time point, three Ct readings for HSPs and three Ct readings for actin were obtained. To account for variability delta-Ct values were calculated for each technical replicate by subtracting the actin Ct from the HSP Ct for replicates 1,2 and 3. Pairwise comparisons were performed using two-tailed Student's t-tests with unequal variance, comparing non-heat-shocked samples to each of the other time points. P-values were categorised as follows: $p < 0.05$ (*), $p < 0.01$ (**) and $p < 0.001$ (***). These significance levels are indicated on the respective graphs.

2.2.13. gDNA extraction

Two ml of late-log phase culture was centrifuged at 2500×g for 3 minutes at room temperature, then washed in PBS. The supernatant was removed, and the pellet resuspended in 100 µl NTE buffer pH 8 (100 mM NaCl, 10 mM Tris, 50 mM EDTA) and 0.5 µl 20% SDS. This was then incubated at 55 °C for 10 minutes before the addition of 50 µl 3M NaOAc. This was incubated on ice for 5 minutes before centrifuging for 5 minutes at a rate of 20,000 × g and a temperature of 4 °C. The supernatant was removed and transferred to a new Eppendorf to which 2 volumes of 100% EtOH was added. This was

then spun in the centrifuge using the same conditions. Once spun down the supernatant was removed and discarded, and the DNA pellet was allowed to airdry before being resuspended in 50 µl of ddH_2O.

2.2.14. PCR

All primers used were specifically designed then ordered from Sigma. Tables for primers used in this study for *T. brucei* (Appendix 1) and *T. congolense* (Appendix 2) tagging are included in the appendix. PCRs were performed with OneTaq DNA polymerase, for each primer pair, components of the reaction are shown in Table 4. For these reactions, the thermocycler was programmed to 94 °C for 30 seconds for an initial denaturation of the DNA. This is followed by 35 cycles of 94 °C for 30 seconds to ensure full denaturation, a variable temperature based on the T_m of the primer pair (see appendix) for 1 minute for primers to anneal, 68 °C for a variable time based on a rate of 1 minute per kb (see appendix) for elongation, to end the cycle 68 °C for 5 minutes as a final extension period.

Table 4 PCR Master Mix

One*Taq* MM	25 µl
H2O	22 µl
Forward Primer (10µM)	1 µl
Reverse Primer (10µM)	1 µl
Template gDNA*	1 µl

*In these reactions, template DNA was gDNA from the relevant species or cell line.

2.2.15. Agarose gel electrophoresis

To separate DNA components by size for visualisation and purification a 1% agarose gel was prepared. To 40 ml of 1 × TAE running buffer (Fisher Scientific), 40 mg of agarose

powder (Melrose) was added, along with 4 µl of SYBR safe (Invitrogen) to visualise the DNA. The agarose powder was dissolved into the buffer in the microwave and cooled before addition of the SYBR safe dye and then poured into a cast. Samples were run alongside 5 µl 100 bp or 1 kb MW ladder (Promega) and 6 × purple loading dye was added to facilitate loading of samples by giving colour and adding density, so samples don't flow out. Gels were run for approximately 25-30 minutes at 115 V. The gels were then images on a BioRad Gel Doc EZ imager.

2.2.16. Gel extraction

The desired band was cut out from an agarose gel using a UV transilluminator (Syngene) for visualisation. The DNA was then extracted from the band using a Thermo Scientific GeneJet Gel Extraction kit according to the manufacturer's instructions provided.

2.2.17. Ligation

Backbones and inserts were ligated using 0.5 µl of T4 DNA ligase (Promega), 0.5 µl of 10× rapid ligation buffer (Promega), 0.5 µl of vector, and 3.5 µl of insert. The reactions were incubated at room temperature overnight.

2.2.18. Transformation

Five µl of plasmid DNA was added to a 25 µl aliquot of high-efficiency *Escherichia coli* competent cells (NEB) and incubated on ice for 10 minutes. The cells were then heat-shocked at 42 °C for 30 seconds and placed back on ice for 5 minutes. After this, the cells were allowed to recover in 150 µl of SOC medium for 30 minutes in a shaking incubator at 37 °C. The cells were then plated onto LB plates containing 100 µg/ml carbenicillin and incubated overnight at 37 °C. For blue-white screening, 30 µl of 0.1 M IPTG (Melford) and 30 µl of 20 µg/ml X-Gal (Thermo) were spread on the plates prior to adding the bacterial cells.

2.2.19. DNA mini-preps

Selected colonies were cultured overnight in 3 ml of LB broth containing 100 μg/ml carbenicillin, in a shaking incubator at 37 °C. The bacterial cells were then pelleted by centrifugation at 3500 × g for 10 minutes. DNA mini-preps were performed using the Thermo Scientific GeneJet Miniprep kit according to the manufacturer's instructions.

2.2.20. DNA midi-preps

One μl of established miniprep was diluted 1/100 with double distilled water. One μl of this was transformed following the transformation protocol and ½ of this transformation was spread onto LB plates with 100 ug/ml Carbenicillin and left overnight at 37 °C. The following morning single colonies were selected cultured overnight in 50 ml of LB, in a shaking incubator at 37 °C. The bacterial cells were then pelleted by centrifugation at 6000 × g for 15 minutes at 4 °C. DNA midi-preps were performed using the QIAGEN Plasmid Midi Kit according to the manufacturer's instructions.

2.2.21. Sequencing

Aliquots of the miniprep products were sent for sequencing at Dundee DNA Sequencing Services using standard or custom primers. The obtained DNA sequences were compared to genomic sequences from TriTrypDB (Aslett et al., 2009) using ApE software (Davis & Jorgensen, 2022).

2.2.22. Restriction Enzyme Digest

For the restriction digestion reactions, 1/10 of the total reaction volume was 10× Cutsmart buffer (NEB), and 1/20 of the total reaction volume was each restriction enzyme (NEB). The reactions were incubated at 37 °C for at least 2 hours.

2.2.23. Ethanol precipitation

Volume of linearised plasmid DNA was reduced using ethanol perception. 1/10 volume of sodium acetate was added to the digest, along with 2 volumes of 100% ethanol. This was vortexed and incubated at -20 °C overnight. After incubation this was centrifuged at 20,000×g for 15 minutes at 4 °C and the supernatant discarded. The pellet was resuspended in 2× volume of 70% ethanol. This was centrifuged under the same conditions for 5 minutes and the subsequent supernatant was removed. The pellet was then air dried and resuspended in 10μl of double distilled water.

2.2.24. Transfection of *T. brucei*

Three μg of plasmid DNA from confirmed mini preps was linearised in a restriction enzyme digest using *Not*I (NEB) and the volume of digested DNA was reduced using ethanol precipitation. Then 2×10^7 cells from a maintained log phase culture were pelleted at 800 × g. The pellet was washed in PBS, re-pelleted and suspended in 100μl of transfection buffer (nucleofector solution and supplement (Lonza)). Cells were added to plasmid DNA, and this was transferred to an Amaxa certified cuvette. The cells were then electroporated using an Amaxa set to programme X-001. Negative controls were carried out without the addition of plasmid DNA. Transfected cells were added to 25ml of media containing 250μl of additional Penicillin Streptomycin (Labetch) and returned to 37 °C. Cells were allowed to recover for a minimum of 6 hours to allow for homologous recombination and the protein for drug resistance to be expressed. Drugs were added dependent on potential drug resistance provide through the plasmid DNA (specific concentrations shown in Table 5) . Cells were plated into 24 well plates with 1ml in each well to allow for drug selection. After 5 days wells were screened to check for complete death in the negative control and surviving single clones in plasmid transfectant cells, these were the cells selected and cultured for analysis.

2.2.25. Transfection of *T. congolense*

For *T. congolense* transfections midi-preps were used to amplify plasmid DNA prior to linearisation as recommended (Awuah- Mensah et al., 2021). Ten µg of plasmid DNA from these midi preps was linearised using *Not*I (NEB) and the volume of digested DNA was reduced using ethanol precipitation. Then 4×10^7 from a maintained log phase culture were pelleted at 800×g. The pellet was washed in PBS, re-pelleted and suspended in 100µl of transfection buffer (nucleofector solution and supplement (Lonza)). Cells were added to plasmid DNA, and this was transferred to an Amaxa certified cuvette. The cells were then electroporated using an Amaxa set to programme Z-001. Negative controls were carried out without the addition of plasmid DNA. Transfected cells were added to 25ml of media containing 250µl of additional Penicillin Streptomycin (Labetch) and returned to 37 °C. Cells were allowed to recover for a minimum of 6 hours to allow for homologous recombination and the protein for drug resistance to be expressed. Drugs were added dependent on potential drug resistance provide through the plasmid DNA (specific concentrations shown in Table 5). Cells were plated into 24 well plates with 1ml in each well to allow for drug selection. After 10 days wells were screened to check for complete death in the negative control and surviving single clones in plasmid transfectant cells, these were the cells selected and cultured for analysis.

Table 5 Drug concentration used for transfected cell lines

Backbone	Drug	Concentration for *T. brucei*	Concentration for *T. congolense*
pEnNmSt0-N	G418 (Melford)	2.5 µl/ml	0.5 µl/ml
pEnNY0	Hygromycin (Melford)	2.5 µl/ml	0.4 µl/ml
pSIS-HHsfG	Hygromycin (Melford)	2.5 µl/ml	0.4 µl/ml

2.2.26. SDS-PAGE

A sample of 4×10^6 cells were prepared then resuspended in 20 µl 2 × SDS loading buffer to coat proteins with a uniform negative charge. These samples were then denatured at 95 °C for 10 minutes. Ten µl of sample was then run on a Mini-PROTEAN TGX precast gel (4-12% gradient Biorad) alongside 5 µl of precision plus protein dual colour standards ladder (Biorad) at 180v for around 40 minutes or until maximum resolution between bands was reached.

2.2.27. Western blot

After running an SDS-PAGE, proteins were transferred on to a PVDF membrane using the Trans-Blot Turbo RTA transfer kit (Biorad), according to manufacturer's instructions. Blots were then blocked for 20 minutes in a 2.5% milk solution. Primary antibody (anti-GFP antibody (Sigma) was added at a concentration of 1/10,000 made up in 2.5% milk solution, this was left overnight on a platform rocker at 4 °C. The following morning the blot was washed in a PBST solution including 3 quick rinses and 2 × 5-minute washes where the blot was covered in PBST and left on the platform rocker at room temperature. Once the wash was removed the secondary antibody (goat-anti mouse, LI-COR) was added at a concentration of 1/20,000 and left to incubate on a platform rocker protected from the light for 1 hour. The washes were repeated before visualisation on the LI-COR Odyssey FC. The process is then repeated on the same blot using antibodies for a loading control, these were anti H3 (primary antibody) and goat-anti mouse (secondary antibody). Secondary antibodies are conjugated with IRDye to allow for visualisation.

3. Profiling thermal tolerance in *T. brucei* and *T. congolense*

3.1. Introduction

The primary objective of the project was to optimise the temperature conditions for inducing heat shock in *T. congolense* by comparing its response to the well characterised heat shock response of *T. brucei*. The established and widely reported heat shock protocol for *T. brucei*, involving a temperature increase to 41 °C, which is 4 °C and 14 °C above standard growth temperatures for bloodstream form (BSF) and procyclic form (PCF) stages, respectively, was used as a reference (Droll et al., 2013). Previous studies have demonstrated that BSF *T. brucei* cells exposed to 41 °C for one hour experience a notable growth lag, extending up to 24 hours post-treatment (Ooi et al., 2020). This phenomenon prompted an in-depth investigation into the reproducibility and implications of the heat shock response in *Trypanosoma spp.*

3.2. Interrogating *T. brucei* BSF growth recovery after variable heat shock timeframes

Growth curves were generated to evaluate growth of cells recovering from heat shock. The aim of this initial experiment was to understand and determine the most effective timeframes for heat shock, when analysing the parasites' ability to recover, what timeframes of analysis were effective, and which would likely offer the best window to interrogate proteins involved in the heat shock response in later stages of this project.

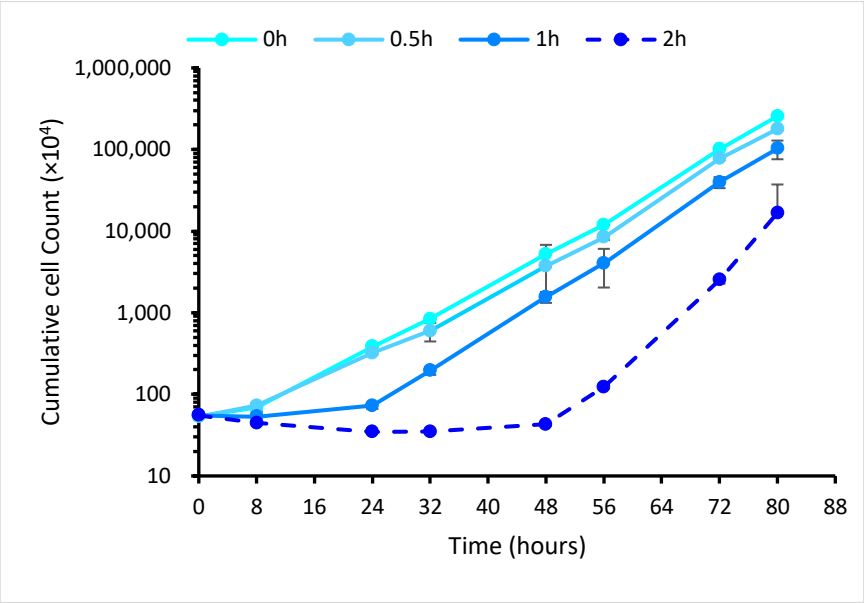

Figure 3.1 Growth Curves of Blood Stream Form *Trypanosoma brucei* Post Heat Shock. Growth curves of bloodstream *T. brucei* cells post heat shock at 41 °C for 0, 0.5, 1 and 2 hours. Cell density was recorded at intervals up to 80 hours post-treatment. Data show mean ± standard deviation, where n=3.

The growth curves highlight the differential response of bloodstream form *T. brucei* to heat shock depending on the duration of exposure. Bloodstream *T. brucei* cells not subjected to heat shock (0-hour control) displayed rapid and exponential growth, demonstrating the typical cellular proliferation of this parasite, reaching a cumulative cell density of 2.5×10^9/ml by the end of the observation period, and providing a benchmark for assessing the effects of heat treatment. Cells exposed to a 0.5-hour heat shock showed a slight temporary growth lag but resumed exponential growth thereafter, understandably, there was no significant difference observed in comparison to the control. Contrastingly, a 1-hour heat shock induced a noticeable and significant difference in growth inhibition compared to the control, with a marked decrease in cell density and severe growth lag during the initial 24 hours. However, the cells gradually recovered, resuming exponential growth after the lag period, demonstrating a significant but reversible impact of the heat shock on cellular proliferation. The most pronounced effect was observed with the 2-hour heat shock, where cell density largely decreased within the first 24 hours, with a severe growth arrest extending up to 48 hours post-treatment. Minimal recovery was seen, with cell density reaching only about 1.6 ×

10^7/ml by the end of the observation period. This suggests that prolonged heat exposure leads to significant cellular damage and a substantial reduction in growth potential.

3.3. *T. brucei* BSF Cell cycle analysis across heat shock recovery timeframe

To further understand the underlying cellular mechanisms, flow cytometry was employed to analyse cell cycle progression post heat shock. *T. brucei* cells were heat-shocked for 0-, 0.5-, 1-, and 2-hours, followed by periodic sampling every hour for the first 9 hours and a final sample at 24 hours.

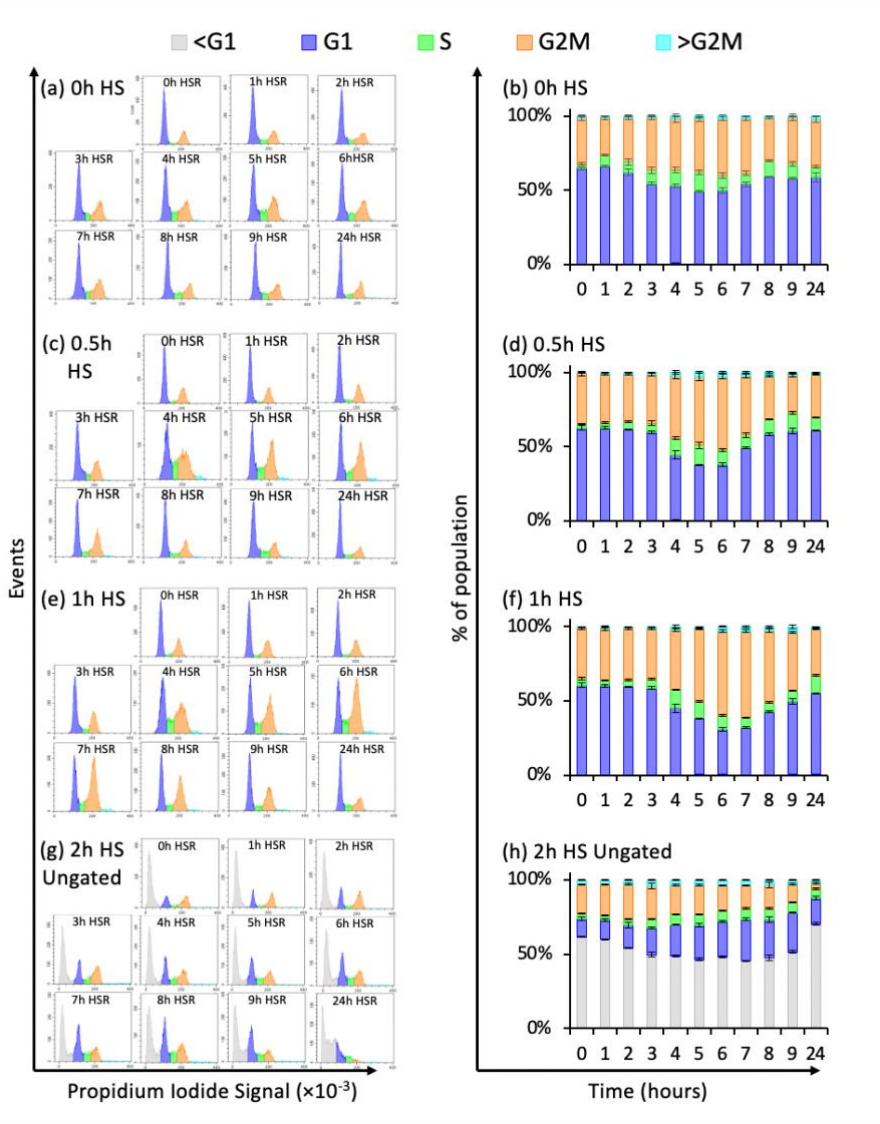

Figure 3.2 BSF *T. brucei* under varying heat shock conditions. Flow cytometry analysis of mid log TbBSF cells (5 × 10^5 cells/ml) post heat shock at 41 °C for 0-, 0.5-, 1-and 2-hours. Samples were taken every hour for 9 hours followed by a 24-hour timepoint. Data

show representative cycles (a, c, e, g) and corresponding relative contribution of cell cycle phases (b, d, f, h). Data are presented as mean ± SD, where n = 3.

In the control group, the G1 phase population initially constituted approximately 65% of the cell population, the S phase around 5% and the G2/M phase around 30%. A minor fraction of cells is observed in the >G2M category and trace amounts in <G1 (Figure 3.2). Over the 24-hour observation period, only minor fluctuations were noted. By the 5-hour mark the G1 phase population had decreased slightly to about 50%, with concurrent increases in the S phase to around 10-15% and in the G2/M phase to about 35-40%. These variations suggest the possibility of a slight stress response, potentially due to methodological factors, but overall, the cell cycle distribution remained stable demonstrating efficient progress through the cell cycle, providing a baseline for determining the effects of heat shock. In line with observations presented in Figure 3.1 a 0.5-hour heat shock did not result in a large shift in cell cycle dynamics, however a slight transient shift was observed. Five-hours post heat shock, it was noted that the key change in cell cycle distribution was a 5% increase in the G2/M population. This increase in G2/M cell numbers was similarly observed in cells at the 6-hour post 1-hour heat shock timepoint. Additionally, there was a notable increase in the S phase to about 10-15% and the G2/M phase to 55-60%, suggesting that a larger fraction of cells were arrested before completing mitosis. The most severe cell cycle disruptions were observed following a 2-hour heat shock (Figure 3.2). Initially, a significant proportion of cells (~55%) were found in the G2/M phase, with a reduction in the G1 phase (~35%) and S phase (~10%), suggesting a strong arrest in the later stages of the cell cycle. Minor fractions were again observed in >G2M and trace amounts in <G1. Over time, there was a gradual increase in the G1 phase, peaking at around 50% by 9 hours, along with a gradual increase in the S phase to around 15%. However, the proportion of cells in G2/M sharply declined to around 25%, and there was a notable increase in cell debris categorized as <G1. This indicates that prolonged heat shock exposure caused significant cell damage, leading to cell death and an inability to progress through the cell cycle. The cells did not recover from this extended heat shock within the 24-hour observation

period, demonstrating that 2-hour exposure to 41 °C causes irreversible cell cycle arrest and considerable cytotoxic effects.

Impact of Gating Removal

Figure 3.2 (g and h) illustrates the cell cycle distribution after a 2-hour heat shock without applying gating criteria. The removal of gating reveals a substantial increase in cell debris categorised within the <G1 fraction, highlighting a more severe impact of heat shock than initially apparent with gating applied (gated data shown in Appendix 5, Figure 8.1). The <G1 fraction, indicative of fragmented or apoptotic cells remained the largest proportion throughout. Initially the second-largest population was G2/M followed by G1. Over time, fluctuations led to changes in this order. The S phase consistently made up the fourth largest population contribution, followed by the >G2/M fraction. This observation potentially underscores the severe, cytotoxic effects of a 2-hour heat shock. Detailed presentation of gating parameters is presented in methods (Section 2.2.6).

3.4. Interrogating *T. brucei* PCF growth recovery after variable heat shock timeframes

The growth curves depicted in Figure 3.3 show the effects of heat shock on the growth dynamics of procyclic form *T. brucei* over an 80-hour period. Heat shocks of varying durations were applied to assess their impact on cell viability and proliferation.

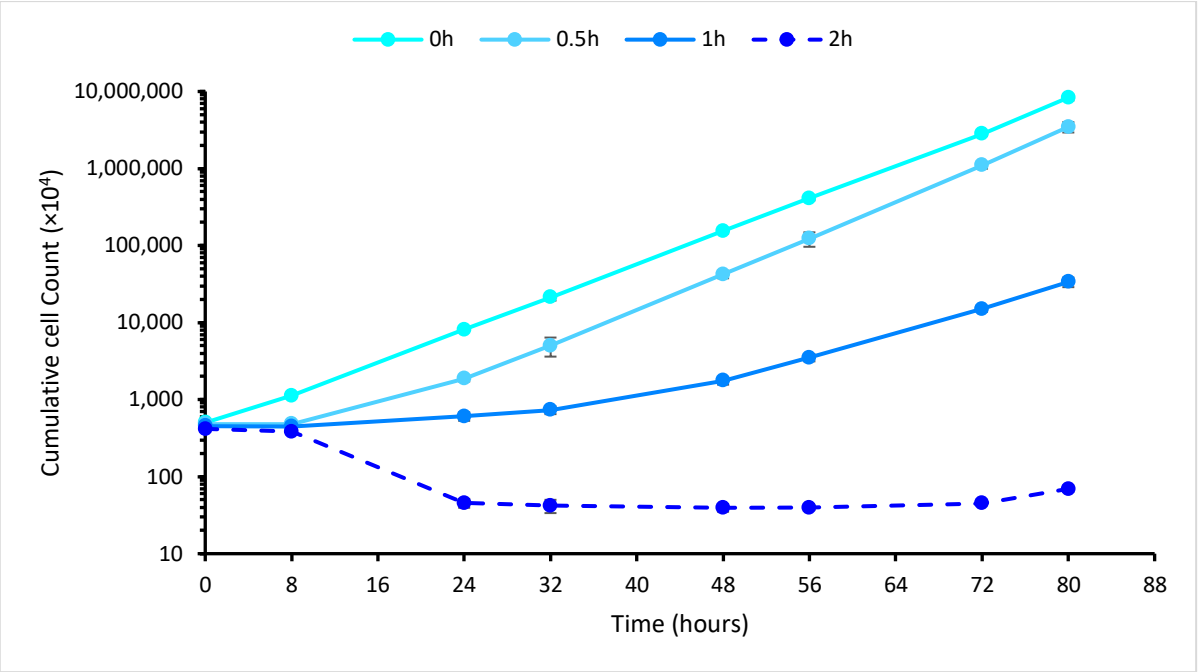

Figure 3.3 Growth Curves of Procyclic Form *Trypanosoma brucei* Post Heat Shock. Growth curves of procyclic *T. brucei* cells post heat shock at 41 °C for 0, 0.5, 1 and 2 hours. Cell density was recorded at intervals up to 80 hours post-treatment. Data show mean ± standard deviation, where n=3.

The growth curves depicted in Figure 3.3 show the effects of heat shock on the growth dynamics of procyclic form *T. brucei* over an 80-hour period. Heat shocks of varying durations were applied to assess their impact on cell viability and proliferation. In line with observations of recovery dynamics of BSFs, Figure 3.1, a slight reduction in growth rate compared to the control was observed after a 0.5-hour heat shock treatment. Despite an initial lag phase, growth resumed and was parallel to the control after 24 hours, although population density remained significantly lower than the control across all replicates ($p \leq 0.05$). Contrastingly, a 1-hour heat shock results in a more pronounced lag in growth, meeting the threshold for significance ($p \leq 0.05$). This treatment resulted in significantly impaired growth across 80-hours, with the population failing to resume exponential growth across this timeframe. Notably, the 2-hour heat shock population exhibited a large reduction in cell density immediately following treatment. With a significant proportion of the population lost by the 8-hour mark, these cells exhibited minimal recovery, and the cell density remained significantly lower than the initial seeding density across the duration of the experiment.

3.5. *T. brucei* PCF Cell cycle analysis across heat shock recovery timeframe

Procyclic *T. brucei* cells not subjected to heat shock (0-hour control) displayed exponential growth, with cell density increasing consistently over the 80-hour period, with doubling times as expected (~8-fold/24-hours).

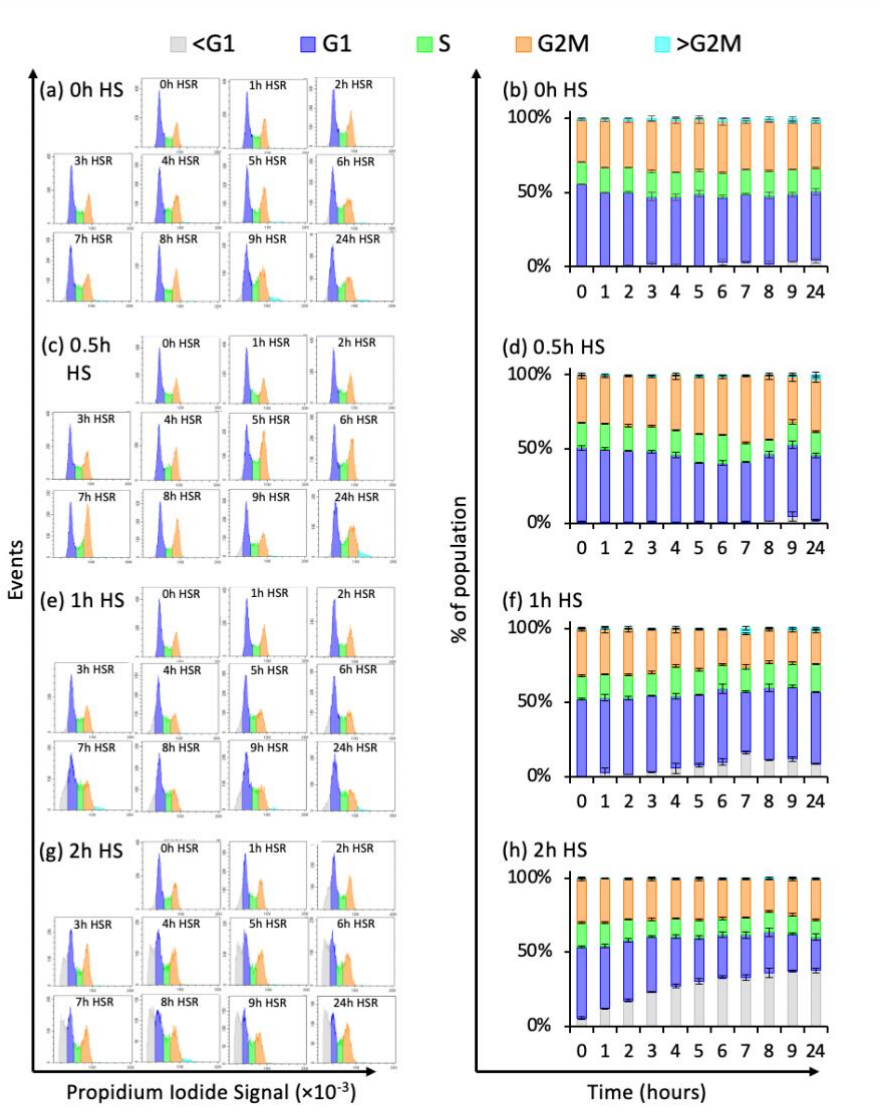

Figure 3.4 Cell Cycle disruption of *Trypanosoma brucei* PCF under varying heat shock conditions. PCF *T. brucei* under varying heat shock conditions. Flow cytometry analysis of mid log TbPCF cells (5 × 10^6 cells/ml) post heat shock at 41 °C for 0-, 0.5-, 1-and 2-hours. Samples were taken every hour for 9 hours followed by a 24-hour timepoint. Data

show representative cycles (a, c, e, g) and corresponding relative contribution of cell cycle phases (b, d, f, h). Data are presented as mean ± SD, where n = 3.

To further understand the conservation of the heat shock response between different life cycle stages, flow cytometry was employed to analyse cell cycle progression post-heat shock. PCF *T. brucei* cells were heat-shocked for 0, 0.5, 1, and 2 hours, followed by periodic sampling every hour for the first 9 hours and a final sample at 24 hours to interrogate the distribution of cells across key cell cycle stages. Initially, Initially, the G1 phase constituted approximately 55% of the cell population, the S phase around 15% and the G2/M phase around 30%, with minor fractions observed in the >G2M category and trace amounts in <G1 (Figure 3.4). Over the 24-hour observation period, only minor and statistically insignificant fluctuations were noted. The proportion of cells in G1 slightly decreased to around 45%, attributed to a slight increase in debris categorised as <G1 and abnormal cells categorised as >G2/M. Samples of the 6-hour post 0.5-hour heat shock population demonstrated that the G1 phase population had decreased to below 40%, indicating a slight delay in the progression through G1. Concurrently, there was an increase in the S phase to about 20% and in the G2/M phase to roughly 40%. By the 9-hour mark, the cell population contained around 50% in G1, 15% in S and 30% in G2/M phases, with minor fractions in >G2M and a slightly increased amount in <G1. However, by 24 hours, the cell population had shifted again, containing around 40% in G1, 15% in S, and 35% in G2/M phases, with slightly increased fractions in >G2M and a slightly reduced amount in <G1. These fluctuations suggest that a 0.5-hour heat shock induces transient stress, leading to temporary alterations in cell cycle progression, particularly a delay in G1, but cells largely recover by 24 hours.

Developing on this observation, cells recovering from a 1-hour heat shock initially contained approximately 50% in G1, 15% in S and 30% in G2/M phases, again with minor fractions in >G2M and trace amounts in <G1 (Figure 3.4). Somewhat surprisingly, by 7 hours post-heat shock, the G1 population had decreased to around 40%, and debris categorized as <G1 had increased to around 15%. However, most notably for this population, the S phase remained around 15%, G2/M decreased to around 20% and

>G2/M remained a remained a minor fraction. This distribution remained relatively stable by 24 hours, with a slight decrease in <G1 and a slight increase in the S phase. The 2-hour heat shock population, however, presented with the most striking changes in cell cycle profile. While initially showing around 5% of cells within <G1, around 45% in G1, around 15% in S, around 30% were in G2/M and trace amounts in >G2M, the population consistently declined in quality, and by 9-hours post-heat shock hours the proportion of cells in <G1 had gradually increased to around 35%, G1 had decreased to around 25%, S remained around 15%, G2/M had decreased to around 25% and minimal fractions remained in >G2M. Taken together, these results indicate that a 2-hour heat shock causes significant and lasting disruptions in the cell cycle, with a substantial increase in debris suggesting extensive cell damage or death.

3.6. Interrogating BSF *T. congolense* growth recovery after variable heat shock timeframes

To assess the impact of heat shock on bloodstream form *T. congolense* cells, they were subjected to 41 °C for different durations of 0, 0.5, 1, and 2 hours. After treatment, cell growth was monitored over an 80-hour period. Cell density measurements were taken at 0, 8, 24, 32, 48, 56, 72, and 80 hours. The growth curve presented below illustrates the capacity of *T. congolense* to progress through the cell cycle following heat shock treatment.

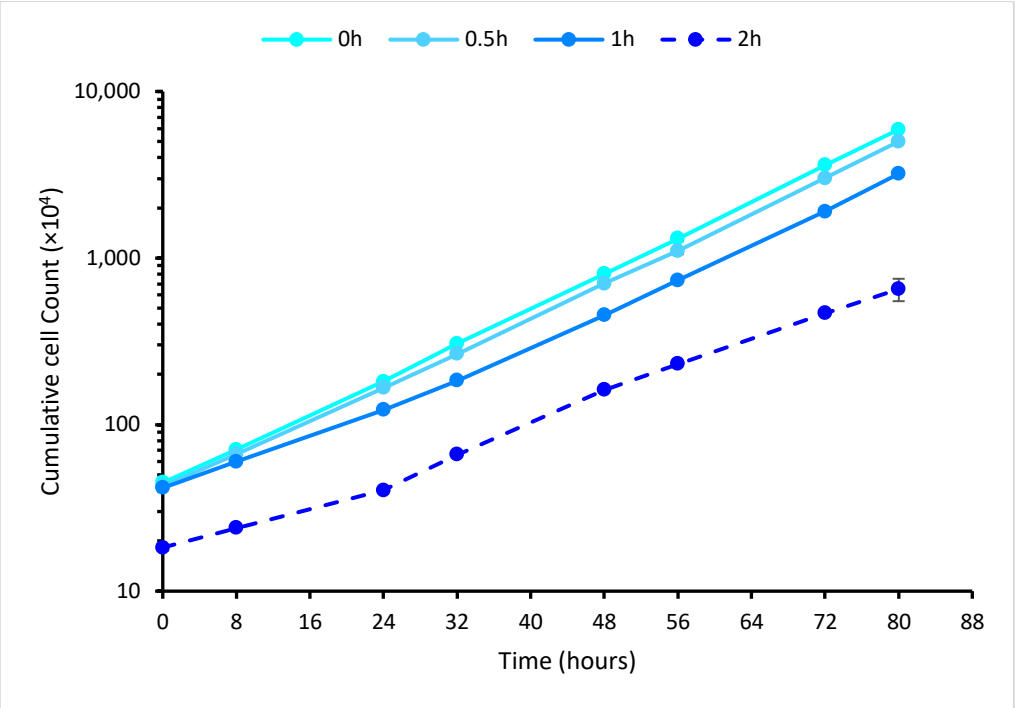

Figure 3.5 Growth Curves of Blood Stream Form *Trypanosoma congolense* Post Heat Shock. Growth curves of bloodstream *T. Congolense* cells post heat shock at 41 °C for 0, 0.5, 1 and 2 hours. Cell density was recorded at intervals up to 80 hours post-treatment. Data show mean ± standard deviation, where n=3.

Cells not exposed to heat shock (0-hour control) exhibited rapid and exponential growth, in line with the expected doubling time. As with PCF and BSF samples, *T. congolense* populations exposed to a 0.5-hour heat shock showed no significant change in growth across the time course of investigation. Similarly, while cells which had undergone a 1-hour heat shock exhibited a statistically significant inhibition of cell growth, with an evident growth lag observed in the first 24 hours, these cells recovered to exponential growth rate soon after. While population growth rose to once again match the control, it is unsurprising that this population remained at a significantly lower cell density than the control at the termination of the experiment. In line with expectations, the most severe effect of heat shock was observed in the 2-hour treatment population. Deviating from expectations however, the most notable change in population dynamics was observed immediately following removal from heat shock conditions, with more than 50% of the population being lost during this time. It is, however, important to note, that surviving cells did not show a considerable reduction in growth rate, almost paralleling

the growth of the control population. A slight lag in growth was observed following the 56-hour timepoint, however cell growth did continue. The rapid death of a large cohort of this population prompted further analysis via flow cytometry, discussed below. These results are consistent with previously observed trends in other *Trypanosoma* species, highlighting that while shorter heat shocks can be tolerated and recovered from, prolonged exposure results in significant cellular stress and impaired growth. This insight is crucial for understanding the thermal tolerance and adaptive responses of *T. congolense*, which could inform strategies for managing infections and improving treatment outcomes.

3.7. BSF *T. congolense* Cell cycle analysis across heat shock recovery timeframe

To elucidate the cellular mechanisms underlying the response to heat shock, flow cytometry was employed to analyse cell cycle progression in bloodstream form (BSF) *T. congolense* cells. The cells were subjected to heat shock at 41 °C for durations of 0, 0.5, 1, and 2 hours. Post-treatment, cells were periodically sampled every hour for the first 9 hours and at the 24-hour mark. The cells were fixed using an optimized protocol (see methods for details) with 70% methanol and stained with propidium iodide to enable DNA content analysis. Gating strategies were implemented to differentiate cell populations based on size, doublets, and DNA content (see methods for details).

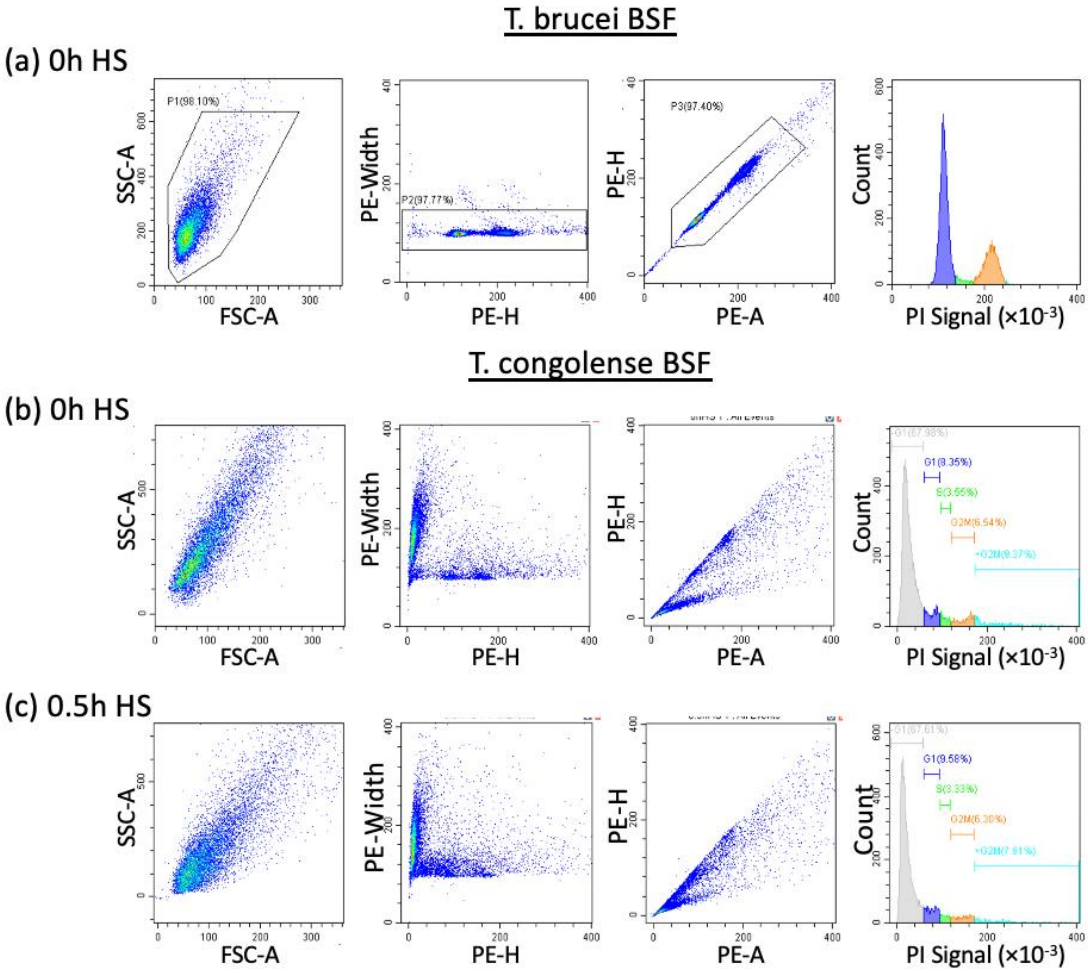

Figure 3.6 Cell Cycle Distribution of *Trypanosoma congolense* after 0 and 0.5 hours of heat shock. Flow cytometry analysis of mid log TcoBSF cells (5×10^5 cells/ml), subjected to heat shock at 41 °C for 0 (b) and 0.5 hours (c). Flow cytometry analysis of mid log TbBSF cells (5×10^5 cells/ml), subjected to heat shock at 41 °C for 0 (a) is shown as a control. Samples were taken immediately post-treatment. Each graph is based on 10,000 recorded events and illustrates side scatter area vs forward scatter area, PE width vs PE height, PE height vs PE area, and gated cell cycle distribution.

Despite replicating the same experimental conditions used successfully for *T. brucei*, the samples from *T. congolense* proved problematic for analysis. It was evident that the acquisition of complete data from these experiments was not feasible. While flow cytometry analysis aimed to record 10,000 events following the previously established protocol, this was largely unsuccessful. In rare instances where 10,000 events were

recorded, it took up to 8.5 minutes, compared to the typical 30 seconds required for *T. brucei* samples. A notable observation was the significantly broader distribution of cell sizes (Side scatter area vs Forward scatter area) in *T. congolense* (Figure 3.6, b and c) populations, compared to *T. brucei* (Figure 3.6, a). Doublet discrimination efforts revealed a substantial proportion of cells with abnormal PE-height to PE-width ratios, leading to the identification of two distinct cell populations (Figure 3.6, b and c). Similarly, gating based on DNA content also displayed two distinct populations. The majority of recorded events in *T. congolense* were classified as <G1 (debris). This phenomenon was observed in both the untreated control sample and the 0.5-hour heat-shocked sample, indicating that it was not an artifact of heat treatment but rather that an element of the methodology likely required further optimisation.

3.8. Optimisation of fixation parameters for flow cytometry

In an effort to resolve this issue, a series of trials with different fixation methods were conducted to identify a suitable protocol that would prevent cell bursting and ensure accurate cell cycle stage fixation. The only variable altered was the fixative. Cells were examined on a slide under a light microscope before fixation to confirm their normal viability and motility, immediately after fixation, and the following morning.

Table 6 Fixation optimisation observations

Fixative	**Immediate Observation**	**Observation Following Morning**
PBS (Control)	Cells appeared normal in shape and motility.	Some cells were alive, others dead.
4% PFA	Cells remained intact and fixed, maintaining good shape.	Some cells remained intact, but others were swollen.

2% Formaldehyde and 0.05% Glutaraldehyde	Most cells remained intact; ~50% showed morphology loss.	Very few cells remained intact.
3.7% Formaldehyde	Most cells remained intact; ~80% showed morphology loss.	Complete debris, no intact cells.

From these results, it is evident that the method of fixation for flow cytometry of *T. congolense* requires further optimisation, as none of the tested protocols were successful. The aim is to develop a fixation method that preserves cells in their current state before the addition of fixative, preventing cell bursting and maintaining cellular morphology. Further research is needed to identify a suitable fixation protocol that meets these criteria.

3.9. Summary

This chapter compared the effects of heat shock on three *Trypanosoma* species (*T. brucei* BSF, PCF, and *T. congolense*) and relates growth reduction to cell cycle disruptions. *T. brucei* cells exposed to increasing heat shock durations (0.5, 1, and 2 hours) showed varied recovery: short heat shock caused minimal growth lag, while prolonged heat shock (2 hours) led to severe growth arrest and reduced cell density. In BSF *T. brucei* cell cycle analysis revealed that longer heat shock caused arrest in G2/M and significant cell damage, with a rise in apoptotic cells. Similarly, PCF *T. brucei* demonstrated disrupted growth and cell cycle arrest after 1- and 2-hour HS, though they recovered better than BSF cells.

In *T. congolense*, growth was significantly impaired after 1- and 2-hour HS, with high cell death. Attempts to analyse *T. congolense's* cell cycle by flow cytometry were hindered by technical issues with fixation and subsequent cell debris. This comparison highlights that while all three cell types can recover from brief heat shock, prolonged exposure can lead to growth arrest and cell damage, particularly impacting BSF *T. brucei* cell cycle

progression in G2/M. Further research on fixation methods for flow cytometry in *T. congolense* is required.

4. Genetic modifications to allow molecular characterisation of the HS response

4.1. Introduction

In *Trypanosoma brucei* procyclic form (PCF) cells, heat shock granules and P-bodies are crucial components of the cellular response to stress arising from temperature elevations, acting as sites for mRNA degradation and storage (Kramer et al., 2008). These granules contain specific proteins that relocate within the cytoplasm to form discrete foci following heat shock treatment at 41 °C for 1 hour. To our knowledge, the dynamics of these structures in BSF *T. brucei* have not been well-characterised. This study attempts to interrogate this response and elucidate the characteristics of the heat shock response in BSF *T. brucei*, as the key lifecycle stage experiencing elevated temperatures within the mammalian bloodstream. In addition to this, the heat shock response has not previously been investigated in *T. congolense,* the major cause of AAT. With recent advances in the testing and development of tools for genetic manipulation, a more rigorous analysis of this stress response is now possible (Awuah-Mensah et al., 2021). Homologues of the proteins chosen for examination in *T. brucei* were identified in *T. congolense* using TriTrypDB, a database of genomes of kinetoplastid organisms (Aslett et al., 2009). Prior investigations within the Urbaniak Laboratory resulted in the generation of five fluorescent reporter fusion proteins, previously used to investigate the heat shock response in *T. brucei* and *T. congolense* (Aelmans, 2022). To develop on this line of questioning, a further three proteins with known heat shock granule or P-body localisation were selected (XRNA, PABP1, and HSP100). This approach was taken to facilitate observation of changes in protein localisation and abundance in response to heat shock (Kramer et al., 2008; Droll et al., 2013; Ooi et al., 2020). This chapter will discuss efforts to generate genetically modified cell lines to facilitate the characterisation of the effects of heat shock in both *T. brucei* and *T. congolense* BSFs.

4.2. In situ tagging of BSF *T. brucei* proteins

In this project *T. brucei* cloning began with two previously completed plasmids PMA5 (pEnNYo-eYFP-TbXRNA) and PMA9 (in pSIS-HH-TbPABP1-sfGFP). These plasmids were digested with *Not*I and linearisation was confirmed via DNA gel electrophoresis. For the ease of presenting these results, a brief schematic and summary of the specific cloning strategy used here is presented, in Methods 2.2.4 (Figure 2.1).

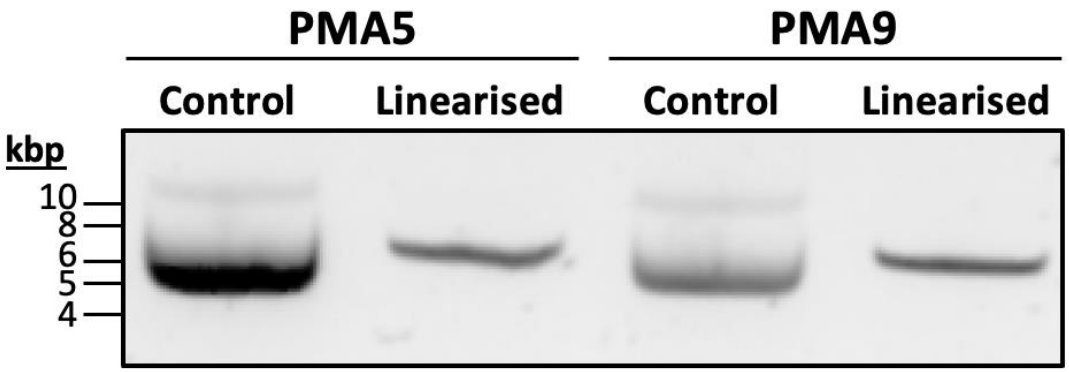

Figure 4.1 Agarose gel electrophoresis of linearised constructs. Lane 1 - intact PMA5 plasmid, Lane 2 displays the NotI linearised PMA5 plasmid (6608 bp). Lane 3 contains the intact PMA9 plasmid, Lane 4 shows the NotI linearised PMA9 plasmid (6576 bp). All constructs ran in line with expected Kbp length.

Figure 4.1 presents the successful linearisation of PMA5 and PMA9, for subsequent transfection. Non-linearised PMA5 plasmid (control), appears around 5 kbp while the *Not*I linearised PMA5 plasmid, ran as expected at around 6 kbp. Linearisation causes the plasmid to take up more surface area, hence running slower and appearing at its expected combined size of the eYFP-TbXRNA PCR products (1064 bp) and the pEnNYo backbone (5544 bp). Non-linearised PMA9 plasmid (control), containing sfGFP-tagged TbPABP1 in a pSIS-HHsfG backbone, also appears around 5 kbp while the *Not*I linearised PMA9 plasmid, runs closer to 6 kbp for the same reasons as described for the PMA5 plasmid, confirming the linearisation with the expected combined size of the TbPABP1-sfGFP PCR products (1052 bp) and the pSIS-HHsfG backbone (5524 bp). The shift in migration distance after Not1 digestion, from approximately 5 kbp to 6 kbp, validates the successful linearisation of both plasmids. These linearised plasmids were then ethanol precipitated and 3 μg of each plasmid was used in transfection with BSF *T.*

brucei, further details of methodology available in methods (Section 2.2.22). 3 clones from each transfection were selected for verification of successful integration of the TbPABP1 and TbXRNA plasmids, with cell lines named cAT1 and cAT2 respectively.

4.2.1. PCR Verification of eYFP-TbXRNA cell lines

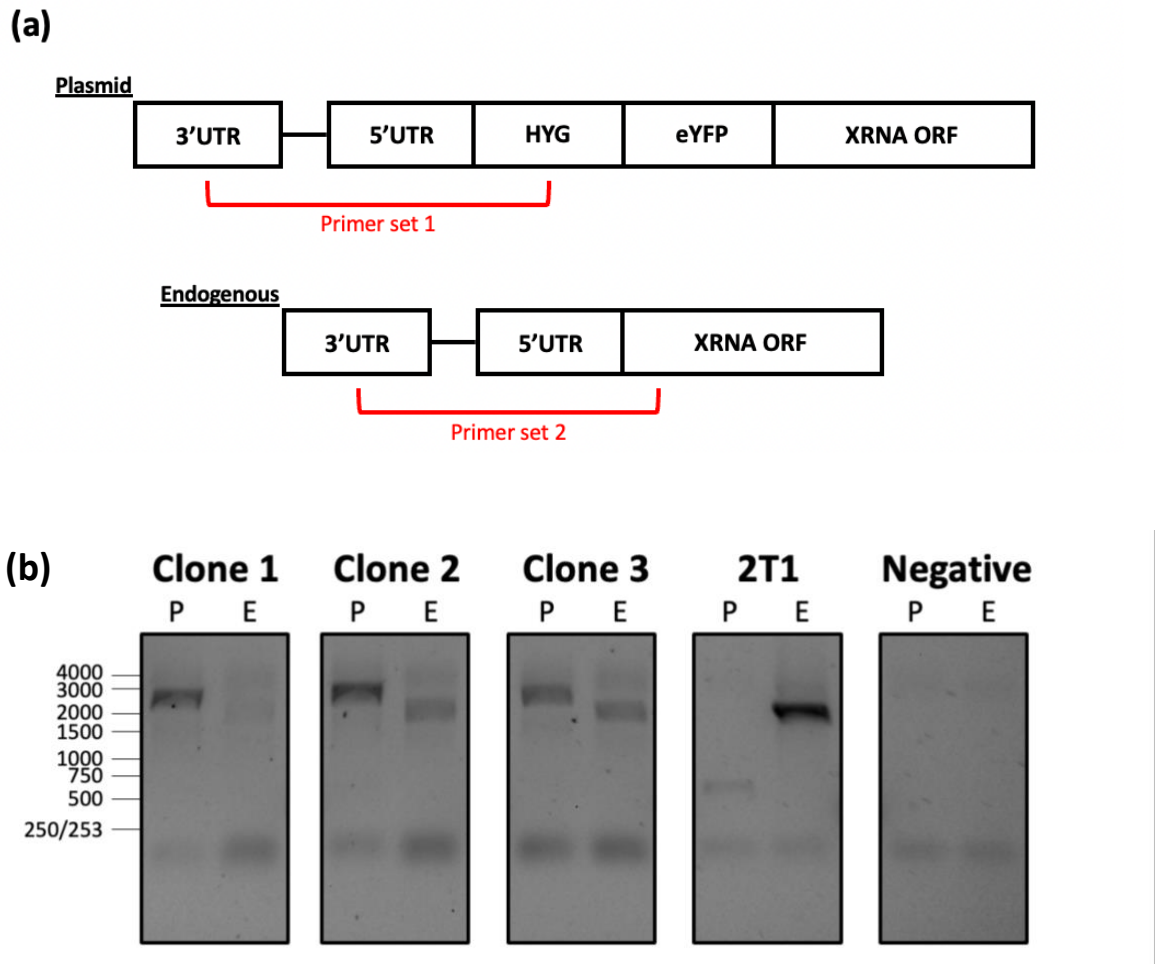

Figure 4.2 Confirmation of eYFP-TbXRNA transfected cell line by PCR. (a) Schematic of PCR primer design. Primer set 1 amplifies 1939 bp region that confirms the successful transfection and integration at the intended locus. Primer set 2 amplifies a 2082 bp region that confirms the presence of the TbXRNA sequence in the normal genomic context. **(b) Agarose Gel Electrophoresis of PCR products confirming Integration into the genome.** PCR products using primer set 1 confirm the integration of the eYFP-tagged TbXRNA plasmid PMA5 into the genome. PCR was performed on genomic DNA (gDNA) extracted from three different clones, with 2T1 *T. brucei* gDNA as a positive control and a no gDNA sample as a negative control.

The schematic (Figure 4.2, a) provides a visual representation of the PCR strategy, demonstrating how these primer sets ensure that one copy of the eYFP-tagged TbXRNA is correctly located within the genome, allowing for both the verification of gene tagging and the integration of the selection marker. The integration of these constructs, in line with the methodology presented in Figure 4.2 (a), was confirmed by PCR and gel electrophoresis, Figure 4.2 (b). Target constructs, indicated by “P”, detected bands of ~2Kbp, in line with the expected amplicon size of 1939 bp, confirming the presence of the vector construct and successful generation of the reporter fusion protein. Correspondingly, amplification with primers specific to the endogenous locus, “E”, results in bands just above 2Kbp, in line with the expected size of 2082 bp, verifying the integration at the correct locus. Clone 1 shows a weak endogenous band suggesting the clone may be double tagged, suggesting this tagging is well tolerated in the genome. Reassuringly, minimal levels of non-specific amplification are seen within the positive control (lane 4), and no bands were observed in the Negative control (lane 5). These results validate that the eYFP-tagged TbXRNA plasmid (PMA5) is correctly integrated into the genome of the transfected *T. brucei* clones, evidenced by the specific amplicon sizes observed in the gel. Clones were then taken forward for further verification and analysis under heat shock conditions.

4.2.2. PCR verification of TbPABP1-sfGFP cell lines

The schematic below, Figure 4.3 (a), provides a visual representation of the PCR strategy, demonstrating how these primer sets ensure that one copy of the sfGFP-tagged TbPABP1 is correctly located within the genome, allowing for both the verification of gene tagging and the integration of the selection marker.

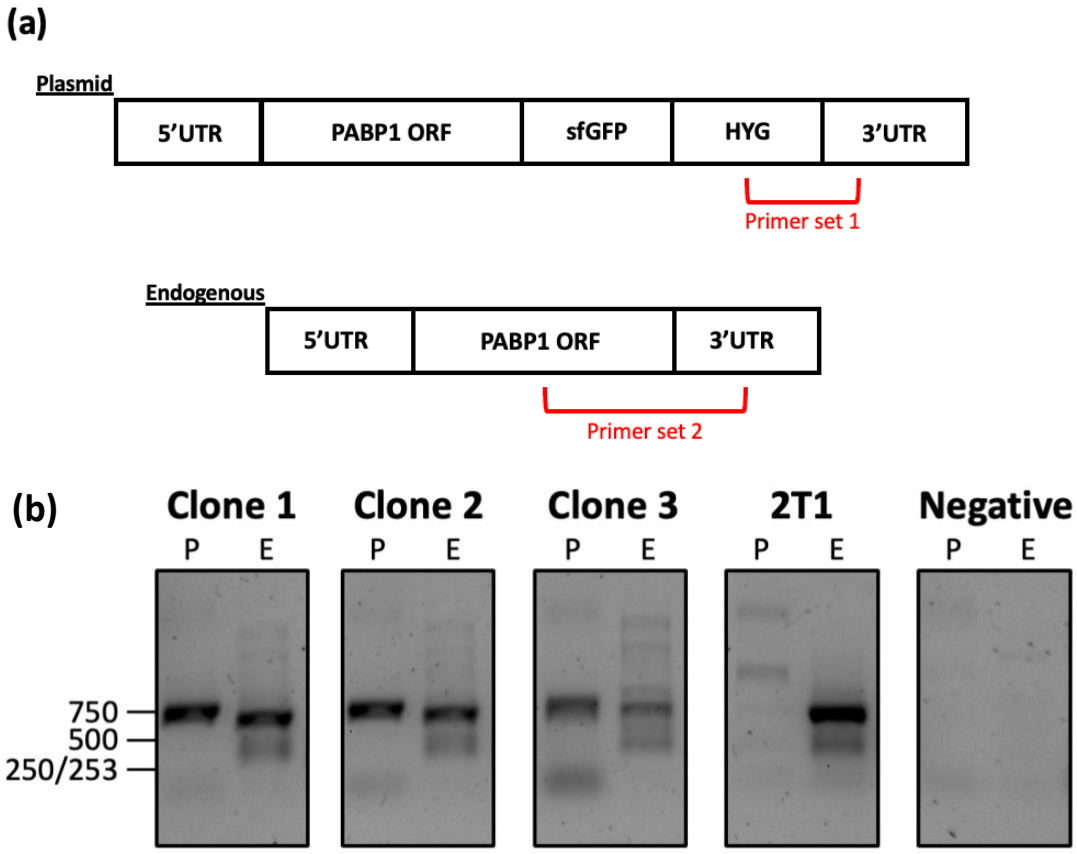

Figure 4.3 Confirmation of TbPABP1-sfGFP transfected cell line by PCR. (a) Schematic of PCR primer design. Primer set 1 amplifies 751 bp region that confirms the successful transfection and integration at the intended locus. Primer set 2 amplifies a 671 bp region that confirms the presence of the TbPABP1 sequence in the normal genomic context. **(b) Agarose Gel Electrophoresis of PCR products confirming Integration into the genome.** PCR products using primer set 1 confirm the integration of the sfGFP-tagged TbPABP1 plasmid PMA9 into the genome. PCR was performed on genomic DNA (gDNA) extracted from three different clones, with 2T1 *T. brucei* gDNA as a positive control and a no gDNA sample as a negative control.

Lanes 1-6 of Figure 27 (b) indicate banding consistent with the expected size of 751 bp, confirming the presence of the plasmid DNA, indicated by "P". Correspondingly, amplification with primers specific to the endogenous locus, "E", results in bands just below 750 bp, in line with the expected size of 671 bp, verifying the integration at the correct locus. While some non-specific bands are seen, indicating non-specific amplification, in the positive control, using plasmid specific primer pairs, amplification

of the endogenous locus again validates specificity. Taken together, these results demonstrate successful integration of the PMA9 plasmid into the genome of *T. brucei* cells and validate that the sfGFP-tagged TbPABP1 plasmid (PMA9) is correctly integrated into the genome of the transfected *T. brucei* clones, evidenced by the specific amplicon sizes observed in the gel.

4.2.3. Western blot verification of eYFP-TbXRNA and TbPABP1-sfGFP cell lines

Western blot analyses (Figure 4.4) was used to confirm the expression of tagged TbPABP1 and tagged TbXRNA in *T. brucei* BSF clones. This also enabled a screening for relative expression levels between clonal populations, to enable selection of the most reliable cell line.

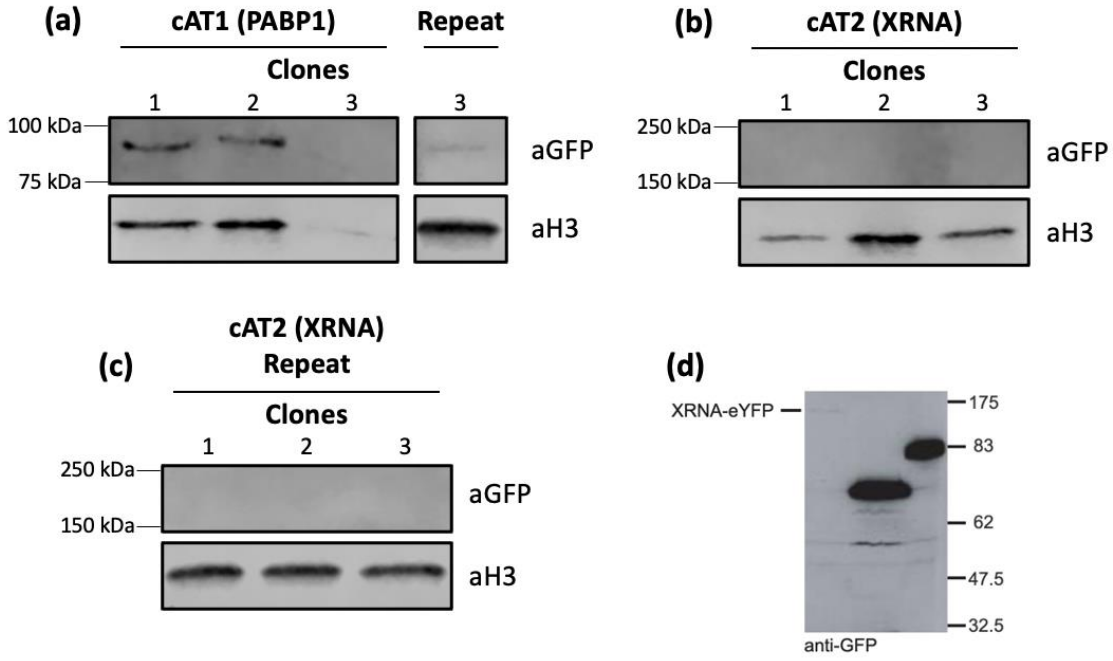

Figure 4.4 Western Blot Analysis of *T. brucei* BSF Clones Expressing TbPABP1-sGFP and eYFP-TbXRNA. (a) Western blot of the TbPABP1-sGFP cell line. Cell lysates from 2×10^6 cells were loaded, including a repeat of clone 3. **(b)** Western blot of the eYFP-TbXRNA cell line. Cell lysates from 2×10^6 cells were loaded. **(c)** Repeat Western blot of the eYFP-TbXRNA cell line with increased cell number. Cell lysates from 4×10^6 cells were loaded. **(d)** Western blot from Kramer et al. (2008) showing YFP-tagged TbXRNA in PCF T. brucei with cell lysates from 1×10^6 cells per lane. Western blots were stained with α-GFP

antibody and visualised using a LI-COR Odyssey FC. H3 protein, detected using an α-H3 primary antibody, served as a loading control.

The western blot of the TbPABP1-sGFP cell line (Figure 4.4, a) shows a distinct band at approximately 88 kDa in all three clones, confirming the presence of the tagged TbPABP1 protein. Initially, no signal was detected for clone 3, but a loading control indicated a loading error. Upon repeating, a signal was successfully detected. The endogenous TbPABP1 protein is around 63 kDa, and the GFP tag adds approximately 25 kDa, resulting in the observed band at around 88 kDa. No signal was detected for the eYFP-TbXRNA cell line using cell lysates from 2×10^6 cells per clone line (Figure 4.4, b). To enhance detection, the blot was repeated (Figure 4.4, c) with lysates from 4×10^6 cells per clone. Despite the increased cell number, no signal was observed for eYFP-TbXRNA. The expected size of the tagged TbXRNA is around 183 kDa (158 kDa for the endogenous protein plus 25 kDa for the tag). For comparison, the western blot from Figure 4.4 (d) successfully detected YFP-tagged TbXRNA in PCF *T. brucei* using α-GFP with lysates from 1×10^6 cells per lane, although the band is very weak (Kramer et al., 2013). This suggests that the lack of detection in our experiment may be due to issues with protein transfer to the blot, potentially related to the large size of the tagged protein. These results confirm the expression of TbPABP1-sGFP in the cell line but indicate difficulties in detecting eYFP-TbXRNA, possibly due to transfer inefficiencies during the blotting process rather than protein concentration. Despite attempts with different blotting methods and buffers, eYFP-TbXRNA was not visualised, suggesting that further optimisation is required for successful detection of this large, tagged protein.

4.2.4. Fluorescence Microscopy Verification of eYFP-TbXRNA

Fluorescence microscopy was used to verify the integration and expression of YFP-tagged TbXRNA in the *T. brucei* genome. This screen was carried out using a DeltaVision Olympus, in line with methodologies outlined in Section 2.2.7. This, in conjunction with data presented in Figure 4.2, gave an additional level of confidence in the selected clone, prior to more detailed interrogation (Figure 4.5).

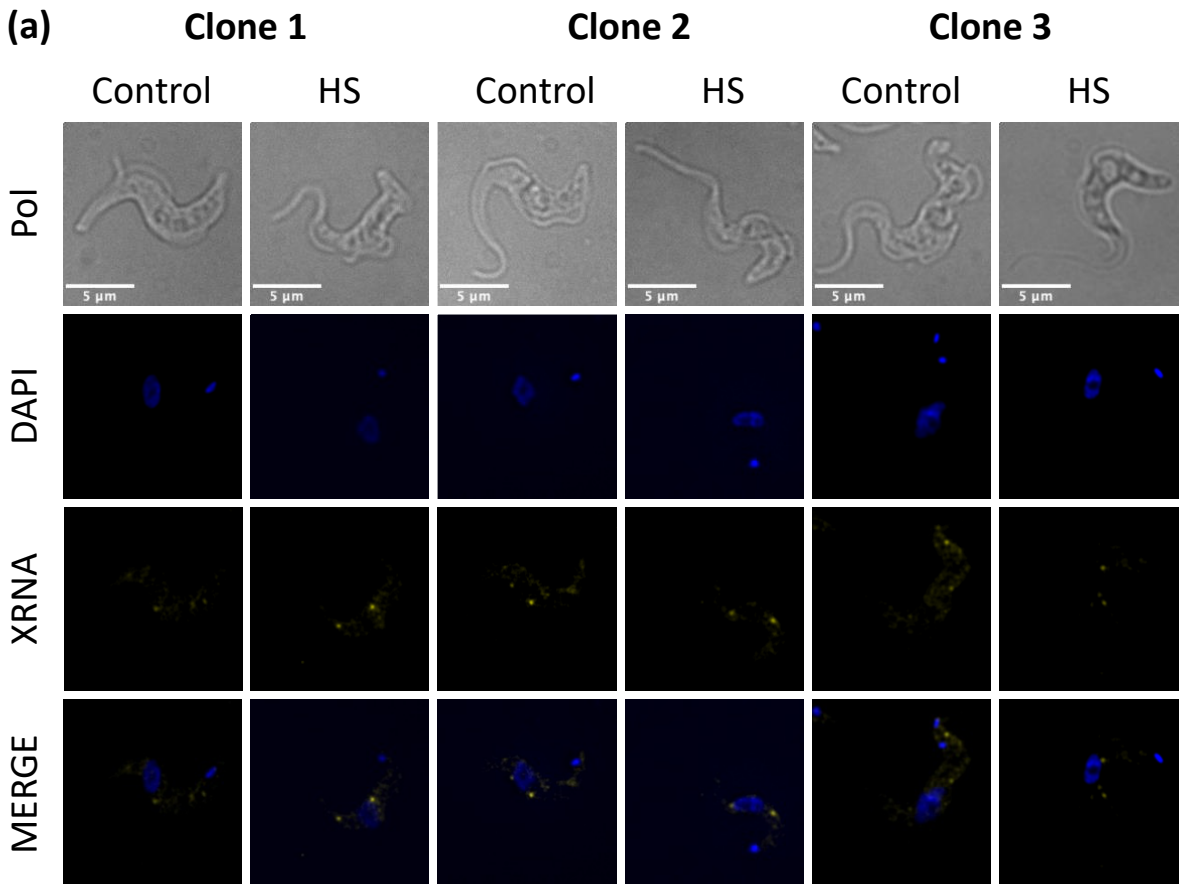

Figure 4.5 Fluorescence Microscopy Images of *T. brucei* BSF eYFP-TbXRNA cell line. Fluorescence microscopy images were taken of *T. brucei* BSF eYFP-TbXRNA cell line clones. For each slide, 5 × 10^5 cells were prepared, imaged using a DeltaVision Elite deconvolution microscope and edited with ImageJ Fiji software. Cells were fixed with 4% paraformaldehyde (PFA) and stained with DAPI to detect the nucleus and kinetoplasts. Images are shown for each of the three clones under two conditions: control (non-heat shocked) and heat shocked (1 hour at 41 °C). For each condition, images include polarised light (POL), DAPI staining, YFP fluorescence (referred to as XRNA), and a merged image of DAPI and YFP channels.

Visualisation of cell lines pre- and post- heat shock, in line with methodologies outlined in Section 2.2.7, allowed selection of the most appropriate cell line to be taken forward for interrogation. The control population in each cell line show YFP signal dispersed

across the cytoplasm with few discrete loci, agreeing with previously reported localisation (Kramer et al., 2008), reliably indicated the presence of eYFP-TbXRNA. Following heat shock treatment (1 hour at 41 °C), YFP signal remains detectable in all clones, confirming the presence of the tagged protein. While no significant changes in fluorescence intensity are observed between control and heat-shocked cells, cytoplasmic localisation appears to reduce slightly after heat shock, these results confirm the successful integration and expression of the YFP-tagged TbXRNA in the *T. brucei* cell lines, validating the detectability of the tagged protein under both control and heat shock conditions. Further experiments will be necessary to explore the effects of heat shock on TbXRNA localisation and expression in more detail.

4.2.5. Fluorescence Microscopy Verification of TbPABP1-sfGFP

Fluorescence microscopy was employed to verify the integration and expression of GFP-tagged TbPABP1 in the *T. brucei* genome, Figure 4.6.

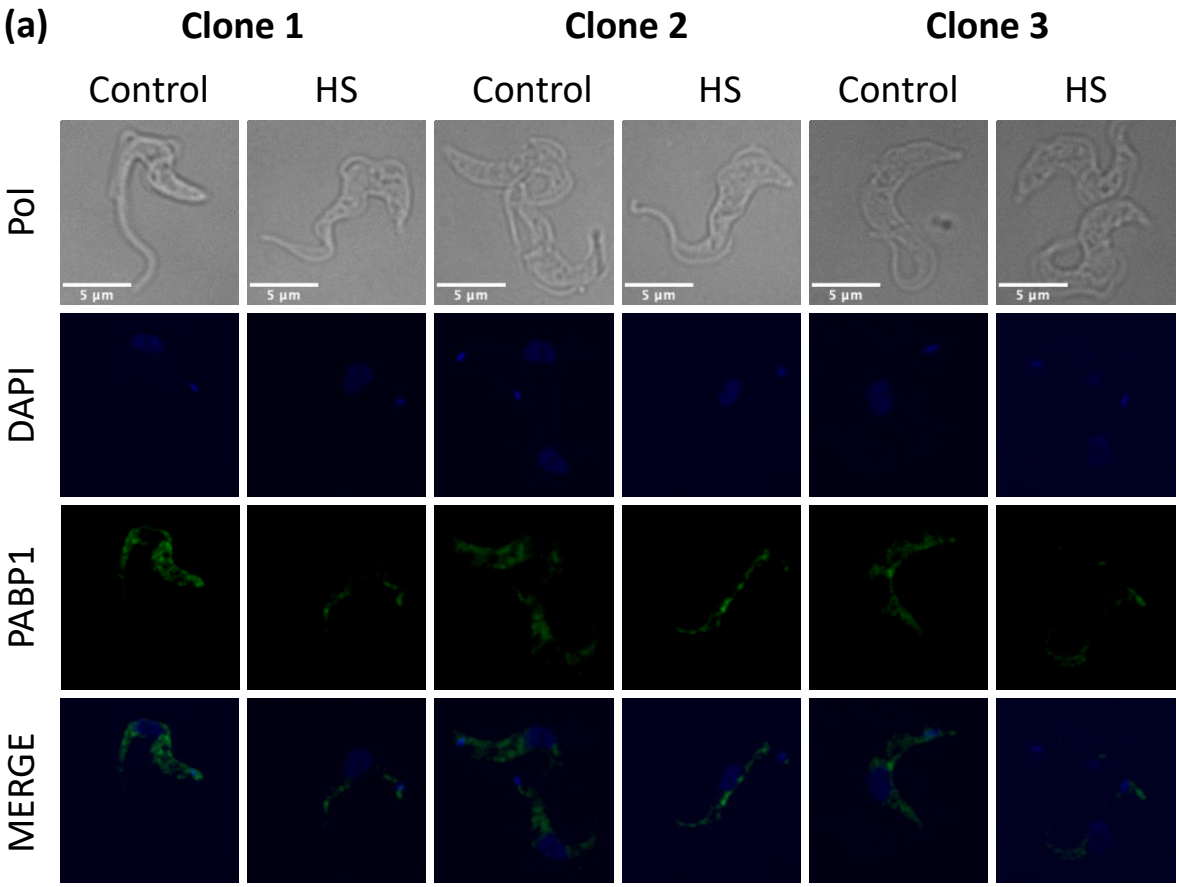

Figure 4.6 Fluorescence Microscopy Images of T. brucei BSF TbPABP1-sfGFP cell line. Fluorescence microscopy images were captured for T. brucei BSF TbPABP1-sfGFP cell line clones. For each slide, 5 × 10^5 cells were prepared, imaged using a DeltaVision Elite deconvolution microscope and edited with ImageJ Fiji software. Cells were fixed with 4% paraformaldehyde (PFA) and stained with DAPI to visualise the nucleus and kinetoplasts. Images are provided for each of the three clones under two conditions: control (non-heat shocked) and heat shocked (1 hour at 41 °C). For each condition, images include polarized light, DAPI staining, GFP fluorescence (referred to as PABP1), and a merged image of DAPI and GFP channels.

Each clone in the control population shows a strong GFP signal dispersed throughout the cytoplasm, indicating the presence of TbPABP1-sfGFP. After heat shock treatment (1 hour at 41 °C), the GFP signal remains detectable in all clones, confirming the detectability of TbPABP1-sfGFP post-heat shock

While this experiment primarily aimed to confirm protein integration and expression, it was observed that post-heat shock, the GFP signal appeared to become more concentrated into foci and localised along one edge of the cytoplasm. In contrast, the signal in non-heat shocked cells was more evenly dispersed throughout the cytoplasm. This potential change in localisation warrants further investigation. These microscopy results confirm the successful integration and expression of GFP-tagged TbPABP1 in the *T. brucei* cell lines, validating the presence of the tagged protein under both control and heat shock conditions. Further experiments will be needed to thoroughly explore the effects of heat shock on TbPABP1 localisation and expression.

4.3. In situ tagging of BSF *T. congolense* proteins

In this project *T. congolense* cloning began with three previously completed plasmids PMA6 (pEnNYo-eYFP-TcoXRNA), PMA8 (pSIS-HHsfG-TcoHSP100-sfGFP) and PMA10 (in pSIS-HHsfG-TcoPABP1-sfGFP). These plasmids were digested with *Not*I and linearisation was confirmed via DNA gel electrophoresis. For the ease of presenting these results, a brief schematic and summary of the specific cloning strategy used here is presented, in Methods 2.2.4 (Figure 2.1).

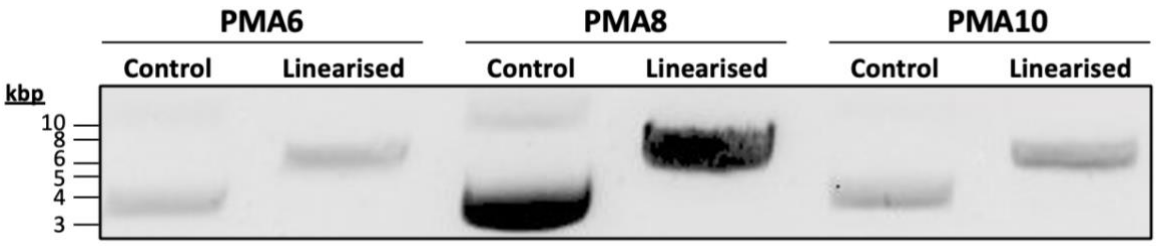

Figure 4.7 Agarose gel electrophoresis of linearised constructs. Lane 1- intact PMA6 plasmid, Lane 2 displays the NotI linearised PMA6 plasmid (6608 bp). Lane 3 contains the intact PMA6 plasmid, Lane 4 shows the NotI linearised PMA6 plasmid (6588 bp). Lane 5 contains the intact PMA10 plasmid, Lane 6 shows the NotI linearised PMA10 plasmid (6588 bp). All constructs ran in line with expected Kbp length.

This DNA gel electrophoresis confirms the successful linearisation of three plasmids, PMA6, PMA8 and PMA10, for subsequent transfection (Figure 4.7). Non-linearised

PMA6 plasmid (control), appears around 4 kbp, while linearised PMA6 plasmid, ran as expected around 6kb. Linearisation causes the plasmid to take up more surface area, hence running slower and appearing at its expected combined size of the eYFP-TcoXRNA PCR products (1064 bp) and the pEnNYo backbone (5544 bp). Non-linearised PMA8 plasmid (control), containing sfGFP-tagged TcoHSP100 in a pSIS-HHsfG backbone, appears between 3 and 4 kbp for the same reasons as described for the PMA6 plasmid. Linearised PMA9 plasmid, runs closer to 6 kbp confirming the linearisation with the expected combined size of the TcoHSP100-sfGFP PCR products (1064 bp) and the pSIS-HHsfG backbone (5524 bp). Non-linearised PMA10 plasmid (control), containing sfGFP-tagged TcoPABP1 in a pSIS-HHsfG backbone, appears around 4 kbp for the same reasons as described for the PMA6 plasmid. Linearised PMA10 plasmid, runs closer to 6 kbp confirming the linearisation with the expected combined size of the TcoPABP1-sfGFP PCR product (1064 bp) and the pSIS-HHsfG backbone (5524 bp). The shift in migration distance after *Not*I digestion, validates the successful linearisation of both plasmids. These linearised plasmids were then ethanol precipitated and 10 μg of each plasmid was used in transfection with BSF *T. congolense*, further details of methodology available in Methods (Section 2.2.22). 3 clones from each transfection were selected for verification of successful integration of the TcoXRNA, TcoHSP100 and TcoPABP1 plasmids, with cell lines named cAT3, cAT4 and cAT5 respectively.

4.3.1. Verification of eYFP-TcoXRNA integration by PCR

Primers were designed for PCR confirmation of plasmid DNA integration into the genome. For cAT3 (eYFP-TcoXRNA) endogenous (E) primers were designed to amplify a region spanning from the start of TcoXRNA ORF to the 3’ end of the upstream gene. This amplification confirms the presence of the TcoXRNA sequence in the correct genomic context. Plasmid (P) primers were designed to amplify a region spanning from the same 3’ end of the upstream gene to the hygromycin resistance cassette. This amplification confirms the integration of the selection marker alongside the TcoXRNA, verifying the successful transfection and integration at the intended locus.

To interrogate whether eYFP-TcoXRNA (PMA6) had been successfully integrated into the genome in selected clonal cell lines, PCR amplification of the tagged locus and native gene sequence was conducted, Figure 4.8.

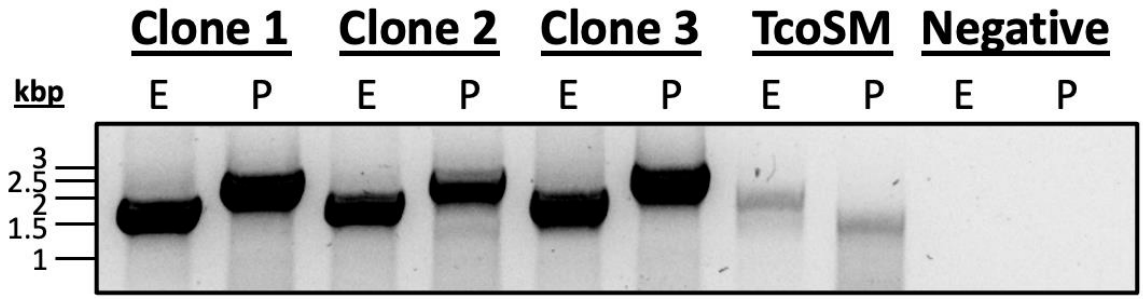

Figure 4.8 DNA Gel Electrophoresis of PCR Products Confirming Integration of PMA6 (eYFP-TcoXRNA). This figure displays the results of DNA gel electrophoresis of PCR products using primers to confirm the integration of the eYFP-tagged TcoXRNA plasmid (PMA6) into the genome. PCR was performed on genomic DNA (gDNA) extracted from three different clones, with BSF TcoSM gDNA as a positive control and a no gDNA sample as a negative control. The first set of primers targets the endogenous (E) DNA, while the second set targets the plasmid (P) DNA.

The gel electrophoresis results, Figure 4.8, demonstrate successful integration of the PMA6 plasmid into the genome of *T. congolense* cells. Plasmid primers, "P", detect bands running around 2 Kbp, in line with the expected construct size of 1.9 kbp, verifying integration at the target locus. Correspondingly, primers engineered for the endogenous locus, "E", are confirmed with a single bands running at the expected size of 1.8 kbp. While there is some non-specific binding in the positive control utilising plasmid sequence specific primers, specific binding is observed using primers targeted to the native locus of the gene. These results validate that the eYFP-TcoXRNA plasmid PMA6 is correctly integrated into the genome of the transfected *T. congolense* clones, evidenced by the specific amplicon sizes observed in the gel. Clones were then taken forward for further verification and analysis under heat shock conditions.

4.3.2. Verification of TcoHSP100-sfGFP integration by PCR

For cAT4 (TcoHSP100-sfGFP) endogenous (E) primers were designed to amplify a region spanning from the TcoHSP100 ORF and 5' end of the downstream gene. This amplification confirms the presence of the TcoHSP100 sequence in the correct genomic context. Plasmid (P) primers were designed to amplify a region spanning from the same 5' end of the gene downstream of the TcoHSP100 ORF, to the PFR2 IGS (found on the pSIS plasmid before the 3'UTR cloning site). This amplification confirms the integration of plasmid DNA alongside the TcoHSP100, verifying the successful transfection and integration at the intended locus.

In order to validate that the sfGFP-tagged TcoHSP100 plasmid (PMA8) is correctly integrated into the genome of the transfected *T. congolense* clones, PCR amplifications were conducted using primers specific to the vector (P) and native sequences (E), Figure 4.9.

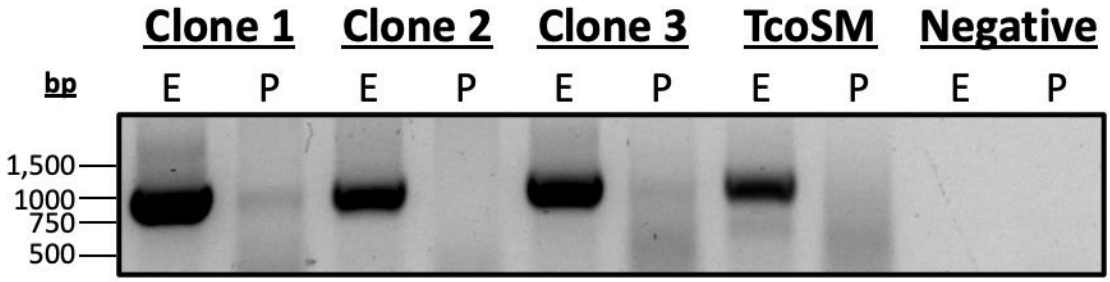

Figure 4.9 DNA Gel Electrophoresis of PCR Products Confirming Integration of PMA8 (sfGFP-tagged TcoHSP100 Plasmid) into the Genome. This figure displays the results of DNA gel electrophoresis of PCR products using primers to confirm the integration of the sfGFP-tagged TcoHSP100 Plasmid (PMA8) into the genome. PCR was performed on genomic DNA (gDNA) extracted from three different clones, with BSF TcoSM gDNA as a positive control and a no gDNA sample as a negative control. The first set of primers targets the endogenous (E) DNA, while the second set targets the plasmid (P) DNA.

While amplification of the endogenous locus was successful with bands observed between 750 and 1000 bp, in line with predicted size of 950bp, there was no detectable amplification of DNA using plasmid specific primers. These results failed to validate the

integration of sfGFP-tagged TcoHSP100 plasmid (PMA8) into the genome of the transfected *T. congolense* clones, evidenced by lack of amplified plasmid DNA observed in the gel.

4.3.3. Verification of TcoPABP1- sfGFP integration by PCR

For cAT5 (TcoPABP1-sfGFP) endogenous (E) primers were designed to amplify a region spanning from the 5' end of the TcoPABP1 ORF and 3' end of the downstream gene. This amplification confirms the presence of the TcoPABP1 sequence in the correct genomic context. Plasmid (P) primers were designed to amplify a region spanning from the same 3' end of the downstream gene to the PFR2 IGS (found on the plasmid before the 3'UTR cloning site). This amplification confirms the integration of plasmid DNA alongside the TcoPABP1, verifying the successful transfection and integration at the intended locus. Successful integration of the final protein to be investigated, TcoPABP1-sfGFP , was confirmed by PCR, utilising vectors which are specific to the plasmid (P) and endogenous (E) sequences.

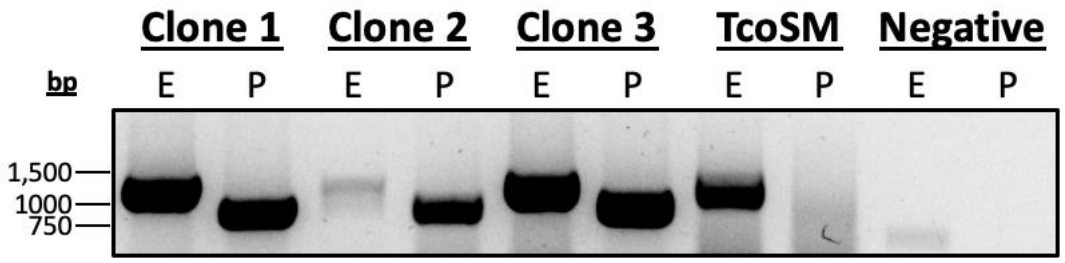

Figure 4.10 DNA Gel Electrophoresis of PCR Products Confirm Integration of PMA10 (sfGFP-tagged TcoPABP1 Plasmid) into the Genome. This figure displays the results of DNA gel electrophoresis of PCR products using primers to confirm the integration of the sfGFP-tagged TcoPABP1 Plasmid (PMA10) into the genome. PCR was performed on genomic DNA (gDNA) extracted from three different clones, with BSF TcoSM gDNA as a positive control and a no gDNA sample as a negative control. The first set of primers targets the endogenous (E) DNA, while the second set targets the plasmid (P) DNA.

Results presented in Figure 4.10 show specific amplification of the plasmid sequence, with bands evident between 750 and 1000 bp, consistent with the expected size of 900 bp, confirming the presence of the plasmid DNA. Correspondingly endogenous Primers (E) specifically amplify bands between 1000 and 2000 bp, which matches the expected size of 1200 bp, verifying the integration at the correct locus. Clone 2 shows a weak endogenous band meaning the clone may be double tagged, suggesting this tagging is well tolerated in the genome. In line with this, successful amplification of the endogenous sequence in the positive control, and lack of amplification of non-specific bands using plasmid-specific primers validated the specificity of this assay and confirmed the reliability of plasmid amplification. Taken together these results validate that the sfGFP-tagged TcoPABP1 Plasmid (PMA10) is correctly integrated into the genome of the transfected *T. congolense* clones, evidenced by the specific amplicon sizes observed in the gel.

4.3.4. Fluorescence Microscopy Verification of *T. congolense* cell lines

Fluorescence microscopy was used to verify the integration and expression of YFP-tagged TcoXRNA, GFP-tagged TcoHSP100 and GFP-tagged TcoPABP1 in the *T. congolense* genome. This initial interrogation also aimed to gain preliminary understanding of protein localisation before and after heat shock, Figure 4.11.

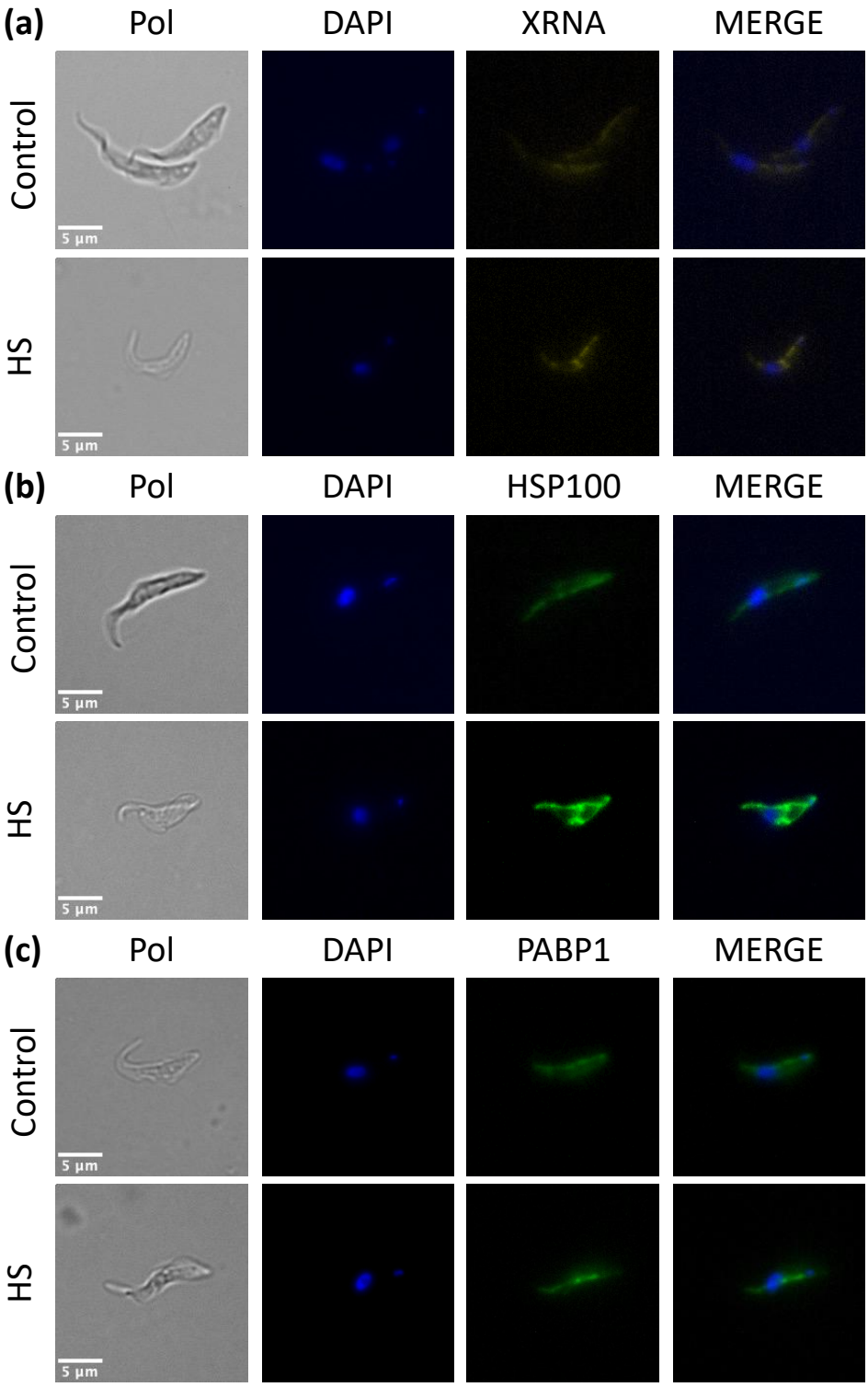

Figure 4.11 Fluorescence Microscopy Images of T. congolense BSF eYFP-TcoXRNA, TcoHSP100-sfGFP and TcoPABP1-sfGFP cell lines. Cells were fixed with 4% paraformaldehyde (PFA), stained with DAPI and imaged using a DeltaVision Elite deconvolution microscope and edited with ImageJ Fiji software. Images are under two conditions: control (non-heat shocked) and heat shocked (1 hour at 41 °C). For each

condition, images include polarized light, DAPI staining, YFP fluorescence (referred to as XRNA) or GFP (referred to as HSP100 or PABP1), and a merged image of DAPI and YFP/GFP channels.

These data indicated that in all three cell lines the tagged proteins exhibit a weak cytoplasmic signal prior to heat shock, although eYFP-TcoXRNA exhibited a lower signal intensity relative to the TcoPABP1-sfGFP, and TcoHSP100-sfGFP. Following heat shock, eYFP-TcoXRNA YFP signal appears to increase, and discrete foci become visible within the cell. Similarly, TcoPABP1-sfGFP signal appears to increase with more concentrated areas of signal becoming visible. Contrastingly, TcoHSP100-sfGFP signal intensity increased markedly, with an accumulation of distinct foci throughout the cell body. These microscopy results align with previously reported behaviour of this heat shock protein and confirm the successful integration and expression of YFP-tagged TcoXRNA, GFP-tagged TcoHSP100 and GFP-tagged TcoPABP1in the *T. congolense* cell lines, validating the presence of the tagged proteins, and that all fusion proteins exhibited altered localisations within the cell body post-heat shock. It was noted in this experiment that cell lines expressing eYFP-TcoXRNA and TcoHSP100-sfGFP fusion proteins exhibited a reduction in cell length after heat shock. Further experiments will be necessary to explore the effects of heat shock on localisation and expression of these proteins in more detail.

4.4. Summary

In this chapter, several genetically modified cell lines of BSF *Trypanosoma brucei* and *T. congolense* were successfully created to study the integration and expression of fluorescently tagged proteins (summarised in Table 7).

Table 7 Summary of cell lines produced and verified

Protein	Tag	Tag Location	PCR Verification			Western Blot Verification			IF Verification		
			Clone			Clone			Clone		
			1	2	3	1	2	3	1	2	3
TbXRNA	eYFP	N-Terminus	✓	✓	✓	X	X	X	✓	✓	✓
TbPABP1	sfGFP	C-Terminus	✓	✓	✓	✓	✓	✓	✓	✓	✓
TcoXRNA	eYFP	N-Terminus	✓	✓	✓	X	X	X	✓	X	X
TcoHSP100	sfGFP	C-Terminus	X	X	X	X	X	X	✓	X	X
TcoPABP1	sfGFP	C-Terminus	✓	✓	✓	X	X	X	✓	X	X

Fluorescence microscopy demonstrated altered protein localisation post-heat shock, with increased signal intensity and the formation of distinct foci in the cells. These findings suggest a dynamic response of the proteins to stress conditions and highlight the potential for further studies on protein function and localisation.

5. Characterisation of protein localisation in response to heat shock

5.1. Introduction

Understanding how *T. brucei* and *T. congolense* respond to environmental stress, such as heat shock, is crucial for elucidating their survival strategies and pathogenicity. This chapter focuses on characterising the protein localisation changes in cell lines generated in Chapter 4, specifically under conditions of heat shock and subsequent recovery. By employing fluorescent tagging of key proteins, we aim to provide insights into the dynamic reorganization of cellular components in response to stress. Systematic observation of protein behaviour was utilised to seek a clearer understanding of their roles and interactions during stress conditions, ultimately contributing to a deeper comprehension of trypanosome biology.

5.2. Characterisation of tagged *T. brucei* cell lines

The characterisation of cell lines expressing fluorescently tagged proteins involved in the *T. brucei* heat shock response, specifically eYFP-TbXRNA and PABP1-sfGFP, was conducted to investigate their behaviour during heat shock and subsequent recovery. Previous studies have demonstrated that TbXRNA, typically dispersed throughout the cytoplasm with a notable focus at the posterior, relocates to P-bodies upon heat shock, with an increase in the size of the posterior granule (Kramer et al., 2008). Similarly, PABP1 has been identified as a stress granule component in PCF *T. brucei* cells, redistributing from a cytoplasmic dispersion to cytoplasmic foci following heat shock (Kramer et al., 2008). The data presented here represent initial characterisations, with further interrogation required to confirm these findings. Results analysis was observational for these characterisations and future quantification needs to be undertaken (ideally in an automated manner to reduce bias).

5.2.1. Characterisation of eYFP-TbXRNA response to heat shock in *T. brucei*

Visualisation of eYFP-TbXRNA was carried out using DeltaVision microscopy, in line with methodologies outlined in Methods Section 2.2.7, with timepoints taken at 0-, 2-, 4-, 6-, 8-, and 24-hours post-heat shock presented alongside a non-heat shocked control (Figure 5.1). In this figure, and those following it, samples taken after the heat shock timeframe are denoted heat shock response timepoints (HSR).

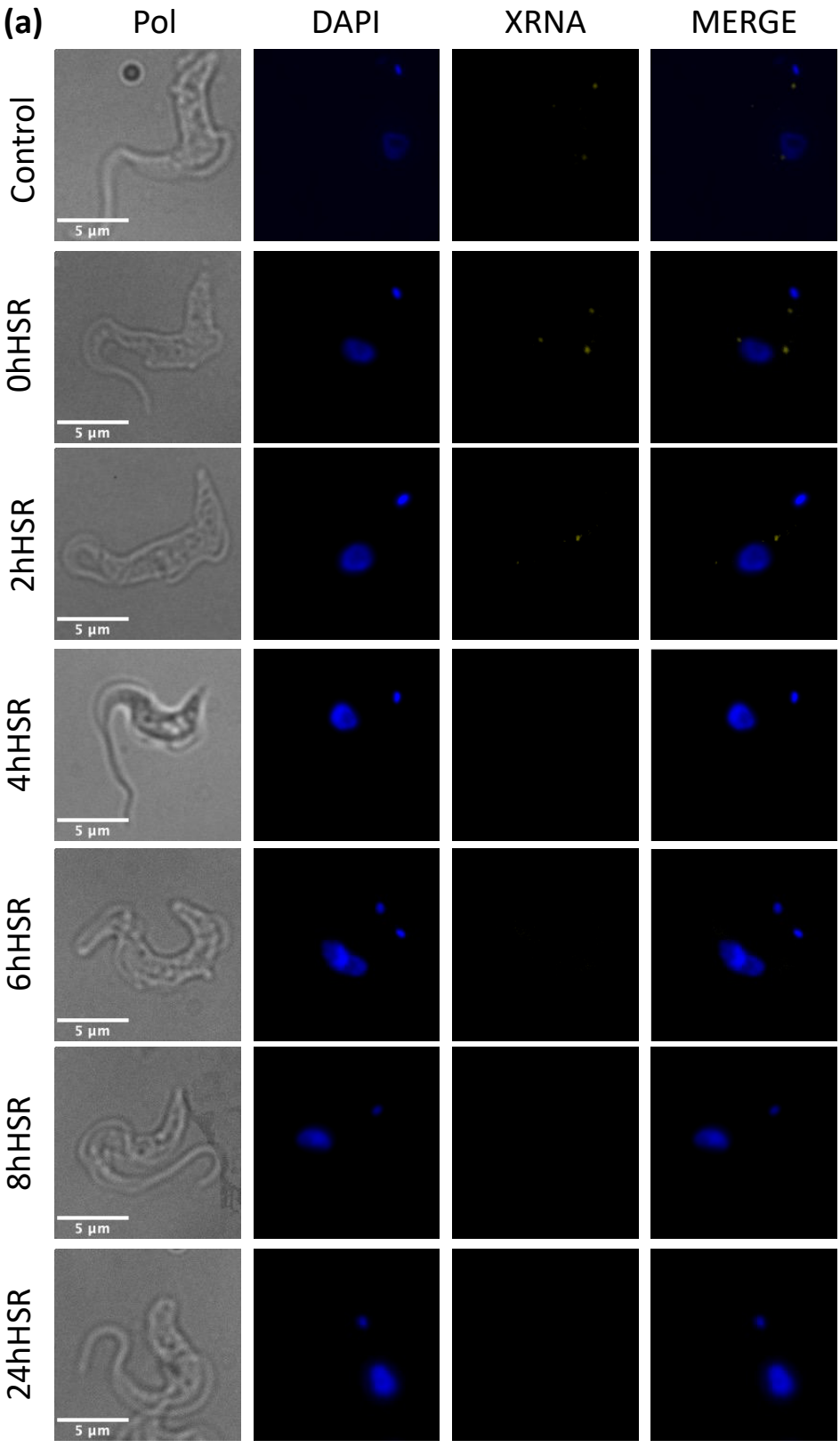

Figure 5.1 Time-Course Analysis of TbXRNA Localisation in *T. brucei* BSF eYFP-TbXRNA Cell Line Following Heat Shock. Cells from the eYFP-TbXRNA cell line were subjected to heat shock at 41 °C for 1 hour. Microscopy samples were prepared immediately post-

heat shock and at subsequent intervals (2, 4, 6, 8, and 24 hours) to monitor changes in TbXRNA localisation and abundance. For each slide, 5×10^5 cells were prepared, imaged using a DeltaVision Elite deconvolution microscope and edited with ImageJ Fiji software. Cells were fixed with 4% paraformaldehyde (PFA) and stained with DAPI to visualise the nucleus and kinetoplasts. Images are presented for each timepoint, including a control sample (non-heat shocked). Each condition includes images under polarized light, DAPI staining, YFP (reffered to as XRNA), and a merged image of DAPI and YFP channels.

These preliminary data demonstrated a subtle, but rapid increase in the number of TbXRNA-eYFP signal in the cell body immediately after heat shock. Fluorescence microscopy was employed to observe the localisation and abundance of eYFP-tagged TbXRNA in *T. brucei* cells following heat shock (Figure 5.1). It was noted that between the cells sampled prior to heat shock and those immediately following this treatment that there was a general shift in foci positioning, with and apparent increase in signal intensity, suggesting higher eYFP-TbXRNA abundance within this locus. Notably, one focus is located at the posterior region of the cell, however when compared to the DAPI and Pol images, it is clear that this point of signal is located anterior to the kinetoplast, rather than at the posterior tip of the cell body. By 2-hours post heat shock, there is a marked decreased in the number of eYFP-TbXRNA foci per cell, with the majority of the population exhibiting only one focus of signal. Further to this, eYFP-TbXRNA foci were often observed to occupy peri-nuclear regions, which could be assumed to be P-bodies. The relevance of this, to the degradation and subsequent dispersion of this protein, leading to minimal detectable signal by 24 hours is discussed further in the discussion. Surprisingly, the number of foci reduces further by 4- to 8- hours, where many cells lack any detectable eYFP-TbXRNA. By 24-hours this eYFP-TbXRNA is no longer detectable within the population, speaking to the continued absence of this protein across a >16-hour period. To develop on this further, co-localisation experiments were performed.

5.2.2. eYFP-TbXRNA does not co-localise with the mitochondria

To further investigate the localisation of XRNA in *T. brucei*, microscopy samples were prepared of pre-heat shock cells and cells subjected to heat shock (1 hour at 41 °C). In addition to DAPI staining for the nucleus and kinetoplasts, MitoTracker was used to stain the mitochondria, providing another cellular landmark for comparison and better insight into TbXRNA localisation.

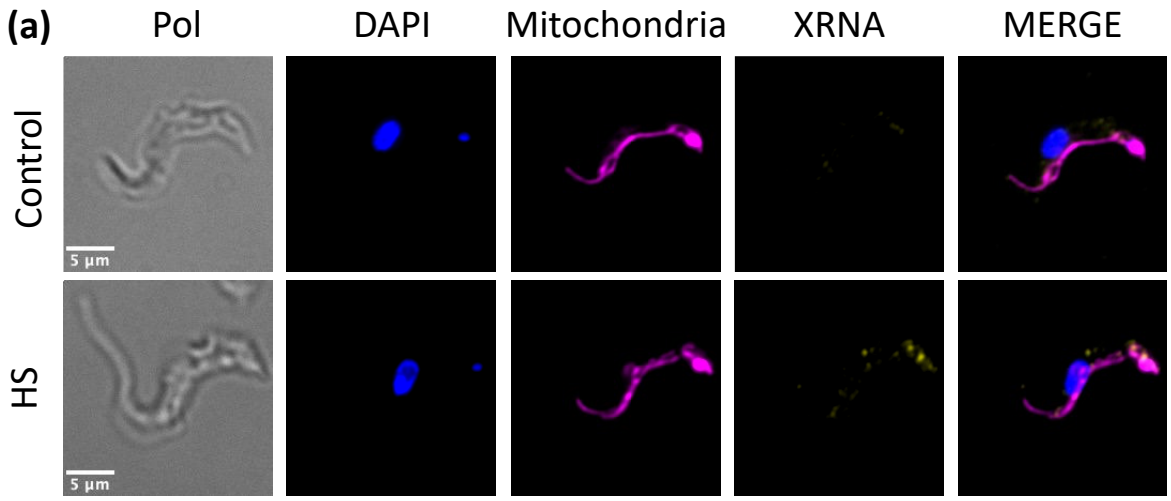

Figure 5.2 Microscopy Analysis of TbXRNA Localisation in *T. brucei* eYFP-TbXRNA Cell Line with Mitochondrial Staining Before and After Heat Shock. Microscopy images of T. brucei BSF eYFP-TbXRNA cell line before and after heat shock Cells from the eYFP-TbXRNA cell line were subjected to heat shock at 41 °C for 1 hour. For each slide, 5×10^5 cells were prepared, imaged using a DeltaVision Elite deconvolution microscope, and processed with ImageJ Fiji software. Cells were stained with MitoTracker to visualise the mitochondria, fixed with 4% paraformaldehyde (PFA), and stained with DAPI to visualise the nucleus and kinetoplasts. Images are presented for control (non-heat shocked) and immediately post-heat shock conditions. Each condition includes images under polarised light, DAPI staining, mitochondrial staining, YFP fluorescence (referred to as XRNA), and a merged image of DAPI, mitochondria, and YFP channels.

Fluorescence visualisation of the location and abundance of eYFP-TbXRNA in *T. brucei* cells, co-stained with MitoTracker to label the mitochondria, revealed a change of signal intensity and distribution following heat shock (Figure 5.2). In non-heat shocked cells, several weak YFP-TbXRNA foci are visible. These foci are typically located near the

kinetoplast at the posterior end of the cell or in the peri-nuclear region. The signal is of low intensity, suggesting a low abundance of eYFP-TbXRNA. There is no clear co-localisation with the mitochondria, however it was noted that foci were observed anterior to the kinetoplast, close to the predicted localisation of the flagella pocket. Immediately following heat shock there was an increase in the number and intensity of TbXRNA foci, suggesting that there is an increase in abundance of eYFP-XRA protein within these foci. Notably, after heat shock, the intensity of this signal increases in the posterior region of the cell body, and foci anterior to the kinetoplast are pronounced. This may suggest that these loci are positioned close to the flagellum pocket. These observations indicate that heat shock induces a notable reorganisation of TbXRNA within the cell, concentrating in specific foci and altering its spatial relationship with cellular landmarks like the mitochondria. Further studies are needed to confirm these findings and elucidate the mechanisms driving TbXRNA re-localisation during heat shock.

5.2.3. Heat shock triggers altered localisation and intensity of PABP1-sfGFP

Fluorescence microscopy was utilised to observe the localisation and abundance of sfGFP-tagged PABP1 in *T. brucei* cells following heat shock (Figure 5.3). Samples were collected prior to heat shock, and at 0-, 2-, 4-, 6-, 8-, and 24-hours post treatment (Figure 5.3 below).

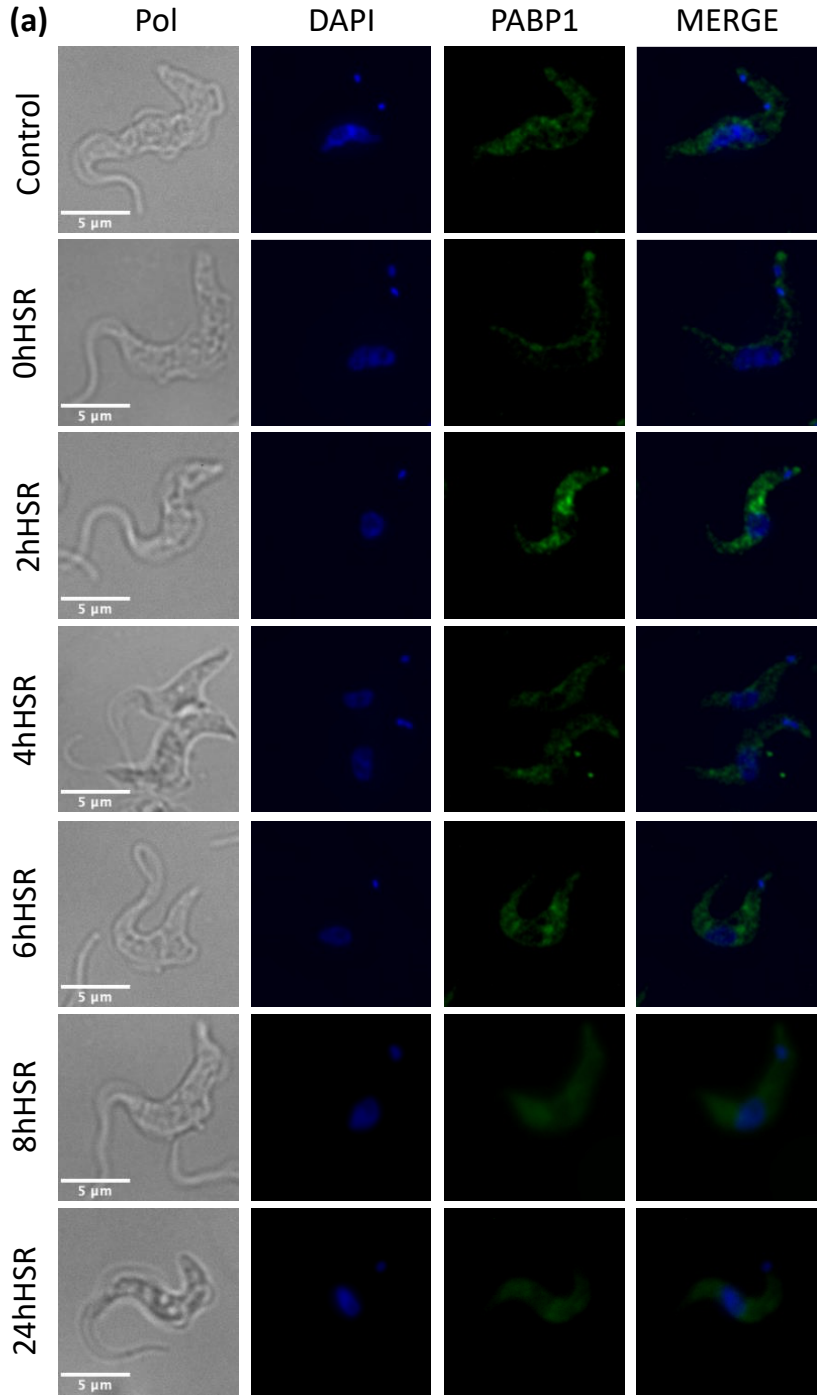

Figure 5.3 Time-Course Analysis of PABP1 Localisation in *T. brucei* BSF PABP1-sfGFP Cell Line Following Heat Shock. Cells from the PABP1-sfGFP cell line were subjected to heat shock at 41 °C for 1 hour. Microscopy samples were prepared immediately post-heat shock and at subsequent intervals (2, 4, 6, 8, and 24 hours) to monitor changes in PABP1 localisation and abundance. For each slide, 5×10^5 cells were prepared, imaged using a DeltaVision Elite deconvolution microscope and edited with ImageJ Fiji software. Cells were fixed with 4% paraformaldehyde (PFA) and stained with DAPI to visualise the

nucleus and kinetoplasts. Images are presented for each timepoint, including a control sample (non-heat shocked). Each condition includes images under polarized light, DAPI staining, GFP fluorescence (indicating PABP1), and a merged image of DAPI and GFP channels.

Fluorescence microscopy visualisation of sfGFP-PABP1 indicated that under standard growth conditions sfGFP-PABP1 localisation is dispersed across the cytoplasm in a punctate pattern. It was noted that some regions exhibited greater signal intensity, particularly in the perinuclear region. Comparatively, immediately following heat shock, this signal becomes polarised to one side of the cell periphery, accompanied by a defined granule at the posterior end of the cell. Within 2-hours of the heat shock recovery, sfGFP-PABP1 signal intensity increases across the cell body, with a central focus of signal posterior to the nucleus. Signal intensity following this, from 4-hours to 24-hours post heat shock results in an overall decrease in sfGFP-PABP1 intensity across the cell body, with discrete foci no longer visible by 8-hours post-heat shock. This distribution remains consistent until 24-hours. To build on this data, this cell line was interrogated further by performing a co-localisation assay.

5.2.4. Regions of high sfGFP-PABP1 signal intensity may co-localise with the mitochondria after heat shock

To further investigate the localisation of PABP1 in *T. brucei* and the effects of different durations of heat shock, microscopy samples were prepared from control (non-heat shocked) cells and cells subjected to heat shock at 41 °C for 0.5-, 1-, and 2-hours. In addition to DAPI staining for the nucleus and kinetoplasts, MitoTracker was used to label the mitochondria, providing an additional cellular landmark for comparison enhancing the analysis of PABP1 localisation. Samples were taken periodically across the 2-hour heat shock timeframe and processed immediately without recovery, targeting a timeframe which had been identified previously as having the highest signal intensity.

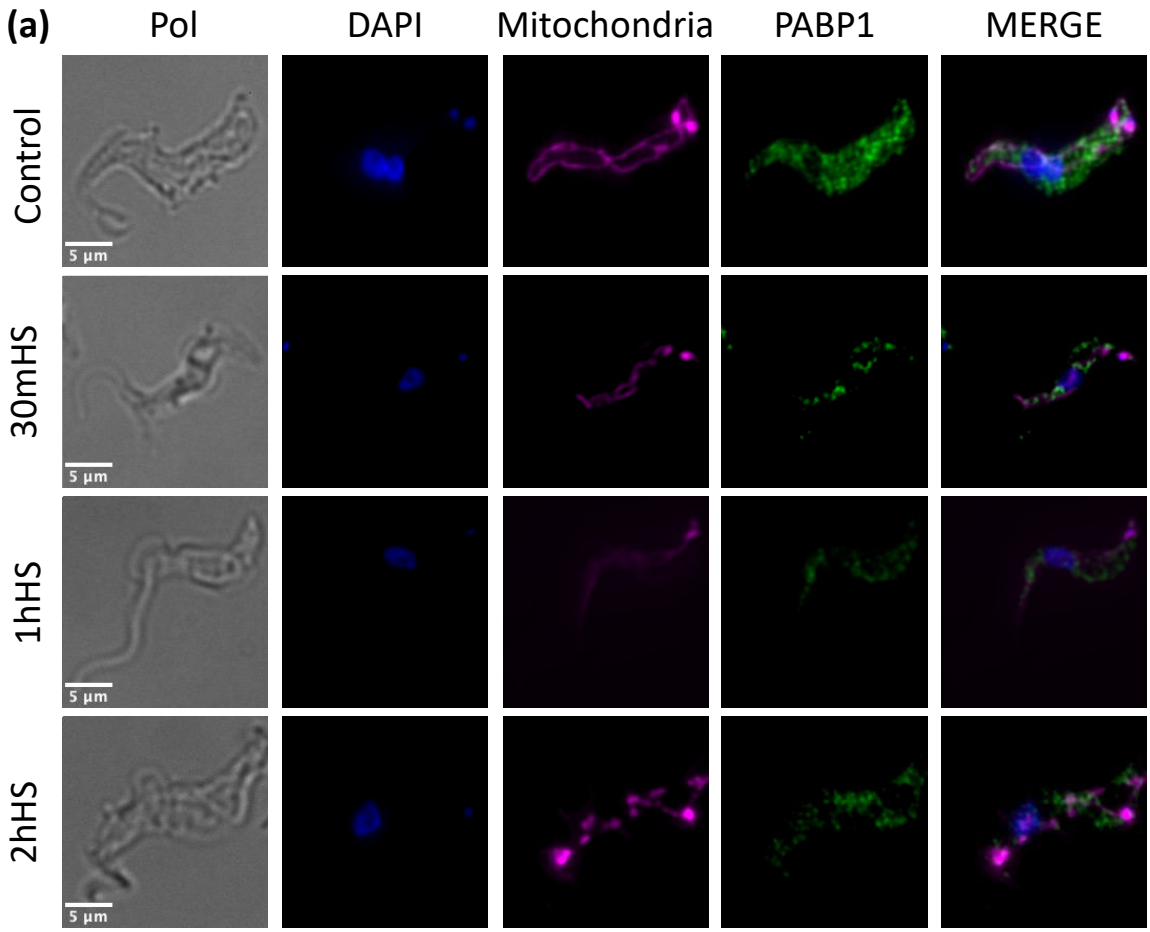

Figure 5.4 Microscopy Analysis of PABP1 Localisation in *T. brucei* PABP1-sfGFP Cell Line with Mitochondrial Staining Before and After Heat Shock. Microscopy images of T. brucei BSF PABP1-sfGFP cell line before and after heat shock. Cells from the PABP1-sfGFP cell line were subjected to heat shock at 41 °C for either 0.5, 1, or 2 hours. For each slide, 5×10^5 cells were prepared, imaged using a DeltaVision Elite deconvolution microscope, and processed with ImageJ Fiji software. Cells were stained with MitoTracker to visualise the mitochondria, fixed with 4% paraformaldehyde (PFA), and stained with DAPI to visualise the nucleus and kinetoplasts. Images are presented for control (non-heat shocked) and immediately post-heat shock conditions. Each condition includes images under polarised light, DAPI staining, mitochondrial staining, GFP fluorescence (indicating PABP1), and a merged image of DAPI, mitochondria, and GFP channels.

In non-heat shocked cells, as previously observed, PABP1-sfGFP signal is mostly evenly dispersed across the cytoplasm, with some areas of speckling indicating higher

concentrations. A few of the areas of higher concentration at the posterior end of the cell are co-localised with the mitochondria. However, immediately post a 0.5-hour heat shock, PABP1-sfGFP signal is localised in discrete foci (stress granules) across the cytoplasm. A high proportion of these foci are adjacent but not co-localised to the mitochondria. Following this, the 1-hour of heat shock condition affirms previous data that PABP1-sfGFP signal is localised in discrete foci (stress granules) polarised to one side of the cell periphery opposite to the mitochondria. Contrastingly with the 1-hour heat shocked cells, 2-hour heat shocked cells in fact exhibit a decrease in discrete PABP1-sfGFP foci (stress granules) across the cytoplasm. A high proportion of these foci are co-localised with the mitochondria. These observations indicate that heat shock induces dynamic changes in the localisation of PABP1 in *T. brucei*, with the formation of stress granules and significant co-localisation with mitochondria. The pattern of PABP1 localisation appears to change with the duration of heat shock, suggesting a complex response mechanism that may involve mitochondrial interaction. Further studies are necessary to elucidate the functional implications of these localisation patterns.

5.3. Heat shock triggers altered localisation and intensity of TbDHH1

Following the behavioural analysis of TbPABP1 and TbXRNA further characterisation of changes in TbDHH1 was carried out. TbDHH1 is a known marker for P-bodies in *T. brucei*. Previous studies on PCF *T. brucei* demonstrated that TbDHH1 co-localises with TbXRNA in cytoplasmic foci, which increase in number upon heat shock (Kramer et al., 2013). TbDHH1 therefore offers a valuable comparator with TbXRNA. To further investigate the role and behaviour of TbDHH1 in BSF *T. brucei* under heat shock stress, a previously generated mSt-TbDHH1 BSF cell line, which underwent preliminary investigation, was utilised (Aelmans, 2022).

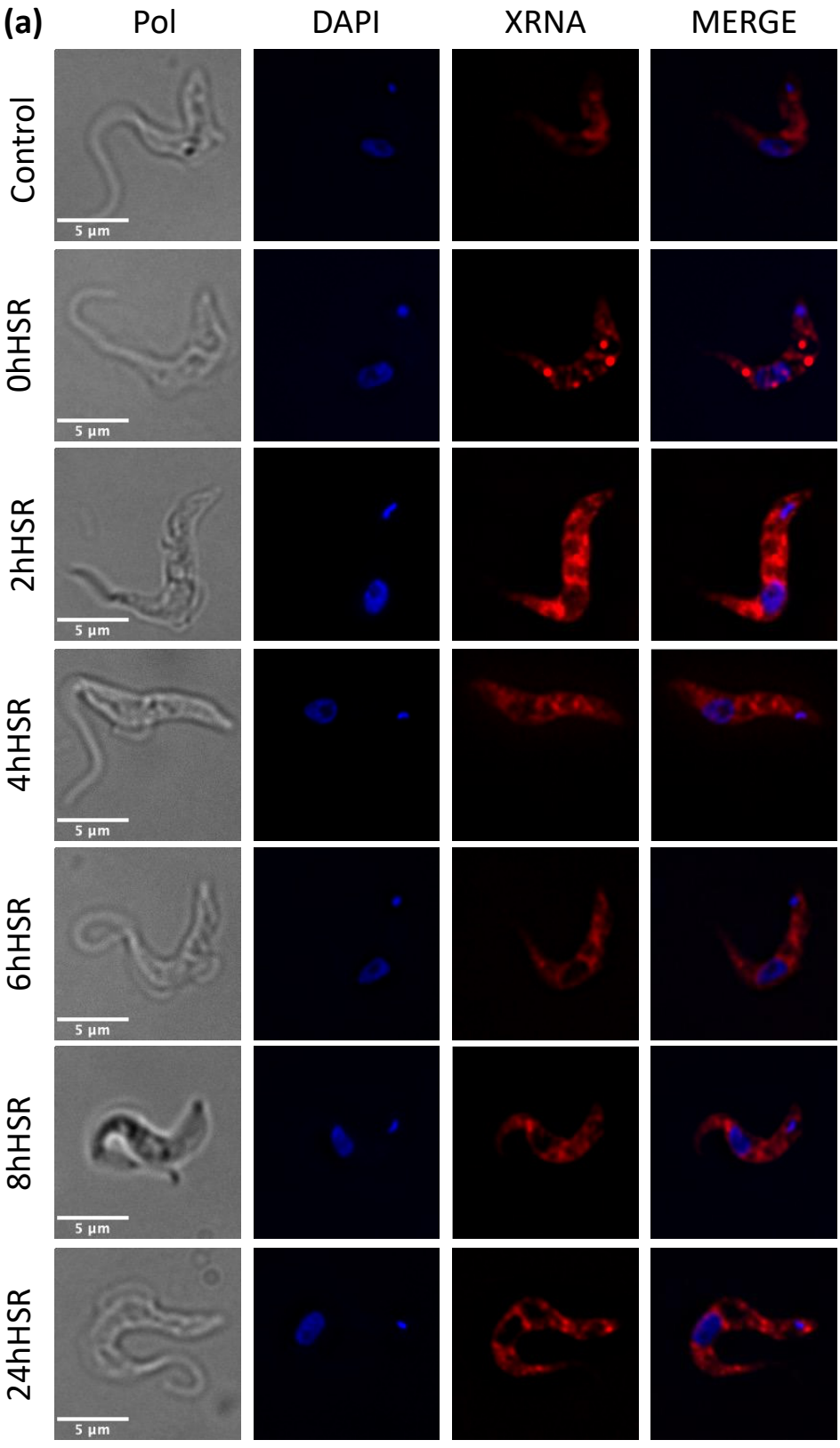

Figure 5.5 Time-Course Analysis of TbDHH1 Localisation in *T. brucei* mSt-TbDHH1 Cell Line Following Heat Shock. Cells from the mSt-TbDHH1 cell line were subjected to heat shock at 41 °C for 1 hour. Microscopy samples were prepared immediately post-heat

shock and at subsequent intervals (2, 4, 6, 8, and 24 hours) to monitor changes in TbDHH1 localisation and abundance. For each slide, 5×10^5 cells were prepared, imaged using a DeltaVision Elite deconvolution microscope and edited with ImageJ Fiji software. Cells were fixed with 4% paraformaldehyde (PFA) and stained with DAPI to visualise the nucleus and kinetoplasts. Images are presented for each timepoint, including a control sample (non-heat shocked). Each condition includes images under polarized light, DAPI staining, mStrawberry fluorescence (referred to as DHH1), and a merged image of DAPI and mStrawberry channels.

The data shown below first highlights that in non-heat shocked cells, TbDHH1-mStrawberry signal is weak with very few foci observed across the cytoplasm. Contrastingly, immediately after heat shock, there is an increase in TbDHH1 signal, with localisation to large, bright, discrete foci, and numerous lower intensity foci distributed throughout the cytoplasm. This signal then further increases, showing a higher number of intense foci across the cytoplasm at 2-hours. By 4-hours post-heat shock, the signal significantly reduces, displaying a weaker, more diffuse cytoplasmic distribution with minimal discrete foci. Surprisingly, this signal did not remain at a low intensity, but increased again by 8-hours, with a more pronounced localisation to discrete foci, before further increasing until 24-hours.

5.4. Summary

This chapter investigated the localisation and dynamics of proteins in BSF *T. brucei* under heat shock conditions, utilising fluorescently tagged cell lines generated in Chapter 4. The findings revealed that proteins involved in the heat shock response, particularly eYFP-TbXRNA and PABP1-sfGFP, undergo significant reorganisation upon exposure to heat. eYFP-TbXRNA was observed to relocate from a dispersed cytoplasmic distribution to distinct foci, indicating a possible shift towards P-bodies, particularly within the peri-nuclear regions and the posterior end of the cell. Similarly, PABP1-sfGFP showed a pronounced polarisation and localisation changes, suggesting its role in stress granule dynamics post-heat shock. Additionally, the characterisation of TbDHH1

indicated a complex response, with fluctuations in its localisation correlating with the stress duration. Collectively, these observations highlight the intricate mechanisms by which *T. brucei* modulates protein localisation in response to heat shock, providing valuable insights into the cellular stress response pathways.

6. Characterisation of heat-induced transcriptional changes in African trypanosomes

6.1. Introduction

Gene regulation in *Trypanosomes* is predominantly controlled post-transcriptionally due to the polycistronic nature of their transcription. This regulation is crucial for modulating gene expression, particularly in response to environmental stress such as heat shock. Previous studies have shown that exposure to 41 °C in *T. brucei* leads to global mRNA degradation and a suppression of translation for some mRNAs, while others escape this heat-induced suppression (Kramer et al., 2008). Additionally, VSG RNAi has been observed to induce similar growth arrest phenotypes similar to those seen after heat shock (Sheader et al., 2005). To elucidate the behaviour of heat shock-responsive proteins, we employed RNA extraction, cDNA synthesis, and qPCR to quantify changes in mRNA levels of known heat shock proteins (HSPs) and variant surface glycoproteins (VSGs). This section of the study aims to provide insights into the temporal dynamics of mRNA production under heat shock and its potential correlation with protein expression and cell cycle changes. This analysis was carried out in both *T. brucei* and *T. congolense* providing novel insight into changes upon heat shock and throughout recovery. Comparative analysis between *T. brucei* and *T. congolense* offers valuable insights into species-specific differences in heat shock response and recovery.

6.2. *T. brucei* mRNA levels exhibit both transient and multiphasic temporal changes due to heat shock

To interrogate whether the mRNA levels of proteins involved in the heat shock response are affected by heat shock, several markers known to be integral to this stress response pathway, were chosen for monitoring. The selected markers included HSP40, HSP70, HSP83, HSP100, and HSP110, as well as two primer sets for VSG2 in *T. brucei* denoted as

VSG2 (Wiedemar et al., 2019) and VSG221 (Black et al., 2020)and finally one set for VSGIL3000 in *T. congolense* (Eyford et al., 2011).

.

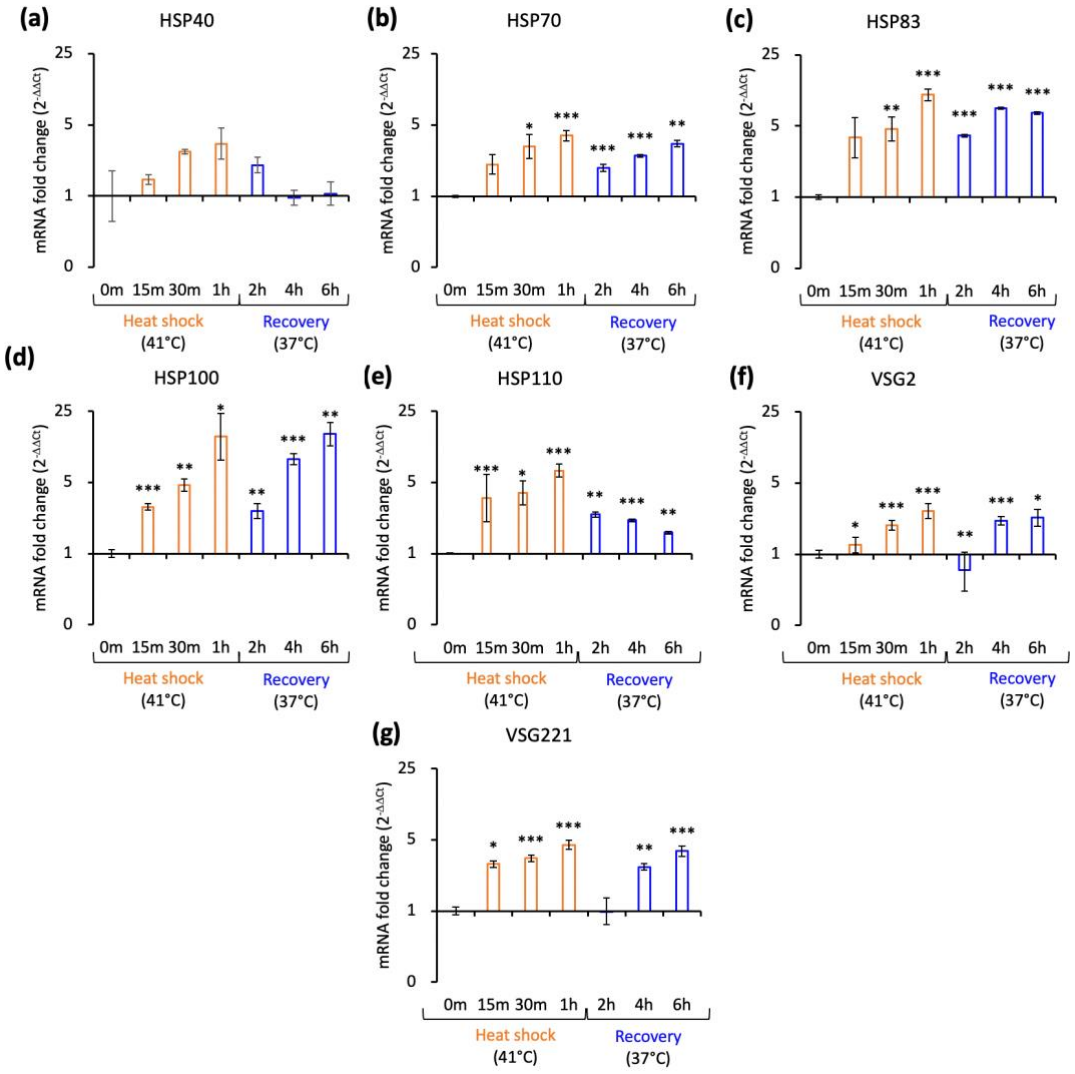

Figure 6.1 Analysis of mRNA Fold Change in Heat Shock Proteins and VSGs in BSF T. brucei During Heat Shock and Recovery. The analysis involved examining mRNA fold changes in T. brucei BSF under heat shock conditions (41 °C) and subsequent recovery at normal culture temperature (37 °C). The target genes include various heat shock proteins (TbHSP40, TbHSP70, TbHSP83, TbHSP100, TbHSP110) and variant surface glycoproteins (TbVSG2 and TbVSG221). The fold change, scaled to log-base-2, represents the expression of the target gene mRNA relative to non-heat-shocked control group, at different time points: 0 minutes (control, non-heat shocked), 15 minutes, 30 minutes, and 1 hour during heat shock, and 2 hours, 4 hours, and 6 hours during

recovery. Results were normalised against an Actin reference gene, with 5×10^6 cells per condition, scale bars are ± standard deviation, where n=3. P-values were categorised as follows: $p < 0.05$ (*), $p < 0.01$ (**) and $p < 0.001$ (***).

TbHSP70, TbHSP83, TbHSP100, TbVSG2, and TbVSG221 displayed variable multiphasic responses, typically characterised by a rapid induction during heat shock followed by a decline and then a secondary increase during recovery. During heat shock TbHSP70 mRNA levels increased gradually with a rapid onset, peaking at almost 4-fold higher than the control by the end of the 1-hour heat shock. By 2 hours of recovery, levels decreased significantly, but remained elevated in comparison to control population, followed by a resurgence, reaching above 3-fold higher than the control by the final 6-hour recovery time point (Figure 6.1, b). This trend is also exemplified strongly in the case of TbHSP100, where mRNA levels significantly increased during heat shock, peaking at average of 14-fold higher than the control by the end of the 1-hour heat shock. By 2 hours of recovery, levels decreased significantly, but also remained elevated in comparison to control population, followed by a resurgence, reaching around 15-fold higher than the control by the final 6-hour recovery time point, (Figure 6.1, d). Interestingly, TbHSP83 also exhibited a similar multiphasic response as TbHSP70 and TbHSP100, with the exception of the 6-hour recovery timepoint where levels exhibited a slight decrease from the 4-hour recovery timepoint resurgence. This is notable as it was unique among proteins exhibiting a multiphasic response to exhibit a decrease in mRNA fold change after the secondary increase, during the measured recovery period.

Interestingly, the mRNA levels for both TbVSG2 proteins (TbVSG2 and TbVSG221) increased gradually during heat shock, reaching peaks of over 3.5-fold and 4-fold, respectively, by the end of the 1-hour period. This is notable, as most mRNA levels are expected to decrease during heat shock; however, TbVSG2 appears to exhibit a similar upregulation pattern to that of heat shock proteins. Contrastingly, by 2 hours of heat shock recovery, TbVSG2 and TbVSG221 mRNA decreased to below or to a similar level as the untreated control respectively. Both TbVSG2 and TbVSG221 mRNA levels

experienced a resurgence reaching above 2-fold higher and just below 4-fold higher than the control respectively, by the final 6-hour recovery time point.

In contrast to proteins exhibiting a multiphasic response, two proteins, TbHSP40, and TbHSP110 exhibited more of a transient response in mRNA fold change following heat shock. Although mRNA fold change increased steadily in these groups over the timeframe of heat shock, both TbHSP40 and TbHSP110 exhibited steadily declining fold change values across the recovery period. In the case of TbHSP40 mRNA levels gradually increased over heat shock peaking at 3-fold higher than the control by the end of the 1-hour heat shock. Over recovery levels gradually declined, returning to near control levels by 6 hours (Figure 6.1, a). Similarly, TbHSP110 mRNA levels initially increased gradually during heat shock, with the addition of an accelerated increase before peaking at approximately 6.5-fold at the end of the 1-hour of heat shock. Over recovery levels gradually declined but remained above control levels by the 6-hour recovery timepoint (Figure 6.1, e).

6.3. *T. congolense* mRNA levels exhibit both transient and multiphasic temporal changes due to heat shock

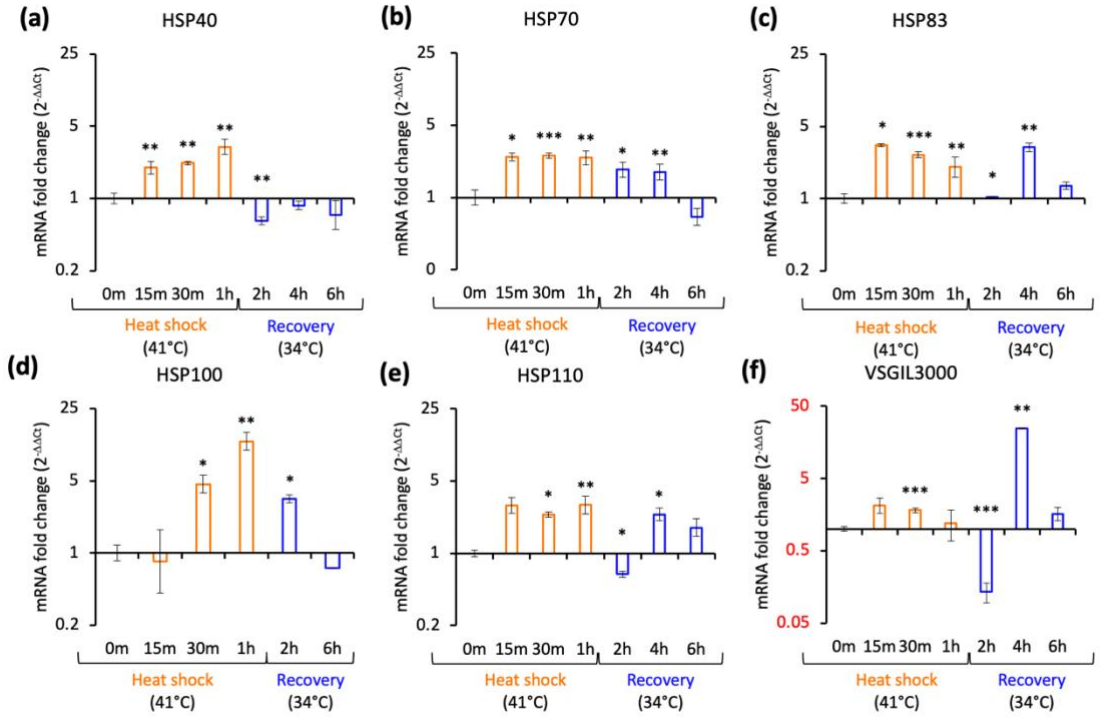

Figure 6.2 Analysis of mRNA Fold Change in Heat Shock Proteins and VSG in BSF T. congolense During Heat Shock and Recovery. The analysis involved examining mRNA fold changes in T. congolense BSF under heat shock conditions (41 °C) and subsequent recovery at normal culture temperature (34 °C). The target genes include various heat shock proteins (TcoHSP40, TcoHSP70, TcoHSP83, TcoHSP100, TcoHSP110) and variant surface glycoprotein TcoVSGIL3000. mRNA levels were quantified using qPCR, with actin used as a control. The fold change, scaled to log-base-2, represents the expression of the target gene mRNA relative to non-heat-shocked control group (set to 1) at different time points: 0 minutes (control, non-heat shocked), 15 minutes, 30 minutes, and 1 hour during heat shock, and 2 hours, 4 hours, and 6 hours during recovery. Results were normalised against an Actin reference gene, with 5 × 10^6 cells per condition, scale bars are ± standard deviation, where n=3. P-values were categorised as follows: p <0.05 (*), p<0.01 (**) and p <0.001 (***).

In *T. congolense* mRNA changes were more dynamic, with some similarities and differences in overall temporal patterns compared to *T. brucei*. In comparison with *T.*

brucei changes in HSP70 mRNA levels, TcoHSP70 mRNA levels appeared to show a more transient trend, notably the initial peak occurred much faster reaching levels 2.5-fold higher than the control by 30 minutes into heat shock. On average by 1 hour of heat shock levels had fallen slight amounts. During recovery levels decreased gradually before plummeting below levels of the control at the final 6-hour recovery time point (Figure 6.2, b). Notably, TcoHSP83 mRNA levels exhibited a dramatic immediate increase, peaking after just 15 minutes to above 3-fold higher than the control, before gradually decreasing throughout the next 45 minutes of heat shock. During initial recovery, levels had continued to decrease but were followed by a resurgence to above 3-fold higher by 4 hours post heat shock. This level declined but remained slightly elevated from the control by 6 hours similarly, to *T. brucei* this also suggests a multiphasic response to heat shock however the manifestation of the two are somewhat dissimilar **(**Figure 6.2, c).

Contrastingly, TcoHSP100 mRNA levels initially decreased during the first 15 minutes of heat shock followed by an accelerated increase during the remainder of it peaking at approximately 6.5-fold at 1 hour of heat shock. During recovery, levels decreased gradually reaching levels below the control by 6 hours post heat shock. Similarly, to *T. brucei* this also suggests a multiphasic response to heat shock however manifestation of the two are drastically dissimilar (Figure 6.2, d). TcoHSP40 mRNA levels showed a transient gradual increase similar to that seen in *T. brucei*. At 1 hour of heat shock mRNA levels peaked at above 3-fold higher than the control. During recovery, mRNA levels rapidly declined, falling below control levels by 2 hours and with variation remained there for up to 6 hours post heat shock, indicating an immediate but overall transient increase to heat shock (Figure 6.2, a).

TcoHSP110 mRNA levels displayed a much more dynamic multiphasic response to heat shock compared with *T. brucei*. Initially TcoHSP110 mRNA levels increased rapidly during heat shock, reaching just under a 3-fold increase in the first 15 minutes of heat shock, however on average this dropped slightly by 30 minutes, returning similar levels by 1 hour of heat shock. During recovery, levels decreased significantly, falling below levels of the control at 2 hours, before resurging to levels 2.5 higher than the control by 4

hours, followed by a final decrease by 6 hours post heat shock to levels still elevated 2-fold higher than the control, suggesting a prolonged dynamic response to heat shock (Figure 6.2, e).

Finally, the VSG ortholog in *T. congolense,* TcoVSGIL3000**,** displayed an unusual trend in mRNA levels. During the first 15 minutes of heat shock there was an initial increase to above 2-fold higher than the control, these levels fell slightly after 30 minutes after and further by 1 hour of heat shock. During recovery, levels fell significantly below the control by 2 hours, followed by a dramatic resurgence to almost 25-fold by 4 hours, then falling dramatically to levels slightly elevated from the control by 6 hours post heat shock, suggesting a drastically variable multiphasic response to heat shock (Figure 6.2, f). The mRNA fold change analysis revealed distinct temporal patterns of heat shock protein and VSG gene expression in response to heat shock and recovery.

In summary TcoHSP40 and HSP70 mRNA displayed a more transient response to heat shock with initial increases that declined throughout the time course, whereas TcoHSP83, TcoHSP100, TcoHSP110 and TcoVSGIL3000 mRNA displayed varying multiphasic responses with multiple periods of increase and decline. These findings provide deeper insights into the molecular mechanisms of the heat shock response in *T. brucei* and *T. congolense* highlighting the complexity and dynamic nature of gene regulation in these organisms.

6.4. Chapter Summary

This chapter explores mRNA production responses of *Trypanosoma brucei* and *Trypanosoma congolense* to heat shock, highlighting the significance of post-transcriptional gene regulation. Comparative analysis between *T. brucei* and *T. congolense* revealed both similarities and distinct differences in their transcriptional responses to heat shock, emphasising species-specific regulatory mechanisms. Overall, the chapter provides novel insights into the complex transcriptional regulation of heat

shock responses in trypanosomes, highlighting the adaptive mechanisms these parasites employ in response to environmental stressors.

7. Discussion

7.1. Growth Recovery

Investigations into the growth recovery of *Trypanosoma* spp. following heat shock revealed distinct, temperature- and time-dependent responses. These findings partially align with previous research, particularly regarding *T. brucei.* As discussed throughout Section 3, BSF *T. brucei* exhibited a transient growth lag following short term heat shock exposure (0.5 hours), with no long-term detrimental effects observed across the time course of study. However, 1 hour heat shock effects were more pronounced and prolonged aligning with the effects observed in other studies under similar conditions (Kramer et al., 2010, Ooi et al., 2020). Prolonged exposure to heat shock (2-hours) resulted in significant and potentially irreversible growth impairment, indicating that *T. brucei* BSF may possess a thermal tolerance threshold beyond which cellular damage may be too severe for recovery. These findings corroborate those reported by Ooi et al. (2020), which similarly identified heat shock duration as a key factor in determining the extent of cellular damage and the potential for recovery, in line with a conserved mechanism of thermal tolerance across eukaryotic organisms and cell types (Mahat et al., 2016; Velichko et al., 2013). Notably, our observation that a 1-hour exposure to 41°C induces a reversible heat shock response without causing irreversible damage highlights the importance of optimising heat shock duration in experimental designs to avoid confounding effects of cell death on subsequent analyses. To our knowledge, no research has explored the effects of heat shock beyond 2 hours, presenting an opportunity for future investigation. This work underscores the significance of heat shock duration as a critical determinant of cellular recovery and survival.

Comparatively, PCF *T. brucei* displayed a similar trend in response to heat shock, albeit with a slower recovery rate following short to mid-length treatments. This slower

recovery in PCF could be indicative of a more complex response mechanism to thermal shock, possibly due to the environmental conditions encountered by this form in the tsetse fly, where fluctuating temperatures are common (Edney and Barrass, 1962). However, it is important to note that our findings diverge significantly from those reported by Kramer et al. (2010), who observed that a 2-hour heat shock did not result in the same level of detrimental effects in PCF and reported much faster recovery times across all conditions compared to what has been observed here. This discrepancy may be attributed to differences in experimental design, particularly in temperature measurement. While this study used a calibrated thermometer, Kramer's study may have relied on a less accurate thermometer or a less stable water bath for conducting the heat shock.

While timeframes of study differ greatly between this work and that of Kramer and colleagues (2010), examination of growth curves between 0-, and 48-hours of both datasets present significant discrepancies. This is most notable in the 2-hour heat shock populations. While Kramer's cells exhibit "negative" movement, indicative of initial cell death, these cells still rapidly resume a profile of growth not far removed from the exponential growth seen in the respective control population. Contrastingly, the work presented in Figure 3.3 of this thesis shows a prolonged growth lag up to 8-hours of recovery, followed by a significant die-off event. These events precede a plateau of non-dividing cells up to 72-hours post-recovery. The key difference between the two experimental designs discussed here, is the stage of growth at which cells were sampled and exposed to heat shock conditions. While Kramer and colleagues utilised PCF *T. brucei* cells grown to 1×10^6, corresponding with late-lag phase, just prior to log-phase, results presented in this thesis reflect the response of a mid-log population. This discrepancy suggests that thermo-tolerance may be determined at the population level, rather than the level of individual cells. This has many implications, although nutrient availability may be greater prior to log-phase, there are also obvious differences in cell cycle phase distribution with greater numbers of cells progressing through the cell cycle. Furthermore, this could speak to something akin to a quorum sensing pathway, as has been widely reported in the BSF *T. brucei* differentiation response (Rojas et al., 2019). Finally, this may reflect population dynamics within and throughout the internal system

of the tsetse fly, where temperature changes are common (Edney and Barrass, 1962). These differences highlight the need for further investigation to reconcile these findings and better understand why population density impacts the ability of cells to progress through the cell cycle.

Moving on to the less studied *T. congolense*, findings outlined in this body of work contradicted what might be anticipated based on its lower optimal growth temperature of 34 °C. Despite this, the *T. congolense* IL3000 strain did not exhibit a severe growth arrest in response to heat shock, particularly when compared to *T. brucei* BSF and PCF. This unexpected resilience could be attributed to the unique characteristics of the IL3000 strain, which is the only lab adapted *T. congolense* strain and aberrantly grows at 34 °C, despite optimal growth in vivo at around 37 °C. As such, these findings may not be directly applicable to strains in the field. Furthermore, due to growth in goat serum rather than bovine serum a key nutritional parameter diverges between *T. congolense* and *T. brucei* within the experimental parameters utilised in this project. The discrepancy between the expected and observed heat shock response may be due to the strain's adaptation to its non-typical culture conditions, which might enhance overall fitness in the culture, thereby enhancing thermal tolerance. Additionally, research has shown that cows' rectal temperatures can exceed 41 °C during fever (Bianca, 1962), suggesting that while *T. brucei* shares the same host range, *T. congolense* may be better adapted to survive under more extreme conditions than those simulated in this experimental design. Previously collected data by Aelmans (2022) indicate that a 42 °C heat shock in *T. congolense* is more effective as a stimulus to phenocopy the fitness cost seen in *T. brucei,* a finding that warrants further investigation. It is well established within the research community that specific adaptations per species or strain are necessary to facilitate optimal and translational growth and fitness. For example, the need for Hemin supplementation in PCF *T. brucei*, and urine for some varieties of Leishmania spp. (Chanmol et al., 2022) illustrates the importance of tailored culture conditions.

7.2. Cell Cycle Disruptions

Our investigation into the effects of heat shock on the cell cycle of *Trypanosoma brucei* revealed significant disruptions, particularly in the BSF of the parasite. After a 1-hour heat shock, BSF *T. brucei* exhibited a marked accumulation of cells in the G2/M phase during recovery. This accumulation suggests that while DNA replication occurs, there may be a disruption to cytokinesis. This was corroborated by nucleus and kinetoplast counts previously generated in the Urbaniak lab, which showed that heat-shocked cells became transiently arrested in a pre-cytokinesis/post-mitosis state (Aelmans, 2021). This phenotype contrasts with the expected behaviour of BSF cells which lack a specific a G2/M checkpoint, regulating mitosis and cytokinesis, although the disruption of other processes such as flagellum elongation and assembly can interfere with both processes (Landfear, 2006; Broadhead et al., 2006). As such, barring significant disruptions to cleavage furrow formation, *T. brucei* BSF should complete the cell cycle despite mitosis being compromised, without experiencing the delays observed in this study (Zhou et al., 2022). Therefore, these data imply that the detrimental effects of heat shock may not target the mitotic process but could interfere with putative pathways or their components which are critical to successful cell division (Zhang et al., 2019). Notably, despite the accumulation of 2K2N cells, monster cells were not observed within the population, which indicates a striking lack of cytokinesis initiation compared to phenotypes due to the loss of CIF proteins which are integral to cleavage furrow formation (Zhang et al., 2019). This contrasts with phenotypes arising from more specific single-defect issues. Finally, it has been noted in *Leishmania donovanii (L. donovanii)* that some cell-cycle regulating cyclin-like proteins regulate cell cycle progression, such as the *Ld*Cyc1 complex which governs S-phase transition. Importantly, this complex is non-heat labile remaining stable under elevated temperatures and suggesting a putative subset of cell-cycle regulating proteins capable of withstanding heat shock (Banerjee et al., 2006).

Conversely, in PCF *T. brucei*, the response to heat shock did not result in a similar G2/M phase accumulation. Instead, there was an increase in cells classified as <G1, known as zoids, which lack nuclear DNA. This observation is unexpected because in PCF, interference with mitosis typically activates a checkpoint that prevents cytokinesis, leading to a cell cycle delay, and the accumulation of “monster” or zoid cells (Kumar & Wang, 2006). The absence of this delay in PCF after heat shock indicates that the

disruption might occur at a different stage or process, not directly related to the core mitotic machinery. A review of previous data collected by Aelmans (2021) identified an increase in 2K1N cells immediate after heat shock, with a further significant increase at 4-hours after treatment. This indicates that there may be a delay between S-phase initiation the entry to G2. Aligning with this by 5-hours post treatment there is a marked rise identified in 2K2N cells, suggesting a sudden progression into G2M. Therefore, this likely suggests that the population stalls briefly after kinetoplast elongation, although no defect in flagellum numbers is identified. This finally suggests that the delay in kinetoplast division could be due to changes in the speed of flagellum assembly prior to reaching the requisite 0.6 of cell body length to trigger kinetoplast division (Briggs et al., 2004).

Given the complexity of mitosis and the numerous factors that regulate it—including proteins acting as activators and repressors under varying environmental conditions—it is plausible that heat shock selectively affects certain mitotic components, leading to downstream effects that manifest differently in BSF and PCF. One potential explanation for the G2/M arrest observed exclusively in BSF is the involvement of Variant Surface Glycoprotein (VSG) synthesis. This arrest phenotype resembles the pre-cytokinesis arrest observed in previous studies, where RNAi targeting VSG led to a similar cell cycle profile (Sheader et al., 2005). This raises the question of whether VSG synthesis continues after heat shock or is reduced, potentially triggering the observed arrest, which does not appear to be the case. VSGs are expressed from the expression site body (ESB), a specialised region within the nucleus responsible exclusively responsible for the translation of the single active VSG (Navarro & Gull, 2001). In line with this, we observed an upregulation of VSG mRNA levels following heat shock, suggesting that VSG transcription is enhanced (López-Escobar et al., 2022). Developing on this, results presented in Figure 6.1 of Section 6.2, show increased mRNA levels of VSG2 in *T. brucei.* While it is unlikely it is uncertain whether there are additional VSGs being transcribed and if they are detectable within/on the cell, this data is still striking in terms of the effect of heat shock on a key aspect of *Trypanosome* biology. Increased VSG mRNA production likely represents the cells attempt to evade the immune response of fever and possibly reflects the need to replenish misfolded or degraded VSG, due to heat stress.

Throughout the parasite's lifecycle, VSGs are constantly endocytosed and recycled, a process requiring transport through endosomes and the Golgi apparatus. Heat shock could potentially disrupt these organelles, leading to a bottleneck in the recycling process or the intracellular accumulation of VSGs. Supporting this hypothesis, studies on the transport receptor protein ERGIC-53 in mammalian cells have shown that heat shock can disrupt normal recycling pathways, leading to protein accumulation within the cell (Spatuzza et al., 2004). The intracellular transport protein ERGIC-53, which is well conserved in *T. brucei*, is involved in the intracellular transport of specific glycoproteins, suggesting a potential parallel in *T. brucei*, where a similar disruption could impact VSG transport and processing (Nihei and Nakanishi, 2021; Spatuzza et al., 2004). While the early divergence of trypanosomes has led to significant differences in basic cell biology comparatively to other eukaryotes, many pathways remain conserved in both their function and elements of their composition, therefore ERGIC-53 may speak to an underlying cause for the defects associated with heat shock in *T. brucei.* Further investigation into the effects of heat shock on these pathways in *T. brucei* could provide valuable insights into the specific mechanisms disrupted by thermal stress.

7.3. Stress granule and P-body formation

When examining the behaviour of the stress granule protein PABP1 after heat shock in both BSF and PCF *T. brucei*, clear similarities were observed. In BSF cells at the typical growth temperature of 37 °C, PABP1 signal was predominantly dispersed throughout the cytoplasm, with a slightly higher concentration in the perinuclear region. This finding aligns with previous work by Kramer and colleagues (2008), who observed that in PCF cells at their normal growth temperature of 27°C, PABP1 was also diffusely distributed across the cytoplasm, with subtle perinuclear elevations. The reproducibility of localisation dynamics was encouraging in light of the use of CRISPR-Cas9 (which can be a more efficient method to engineer fusion proteins), as well as dual-tagging of both N- and C-termini, suggesting neither change resulted in aberrant protein dynamics. Upon heat shock at 41 °C, PABP1 in both BSF and PCF localised to granules along the cell

periphery, with a particularly prominent granule forming at the posterior end of the cell. Interestingly, the heat shock phenotype observed in PCF after 2 hours was more pronounced comparable to that seen in BSF after 1 hour, supporting the hypothesis of a more complex or robust heat shock response in the PCF stage of the parasite. Similar to the findings in PCF by Kramer et al. (2008), that formation of these stress granules was fully reversible with granules disappearing after 5-6 hours in PCF, after 6-8 hours in BSF the granules containing PABP1 had also disappeared.

The behaviour of P-body proteins TbXRNA and TbDHH1 in response to heat shock was also notably consistent across BSF and PCF stages. Kramer and colleagues (2008) observed a significant increase in P-bodies containing both TbXRNA and TbDHH1 in PCF cells after heat shock, with TbXRNA specifically forming a granule at the posterior pole that intensified under heat stress. Our study corroborated these findings in BSF cells, where similar increases in P-bodies and posterior TbXRNA granules were observed. Additionally, across both forms of the parasite, TbXRNA exhibited higher intensity localisations in the perinuclear region, underscoring its role in mRNA degradation. This perinuclear localisation likely indicates an increased demand for mRNA degradation near the nucleus, which could be a mechanism to rapidly remove misfolded or damaged mRNAs that accumulate due to heat shock. This localised degradation could also play a role in gene regulation during the stress response, ensuring that only essential mRNAs are translated under these conditions.

The formation of a specific TbXRNA granule at the posterior end of the cell suggests the presence of a specialised degradation zone for mRNAs associated with this region. Co-staining with MitoTracker revealed that this posterior granule might be localised near the flagellar pocket, a critical site for endocytosis and exocytosis in trypanosomes. Co-staining with MitoTracker did not reveal mitochondrial co-localisation but the added cellular landmark did suggest a close localisation to the flagellum pocket. Heat shock may disrupt the normal function of flagellar proteins, necessitating the selective degradation of their mRNAs to prevent the synthesis of defective proteins. This could suggest a broader role for TbXRNA in maintaining cellular homeostasis by targeting specific degraded mRNAs for exocytosis in response to environmental stress.

7.4. mRNA changes after HS

This study utilised qPCR analysis to investigate the dynamic changes in mRNA levels of heat shock proteins (HSPs) and VSGs in *T. brucei* and *T. congolense* across different phases of heat shock. The results revealed that some mRNAs exhibited a transient increase in response to heat shock, while others showed a multiphasic response, with multiple periods of upregulation and downregulation throughout the stress and recovery phases. These differing mRNA response patterns likely reflect the diverse roles of the encoded proteins and the complex regulatory mechanisms governing gene expression under stress conditions.

The transient mRNA response observed in certain genes suggests that these mRNAs are involved in the immediate stress response. Proteins encoded by these mRNAs are crucial for the initial mitigation of stress-induced damage but are not required for long-term recovery. As the acute phase of stress subsides, the mRNA levels decrease, likely due to rapid degradation mediated by post-transcriptional mechanisms such as mRNA decay pathways. This rapid turnover may help the cell conserve resources and prevents the unnecessary accumulation of stress-related proteins once the immediate threat has been managed.

In contrast, the multiphasic mRNA response, characterised by multiple peaks of expression over recovery time, suggests a more complex regulatory mechanism. This pattern likely reflects the cell's need to balance immediate stress responses with longer-term adaptation and recovery. mRNAs showing multiphasic responses may encode proteins involved in both immediate damage control and subsequent repair processes, although immediate responders may trigger cascade events with down-stream long-term recovery functions. Interestingly, the timing of these secondary peaks around the 4–6-hour mark could correlate with the dissolution of stress granules or P-bodies seen in this study, which are known to temporarily store mRNAs during stress. As these structures dissolve, stored mRNAs may be released, facilitating additional waves of protein synthesis necessary for cellular adaptation and the re-establishment of normal

functions. This release of stored mRNA could account for the observed secondary peak in HSP mRNA expression.

The regulatory mechanisms underlying these responses are likely distinct. Transient responses may involve straightforward regulation, where mRNAs are quickly transcribed and then degraded. In contrast, multiphasic responses suggest the involvement of more complex post-transcriptional controls, such as the interplay between RNA-binding proteins, small non-coding RNAs, and feedback loops that modulate mRNA stability, translation, and degradation over time. The polycistronic nature of trypanosome genomes, where multiple genes are transcribed as a single mRNA, further complicates these regulatory mechanisms, requiring precise temporal and spatial control to ensure appropriate protein synthesis during stress. Additionally, the process of SL addition, which is conserved in *T. brucei* but absent in mammals, plays a critical role in the maturation of mRNA transcripts in trypanosomes (Clayton, 2019; Nilsen, 2001). This unique mechanism introduces an extra layer of post-transcriptional regulation, potentially influencing the timing and efficiency of mRNA processing and translation during stress responses.

One important consideration in this study was the normalisation of qPCR data. Actin was used as a reference gene for normalisation, under the assumption that its expression remains stable during heat shock. However, given that global cellular processes are disrupted during heat shock, there is a risk that actin expression itself may change, potentially skewing the results. To mitigate this, future studies should include additional reference genes or proteins known to be stable during heat shock, to provide more robust normalisation. A limitation of this type of investigation is only being able to normalise to the number of cells, as normalising to mRNA levels could reflect recovery rather than actual changes in mRNA abundance.

The findings of this study highlight the intricate post-transcriptional regulation that occurs in response to heat shock in *trypanosomes*. The observed mRNA dynamics suggest that these parasites employ both transient and multiphasic strategies to manage stress, ensuring that they can rapidly respond to immediate threats while also preparing

for longer-term recovery. This dual approach likely reflects an evolutionary adaptation to the fluctuating environments encountered by these organisms, such as the transition between the tsetse fly vector and the mammalian host.

Previous research has investigated the regulatory mechanisms that allow HSP70 mRNA to be maintained or upregulated in response to heat shock (Lee, 1998). The study revealed that, unlike in eukaryotes, PCF *T. brucei* does not increase transcription efficiency of heat shock proteins but instead relies on post-transcriptional control. It found that the addition of the 3'UTR from the HSP70 gene to a reporter gene driven by promoters allowed for the maintenance of high-level mRNA expression during heat shock. This suggests that the 3' UTR of the HSP70 gene is primarily responsible for its mRNA stability during heat shock. Future research should further explore the specific regulatory mechanisms that drive these different mRNA responses, including the role of RNA-binding proteins and non-coding RNAs in modulating mRNA stability and translation. While RNA sequencing (RNA-seq) could provide a broader perspective on transcriptional and mRNA abundance changes, it has limitations in identifying RNAs that are regulated at the level of translation or sequestered into granules without changing their abundance. To address this, integrating RNA-seq with whole-cell proteomics at the same timepoints would allow for a more comprehensive understanding of both RNA and protein dynamics. This approach could reveal how translation efficiency and protein turnover contribute to the stress response, providing insights into how trypanosomes prioritise specific mRNAs and proteins under heat shock or other stress conditions.

7.5. Summary

This study delved into the multifaceted responses of *T. brucei* and *T. congolense* to heat shock, revealing significant findings across various aspects of their biology. The investigation into growth recovery highlighted that the duration of heat shock exposure is a critical determinant of cellular survival and recovery, with *T. brucei* BSF showing a threshold of thermal tolerance, beyond which recovery becomes challenging. The PCF displayed a more robust recovery, likely due to their evolutionary adaptation to the

fluctuating temperatures in the tsetse fly. Meanwhile, the unique behaviour of *T. congolense* IL3000 strain under heat shock, despite its lower optimal growth temperature, underscored the challenges of studying this species and the need for more representative strains.

The study also uncovered significant disruptions in the cell cycle of *T. brucei* BSF after heat shock, with a marked accumulation of cells in the G2/M phase, potentially linked to issues in VSG synthesis and trafficking. Conversely, PCF exhibited an increase in zoid cells, suggesting that heat shock affects distinct processes in these forms. This points to the complexity of mitosis and the selective impact of heat shock on specific components of cell division.

Furthermore, the research into stress granule and P-body formation provided insights into the conserved mechanisms between BSF and PCF, with both forms showing similar responses in the localisation and behaviour of proteins like TbPABP1, TbXRNA, and TbDHH1. The study highlighted the perinuclear localisation of TbXRNA, emphasising its role in mRNA degradation and stress response, particularly in proximity to the flagellar pocket—a key site for cellular trafficking.

The qPCR analysis of mRNA changes after heat shock revealed diverse response patterns, including transient and multiphasic responses, reflecting the complex regulatory mechanisms that govern gene expression under stress. The findings emphasise the sophisticated post-transcriptional controls that trypanosomes employ to balance immediate stress responses with long-term adaptation and recovery.

Overall, this study contributes valuable knowledge to the understanding of the heat shock response in trypanosomes, highlighting the importance of continued research into the specific regulatory mechanisms involved. These insights not only deepen our comprehension of parasite biology but also suggest potential avenues for therapeutic intervention.

8. Appendices

Appendix 1 Table of primers for used for *T. brucei* tagging

Primer name	Sequence	Orientation	Target protein ID	Target	Annealing temperature (° C)	Product size (bp)	Enzymes
MA17	ACATTATCTAGAG GTGTTCCAAAATTC TTTCG	Forward	Tb927.7.4 900	XRNA ORF (*T. brucei*)	46	532	XbaI
MA18	CGTATTGGATCCG CGGCCGCATAACG CTACAGTTTTGCCA	Reverse	Tb927.7.4 900	XRNA ORF (*T. brucei*)	46	532	Bam HI NotI
MA19	ACATTATCTAGAG CGGCCGCAAATAC AAAGGAAAAAAAA GAAGTTG	Forward	Tb927.7.4 900	XRNA 5'UTR (*T. brucei*)	45	532	XbaI
MA20	CGTATTGGATCCG TCTACACGTARTAT ATAAACTGTTTCG	Reverse	Tb927.7.4 900	XRNA 5'UTR (*T. brucei*)	45	532	Bam HI NotI
MA33	ACATTAAAGCTTG CGGCCGCTGCACC ATATGCATCCTCCT CC	Forward	Tb927.9.9 290	PABP1 ORF (*T. brucei*)	57	532	*Avr*II *Not*I
MA34	CGTATTCCTAGGA GCGCTTGAGGCGT GTACCT	Reverse	Tb927.9.9 290	PABP1 ORF (*T. brucei*)	57	532	*Hind*III
MA35	ACATTAAAGCTTA GTTGATTTTGTGA GTGAAAGT	Forward	Tb927.9.9 290	PABP1 3'UTR (*T. brucei*)	46	532	*Avr*II *Not*I
MA36	CGTATTCCTAGGG CGGCCGCACAAGT AGGATACTTCACG A	Reverse	Tb927.9.9 290	PABP1 3'UTR (*T. brucei*)	46	532	*Hind*III

Appendix 2 Table of primers for used for *T. congolense* tagging

Primer name	Sequence	Orientation	Target protein ID	Target	Annealing temperature (° C)	Product size (bp)	Enzymes
MA21	ACATTATCTAGAG GGGTTCCAAA GTTTTTCCG	Forward	TcIL3000_ 7_4 080	XRNA ORF (*T. congolense*)	51	532	XbaI
MA22	CGTATTCTCGAGGC GGCCGCTACACAA CTTTGCAACTTTGC C	Reverse	TcIL3000_ 7_4 080	XRNA ORF (*T. congolense*)	51	532	XhoI NotI
MA23	ACATTATCTAGAGC GGCCGCGAGGTGA GAGGTCAGACACG	Forward	TcIL3000_ 7_4 080	XRNA 5'UTR (*T. congolense*)	50	532	XbaI
MA24	CGTATTCTCGAGG ATTTTGGCTCGATA CCGTT	Reverse	TcIL3000_ 7_4 080	XRNA 5'UTR (*T. congolense*)	50	532	XhoI NotI
MA29	ACATTAGCGGCCG CACACGCATGGGC GCA	Forward	TcIL3000_ 2_1 630	HSP100 ORF (*T. congolense*)	57	532	*Avr*II *Not*I
MA30	CGTATTCCTAGGA GAATTCACAGCAG CGCGCT	Reverse	TcIL3000_ 2_1 630	HSP100 ORF (*T. congolense*)	57	532	*Hind*III
MA31	ACATTAAAGCTTTT GGTACGGTGGAGC	Forward	TcIL3000_ 2_1 630	HSP100 3'UTR (*T. congolense*)	47	532	*Avr*II *Not*I
MA32	CGTATTCCTAGGGC GGCCGCCAATAAA GCGCTCCCTTAAA	Reverse	TcIL3000_ 2_1 630	HSP100 3'UTR (*T. congolense*)	47	532	*Hind*III
MA37	ACATTAAAGCTTGC GGCCGCC CAT GCTGAGGTTACAG CTG	Forward	TcIL3000_ 9_3 370	PABP1 ORF (*T. congolense*)	52	532	*Avr*II *Not*I
MA38	CGTATTCCTAGGA GAATTTGAGGCGT GCACTT	Reverse	TcIL3000_ 9_3 370	PABP1 ORF (*T. congolense*)	52	532	*Hind*III
MA39	ACATTAAAGCTTG GCATATAGTTTACT GAAGGTG	Forward	TcIL3000_ 9_3 370	PABP1 3'UTR (*T. congolense*)	47	532	*Avr*II *Not*I
MA40	CGTATTCCTAGGGC GGCCGCCAAATTA CAGAACATGCATG TG	Reverse	TcIL3000_ 9_3 370	PABP1 3'UTR (*T. congolense*)	47	532	*Hind*III

Appendix 3 Vector Map of pEnNYO

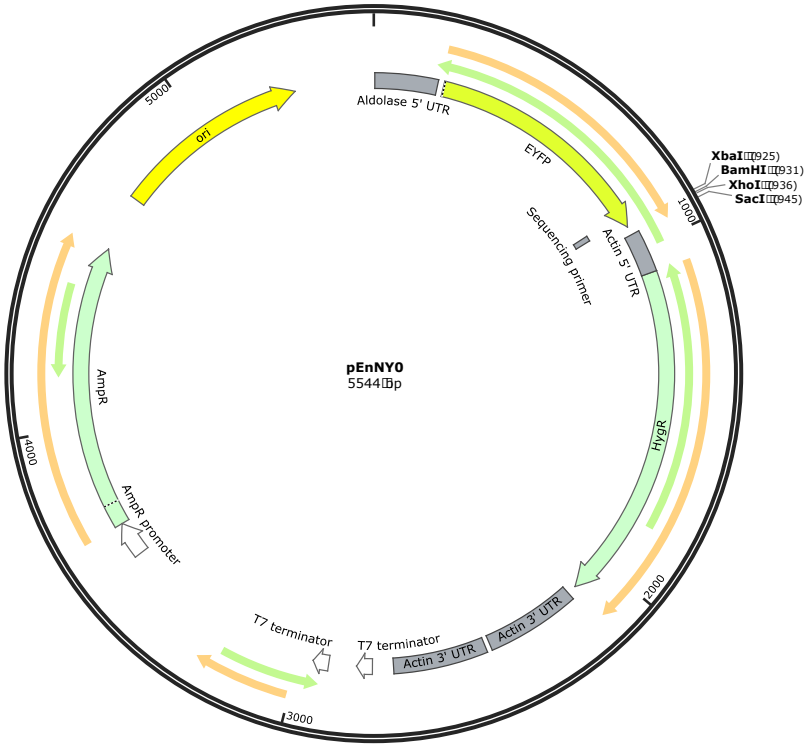

Appendix 4 Vector Map of pSiS-HhsfG

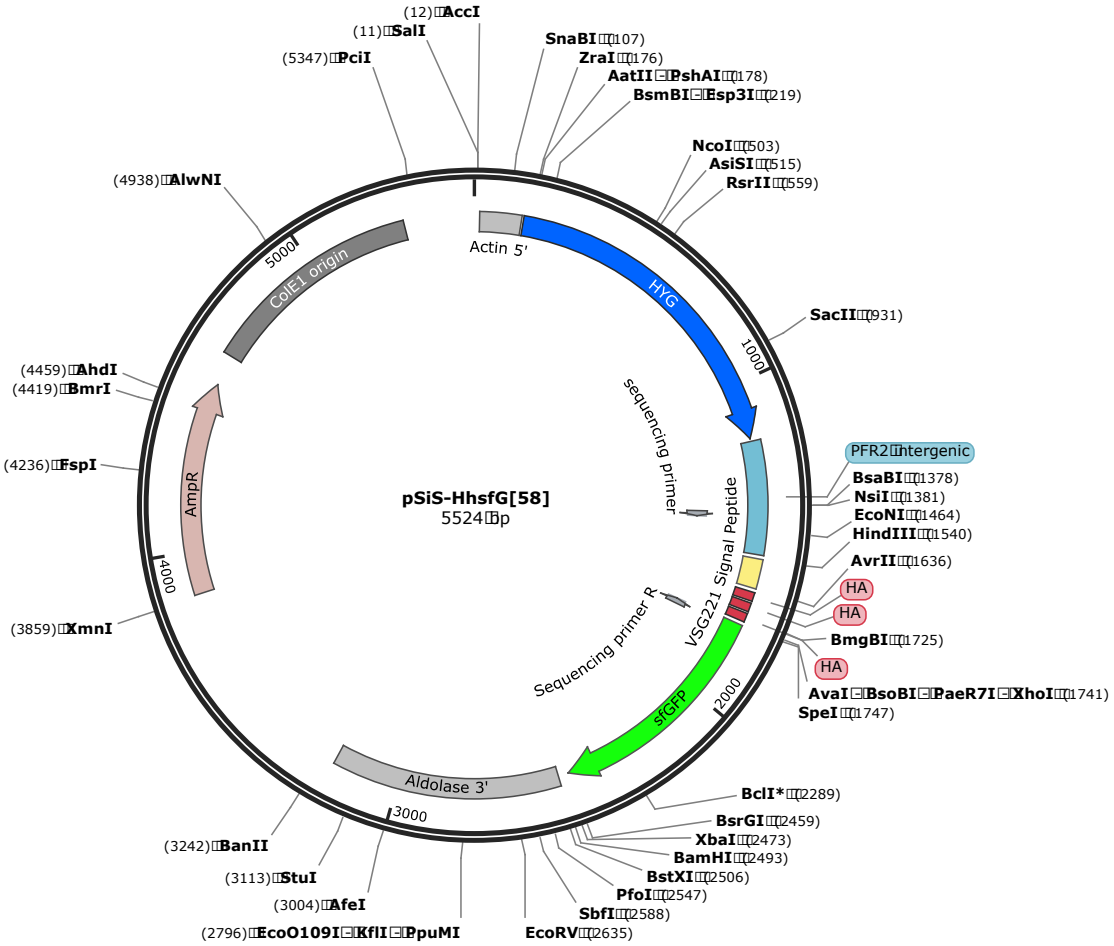

Appendix 5 Gated 2-hour Heat Shock Flow Cytometry Data

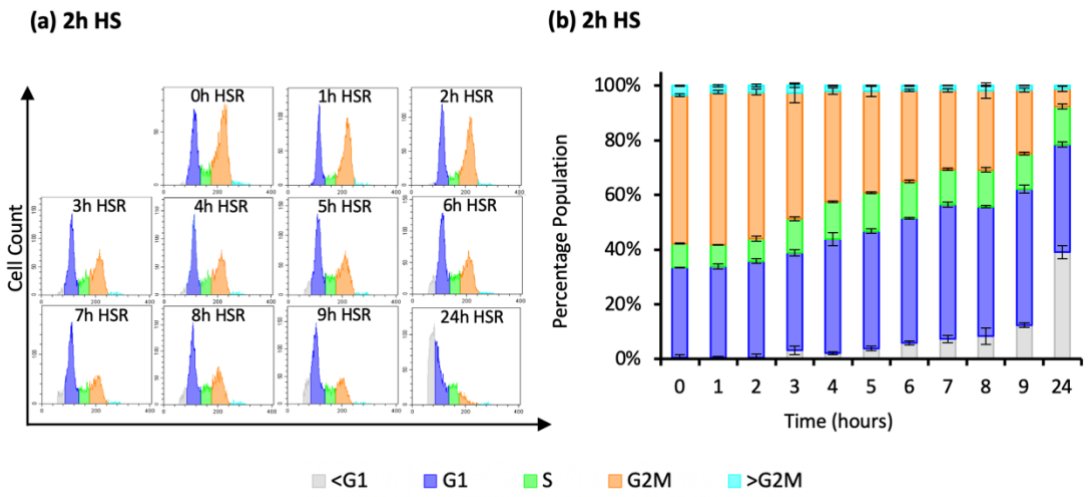

Figure 8.1 Cell cycle analysis of BSF *T. brucei* after heat shock. Flow cytometry analysis of mid log TbBSF cells (5×10^5 cells/ml) post heat shock at 41 °C for 2-hours. Samples were taken every hour for 9 hours followed by a 24-hour timepoint. Data show representative cycles (a) and corresponding relative contribution of cell cycle phases (b). Data are presented as mean ± SD, where n = 3 and gating has been applied from a 0-hour heat shock control.

References

Alagar Boopathy, L.R. et al. (2022) 'Mechanisms tailoring the expression of heat shock proteins to proteostasis challenges', Journal of Biological Chemistry, 298(5), p. 101796. doi:10.1016/j.jbc.2022.101796.

Alsford, S. et al. (2005) 'Tagging a T. brucei RRNA locus improves stable transfection efficiency and circumvents inducible expression position effects', Molecular and Biochemical Parasitology, 144(2), pp. 142–148. doi:10.1016/j.molbiopara.2005.08.009.

Aslett, M. et al. (2009) 'TriTrypDB: A functional genomic resource for the Trypanosomatidae', Nucleic Acids Research, 38(suppl_1). doi:10.1093/nar/gkp851.

Awuah-Mensah, G. et al. (2021) 'Reliable, scalable functional genetics in bloodstream-form Trypanosoma congolense in vitro and in vivo', PLOS Pathogens, 17(1). doi:10.1371/journal.ppat.1009224.

Banerjee, S. et al. (2006) 'Leishmania donovani cyclin 1 (LdCyc1) forms a complex with cell cycle kinase subunit CRK3 (LdCRK3) and is possibly involved in S-phase-related activities', FEMS Microbiology Letters, 256(1), pp. 75–82. doi:10.1111/j.1574-6968.2006.00105.x.

Bianca, W. (1963) 'Rectal temperature and respiratory rate as indicators of heat tolerance in cattle', The Journal of Agricultural Science, 60(1), pp. 113–120. doi:10.1017/s0021859600015902.

Black, J.A. et al. (2020) 'Trypanosoma brucei ATR links DNA damage signaling during antigenic variation with regulation of RNA polymerase I-transcribed surface antigens', Cell Reports, 30(3). doi:10.1016/j.celrep.2019.12.049.

Briggs, L.J. et al. (2004) ‘The flagella connector oftrypanosoma brucei: An unusual mobile transmembrane junction’, Journal of Cell Science, 117(9), pp. 1641–1651. doi:10.1242/jcs.00995.

Broadhead, R. et al. (2006) ‘Flagellar motility is required for the viability of the bloodstream trypanosome’, Nature, 440(7081), pp. 224–227. doi:10.1038/nature04541.

CDC Trypanosomiasis, African (2019) Centers for Disease Control and Prevention. Available at: https://www.cdc.gov/dpdx/trypanosomiasisafrican/index.html (Accessed: 28 September 2024).

Chanmol, W. et al. (2022) ‘Stimulation of metacyclogenesis in Leishmania (mundinia) orientalis for mass production of metacyclic promastigotes’, Frontiers in Cellular and Infection Microbiology, 12. doi:10.3389/fcimb.2022.992741.

Chappuis, F. et al. (2005) ‘Eflornithine is safer than Melarsoprol for the treatment of second-stage trypanosoma brucei gambiense human African trypanosomiasis’, Clinical Infectious Diseases, 41(5), pp. 748–751. doi:10.1086/432576.

Clayton, C. (2019) ‘Regulation of gene expression in trypanosomatids: Living with Polycistronic Transcription’, Open Biology, 9(6). doi:10.1098/rsob.190072.

Coustou, V. et al. (2010) ‘Complete in vitro life cycle of Trypanosoma congolense: Development of genetic tools’, PLoS Neglected Tropical Diseases, 4(3). doi:10.1371/journal.pntd.0000618.

Davis, M.W. and Jorgensen, E.M. (2022) ‘Ape, a plasmid editor: A freely available DNA manipulation and visualization program’, Frontiers in Bioinformatics, 2. doi:10.3389/fbinf.2022.818619.

Droll, D. et al. (2013) ‘Post-transcriptional regulation of the trypanosome heat shock response by a zinc finger protein’, PLoS Pathogens, 9(4). doi:10.1371/journal.ppat.1003286.

Eyford, B.A. et al. (2011) 'Differential protein expression throughout the life cycle of Trypanosoma congolense, a major parasite of cattle in Africa', Molecular and Biochemical Parasitology, 177(2), pp. 116–125. doi:10.1016/j.molbiopara.2011.02.009.

Edney, E. B. and Barrass, R. (1962) 'The body temperature of the tsetse fly, Glossina morsitans Westwood (Diptera, Muscidae)', *Journal of Insect Physiology*. Pergamon, 8(4), pp. 469–481. doi: 10.1016/0022-1910(62)90079-3.

Hirumi, H. and Hirumi, K. (1989) 'Continuous cultivation of Trypanosoma brucei blood stream forms in a medium containing a low concentration of serum protein without feeder cell layers', The Journal of Parasitology, 75(6), p. 985. doi:10.2307/3282883.

Kedersha, N.L. et al. (1999) 'RNA-binding proteins TIA-1 and Tiar link the phosphorylation of EIF-2α to the Assembly of mammalian stress granules', The Journal of Cell Biology, 147(7), pp. 1431–1442. doi:10.1083/jcb.147.7.1431.

Kramer, S. et al. (2008) 'Heat shock causes a decrease in polysomes and the appearance of stress granules in trypanosomes independently of eIF2α phosphorylation at thr169', Journal of Cell Science, 121(18), pp. 3002–3014. doi:10.1242/jcs.031823.

Kramer, S. et al. (2013) 'Differential localization of the two T. brucei poly(a) binding proteins to the nucleus and RNP granules suggests binding to distinct mrna pools', PLoS ONE, 8(1). doi:10.1371/journal.pone.0054004.

Kumar, P. and Wang, C.C. (2006) 'Dissociation of cytokinesis initiation from mitotic control in a eukaryote', Eukaryotic Cell, 5(1), pp. 92–102. doi:10.1128/ec.5.1.92-102.2006.

Landfear, S.M. (2006) 'When the tail wags the dog', Nature, 440(7081), pp. 153–154. doi:10.1038/440153a.

Lee, M. (1998) 'The 3' untranslated region of the HSP 70 genes maintains the level of steady state mrna in Trypanosoma brucei upon heat shock', Nucleic Acids Research, 26(17), pp. 4025–4033. doi:10.1093/nar/26.17.4025.

López-Escobar, L. et al. (2022) ‘Stage-specific transcription activator ESB1 regulates monoallelic antigen expression in Trypanosoma brucei’, Nature Microbiology, 7(8), pp. 1280–1290. doi:10.1038/s41564-022-01175-z.

Mahat, D.B. *et al.* (2016) ‘Mammalian heat shock response and mechanisms underlying its genome-wide transcriptional regulation’, *Molecular Cell*, 62(1), pp. 63–78. doi:10.1016/j.molcel.2016.02.025.

Masser, A.E., Ciccarelli, M. and Andréasson, C. (2020) ‘HSF1 on a leash – controlling the heat shock response by chaperone titration’, Experimental Cell Research, 396(1), p. 112246. doi:10.1016/j.yexcr.2020.112246.

Muhich, M.L. and Boothroyd, J.C. (1988) ‘Polycistronic transcripts in trypanosomes and their accumulation during heat shock: Evidence for a precursor role in mrna synthesis.’, Molecular and Cellular Biology, 8(9), pp. 3837–3846. doi:10.1128/mcb.8.9.3837.

Muhich, M.L. and Boothroyd, J.C. (1989) ‘Synthesis of trypanosome hsp70 mrna is resistant to disruption of trans-splicing by heat shock’, Journal of Biological Chemistry, 264(13), pp. 7107–7110. doi:10.1016/s0021-9258(18)83206-9.

Muhich, M.L. and Boothroyd, J.C. (1989) ‘Heat-shock disruption of trans-splicing in trypanosomes: Effect on hsp70, HSP85 and tubulin mrna synthesis’, Gene, 82(1), pp. 169–175. doi:10.1016/0378-1119(89)90042-5.

Nihei, C. and Nakanishi, M. (2021) ‘Cargo selection in the early secretory pathway of African trypanosomes’, Parasitology International, 84, p. 102379. doi:10.1016/j.parint.2021.102379.

Nilsen, T.W. (2001) ‘Evolutionary origin of SL-addition trans-splicing: Still an enigma’, Trends in Genetics, 17(12), pp. 678–680. doi:10.1016/s0168-9525(01)02499-4.

Ooi, C.P., Benz, C. and Urbaniak, M.D. (2020) ‘Phosphoproteomic analysis of mammalian infective trypanosoma brucei subjected to heat shock suggests atypical mechanisms for thermotolerance’, Journal of Proteomics, 219, p. 103735. doi:10.1016/j.jprot.2020.103735.

Rojas, F. et al. (2019) ‘Oligopeptide signaling through tbgpr89 drives trypanosome quorum sensing’, Cell, 176(1–2). doi:10.1016/j.cell.2018.10.041.

Ross, R. and Thomson, D. (1910) ‘A case of sleeping sickness showing regular periodical increase of the parasites disclosed’, BMJ, 1(2582), pp. 1544–1545. doi:10.1136/bmj.1.2582.1544.

Sheader, K. et al. (2005) ‘Variant surface glycoprotein RNA interference triggers a precytokinesis cell cycle arrest in African trypanosomes’, Proceedings of the National Academy of Sciences, 102(24), pp. 8716–8721. doi:10.1073/pnas.0501886102.

Singh, A. et al. (2014) ‘Trypanosome MKT1 and the RNA-binding protein ZC3H11: Interactions and potential roles in post-transcriptional regulatory networks’, Nucleic Acids Research, 42(7), pp. 4652–4668. doi:10.1093/nar/gkt1416.

Navarro, M. and Gull, K. (2001) ‘A Pol I transcriptional body associated with VSG mono-allelic expression in Trypanosoma brucei’, Nature, 414(6865), pp. 759–763. doi:10.1038/414759a.

Spatuzza, C. et al. (2004) ‘Heat shock induces preferential translation of ERGIC-53 and affects its recycling pathway’, Journal of Biological Chemistry, 279(41), pp. 42535–42544. doi:10.1074/jbc.m401860200.

Tarral, A. et al. (2023) ‘Determination of the optimal single dose treatment for Acoziborole, a novel drug for the treatment of human African trypanosomiasis: First-in-human study’, Clinical Pharmacokinetics, 62(3), pp. 481–491. doi:10.1007/s40262-023-01216-8.

Velichko, A.K. *et al.* (2013a) ‘Mechanisms of heat shock response in mammals’, *Cellular and Molecular Life Sciences*, 70(22), pp. 4229–4241. doi:10.1007/s00018-013-1348-7.

Venturelli, A. et al. (2022) ‘Current treatments to control African trypanosomiasis and one health perspective’, Microorganisms, 10(7), p. 1298. doi:10.3390/microorganisms10071298.

Wickstead, B. et al. (2010) ‘The expanded kinesin-13 repertoire of trypanosomes contains only one mitotic kinesin indicating multiple extra-nuclear roles’, PLoS ONE, 5(11). doi:10.1371/journal.pone.0015020.

Wiedemar, N. et al. (2019) ‘Expression of a specific variant surface glycoprotein has a major impact on suramin sensitivity and endocytosis intrypanosoma brucei’, FASEB BioAdvances, 1(10), pp. 595–608. doi:10.1096/fba.2019-00033.

Zhang, H. et al. (2019) ‘Chromatin structure dynamics during the mitosis-to-G1 phase transition’, Nature, 576(7785), pp. 158–162. doi:10.1038/s41586-019-1778-y.

Zhou, Q., Hu, H. and Li, Z. (2022) ‘KLIF-associated cytoskeletal proteins in Trypanosoma brucei regulate cytokinesis by promoting cleavage furrow positioning and ingression’, Journal of Biological Chemistry, 298(6), p. 101943. doi:10.1016/j.jbc.2022.101943.